INTERFERENCE MANAGEMENT IN ENERGY-EFFICIENT HETEROGENEOUS NETWORKS

by

Can Altay

B.S., Electronics and Communication Engineering, Yıldız Technical University, 2010

M.S., Electrical and Electronics Engineering, Boğaziçi University, 2013

Submitted to the Institute for Graduate Studies in
Science and Engineering in partial fulfillment of
the requirements for the degree of
Doctor of Philosophy

Graduate Program in Electrical and Electronics Engineering

Boğaziçi University

2023

ACKNOWLEDGEMENTS

I would like to express my gratitude to my supervisor, Prof. Mutlu Koca, for his patience and encouragement throughout the work of this thesis. Beside his guidance and contribution to this thesis, working with him has shaped my perspective on academia and industry for my later research career.

I am grateful to Prof. Emin Anarım and Prof. Cem Ersoy for their valuable evaluation in each progress term and final defense presentations. I am thankful to Prof. Hakan Ali Çırpan and Prof. Tayfun Akgül for allocating their valuable time for evaluating this thesis. Their comments and suggestions have significant effect on improving quality of this work.

My special thanks goes to my parents Tayfun and Nigâr, and my brother Gökhan. They have been keen followers of all ups and downs through my career and continuous supporters to my decisions.

I would like to thank to all classmates from Boğaziçi University for their friendly environment. I thank to all of my colleagues from Argela Technologies and later from Juniper Networks for letting me experience fruitful team work on our projects outside the university. I am thankful to all my friends from the 3rd street of Hisarüstü District for all joyful time we spent together. I am also thankful to my friends from running societies of Istanbul for all of colorful activities we did together. Lastly, I would like thank to two close friends, Hüseyin and Sinan, for their supportive and trustworthy friendship.

This thesis has been supported in part by the Scientic and Technical Research Council of Turkey (TUBITAK) with grant number 119N154.

ABSTRACT

INTERFERENCE MANAGEMENT IN ENERGY-EFFICIENT HETEROGENEOUS NETWORKS

By the densification of the cellular networks, the performance of the users, who are close to coverage boundaries, significantly degrades due to severe interference. The statistical characteristics of the interfering signal gets complicated by heterogeneity of the base station deployment and employing non-orthogonal multiple access (NOMA). In this thesis, stochastic geometry analysis is presented to reveal the statistical characteristics of the user performance. The interference experienced by the user includes the signals coming from the neighbor base stations with different transmit power capabilities and also from user's own serving base station for NOMA. Coverage probabilities of strict fractional frequency reuse (FFR) and soft frequency reuse (SFR) techniques are derived for NOMA-based heterogeneous network to indicate their performance under such interference. Parameter optimization problems for strict FFR and almost blank sub-frame (ABS) are modelled for maximization of energy efficiency by the capacity derivations of stochastic geometry analysis. A hybrid multiple access method, where NOMA and orthogonal multiple access (OMA) jointly deployed for improving edge user performance, is proposed and compared with conventional NOMA. For uplink NOMA, a decode order optimization problem is presented with its solution for avoidance of intra-cell interference under the user transmit power constraints.

ÖZET

ENERJİ VERİMLİ ÇOKTÜREL AĞLARDA GİRİŞİM YÖNETİMİ

Baz istasyonu kurulumlarının sıklaşmasından dolayı kapsama alanı sınırlarına yakın kullanıcıların performasları şiddetli girişim yüzünden düşmektedir. Girişim sinyalinin istatistiksel karakteristiği baz istasyonu kurulumlarının çoktürel olması ve dikey olmayan çoklu erişim kullanılmasıyla karmaşıklaşmaktadır. Bu tezde, kullanıcı performansının istatistiksel karakteristiklerini açığa çıkarmak için rastgele geometri analizi yapılmaktadır. Kullanıcı tarafından algılanan girişim, farklı yayın gücü kapasitelerine sahip komşu baz istasyonlarının sinyallerini ve dikey olmayan çoklu erişim kullanılması durumda kullanıcının kendi baz istasyonunun da sinyalini içerir. Bu girişim sinyali altında dikey olmayan çoklu erişim kullanan çoktürel ağlar için mutlak oranlı frekans yeniden kullanımı ve yumuşak frekans yeniden kullanımı yöntemlerinin kapsama olasılıkları türetilmiştir. Rastgele geometri anailizinin kapasite türetimleri kullanılarak, mutlak oranlı frekans yeniden kullanımı ve boşa yakın alt-çerçeve yöntemleri için enerji verimliliğini en üst düzeye çıkaran parametre eniyileme problemleri modellenmiş ve çözümleri sunulmuştur. Kıyı kullanıcılarının performansını arttırmak için dikey olmayan ve dikey çoklu erişim yöntemlerinin beraber kullanıldığı bir melez çoklu erişim yöntemi önerilmiş ve bu yöntemin performansı uzlaşımsal dikey olmayan çoklu erişim yöntemi ile karşılaştırılmıştır. Yukarı yönlü dikey olmayan çoklu erişimde hücre içi girişimin engellenmesi için, kullanıcı yayın gücü limitleri düşünülerek kullanıcı sinyallerinin çözümlenme sırasının eniyilemesi problemi çözümüyle beraber sunulmuştur.

TABLE OF CONTENTS

LIST OF FIGURES

LIST OF TABLES

LIST OF SYMBOLS

$a_{i,j}^{\text{far}}$	Power coefficient of far user for user pair i, j
a_{t}^{far}	Power coefficient of far user for base station tier t
$a_{i,j}^{\text{near}}$	Power coefficient of near user for user pair i, j
a_{t}^{near}	Power coefficient for near user for base station tier t
$\mathfrak{b}$	Base station selection bias for 2-tier network
B	Frequency bandwidth of base station in Hertz
B_{RB}	Frequency bandwidth of resource block in Hertz
$\mathcal{B}$	Frequency bandwidth of base station in Nats ($B \times \log_2(e)$)
$\mathcal{B}_{\text{I}}$	Frequency bandwidth of base station for interior users in Nats
$\mathcal{B}_{\text{E}}$	Frequency bandwidth of base station for edge users in Nats
$\mathcal{B}_{\text{RB}}$	Frequency bandwidth of resource block in Nats
$\mathcal{C}_{\text{M}}^{\text{I}}$	Capacity of macro interior users without bandwidth
$\mathcal{C}_{\text{M}}^{\text{E}}$	Capacity of macro edge users without bandwidth
$\mathcal{C}_{\text{M}}^{\text{Worst}}$	Capacity of macro the worst region users without bandwidth
$\mathcal{C}_{i,j}^{\text{near}}$	Capacity of near users without bandwidth for user pair i, j
$\mathcal{C}_{i,j}^{\text{far}}$	Capacity of far users without bandwidth for user pair i, j
$\mathcal{C}^{\text{OMA}}$	Capacity of OMA users without bandwidth
$\mathcal{C}_{i \to j}^{\text{Up.RB}}$	Total capacity in an uplink resource block without bandwidth for decoding order ($i \to j$)
$\mathbb{C}_{\text{M.BS}}$	Bit-rate of a macro base station
$\mathbb{C}_{\text{M.BS}}^{\text{I}}$	Bit-rate of a macro base station for interior users
$\mathbb{C}_{\text{M.BS}}^{\text{E}}$	Bit-rate of a macro base station for edge users
$\mathbb{C}_{\text{P.BS}}$	Bit-rate of a pico base station
$\mathbb{C}_{\text{P.BS}}^{\text{I}}$	Bit-rate of a pico base station for interior users
$\mathbb{C}_{\text{P.BS}}^{\text{E}}$	Bit-rate of a pico base station for edge users
$\mathbb{C}_{\text{P.BS}}^{\text{Hybrid}}$	Bit-rate of a pico base station for hybrid model
$\mathbb{C}_{\text{P.BS}}^{\text{NOMA}}$	Bit-rate of s pico base station for NOMA
$\mathbb{C}_{\text{P.BS}}^{\text{OMA}}$	Bit-rate of a pico base station for OMA

$\mathbb{C}_{\text{M.User}}$	Bit-rate of a macro user
$\mathbb{C}_{\text{P.User}}$	Bit-rate of pico user
$\mathbb{C}^{\text{W}}_{\text{M.User}}$	Bit-rate of a macro user in the worst-region
$\mathbb{C}^{\text{I-W}}_{\text{M.User}}$	Bit-rate of a macro interior user in the worst-region
$\mathbb{C}^{\text{E-W}}_{\text{M.User}}$	Bit-rate of a macro edge user in the worst-region
$\mathbb{C}^{\text{W}}_{\text{P.User}}$	Bit-rate of a pico user in the worst-region
$\mathbb{C}^{\text{I-W}}_{\text{P.User}}$	Bit-rate of a pico interior user in the worst-region
$\mathbb{C}^{\text{E-W}}_{\text{P.User}}$	Bit-rate of a pico edge user for in worst-region
$\mathbb{C}^{\text{Hybrid}}_{\text{Edge P.User}}$	Bit-rate of a pico user in hybrid model
$\mathbb{C}^{\text{NOMA}}_{\text{Edge P.User}}$	Bit-rate of a pico edge user in NOMA
$\mathbb{C}^{\text{OMA}}_{\text{Edge P.User}}$	Bit-rate of a pico edge user in OMA
D_i	Uplink bit-rate demand of user i
EC'_{M}	Energy consumption of a macro base station
EC_{M}	Simplified energy consumption of a macro base station
EC_{P}	Simplified energy consumption of a pico base station
f_i	Frequency part i
f_{I}	Frequency part for interior users
$f_x(\cdot)$	PDF of random variable x
F	Number of frequency resources
F_{I}	Number of frequency resources for interior users
$\mathcal{F}_x(\cdot)$	CDF of random variable x
g_i	Uplink channel power gain for user i
h	Downlink channel power gain for the user
h_i	Downlink channel power gain for interfering user i
$I_t^{\text{sFFR-I}}$	Interference for strict FFR in interior frequency part for base station tier t
$I_{t,s}^{\text{sFFR-E}}$	Interference for strict FFR in edge-s frequency part for base station tier t
I_t^{SFR}	Interference for SFR for base station tier t
k_M	Number of ABS's in a frame for macro base stations
k_P	Number of ABS's in a frame for pico base stations

K	Number of sub-frames in a frame
N	Number of users
N_{M}	Number of users connected to macro base station
$N_{\mathrm{M}}^{\mathrm{I}}$	Number of interior users connected to macro base station
$N_{\mathrm{M}}^{\mathrm{E}}$	Number of edge users connected to macro base station
N_{P}	Number of users connected to pico base station
$N_{\mathrm{P}}^{\mathrm{I}}$	Number of interior users connected to pico base station
$N_{\mathrm{P}}^{\mathrm{E}}$	Number of edge users connected to pico base station
p_i	Uplink transmit power of user i
$p_i^{\max}$	Maximum uplink transmit power of user i
P_{M}	Downlink transmit power of macro base station
P_{P}	Downlink transmit power of pico base station
P_t	Downlink transmit power of tier t base stations
$\mathfrak{p}_{\mathrm{M}}$	Probability of selecting macro base station tier
$\mathfrak{p}_{\mathrm{P}}$	Probability of selecting pico base station tier
$\mathfrak{p}_t$	Probability of selecting base station tier t
$P_{\mathrm{M}}^{\max}$	Maximum downlink transmit power of a macro base station
p_{worst}	Probability of the worst-region
$\mathcal{P}_{\mathrm{M}}^{\mathrm{E}}$	Probability of grouping a macro user as edge user
$\mathcal{P}_{\mathrm{P}}^{\mathrm{E}}$	Probability of grouping a pico user as edge user
$\mathcal{P}_t^{\mathrm{E}}$	Probability of grouping a tier t user as edge user
$\mathbb{P}(\cdot)$	User pairing set
$\mathfrak{P}_t$	Probability of grouping a tier t user as far user
$q_{s\|t}$	Minimum distance of interfering base stations of tier s to the user of tier t
r	Distance between the user and serving base station
r_i	Distance between the user and interfering base station i
$S_{\mathrm{M}}^{\mathrm{I}}$	Capacity with user grouping probability for macro interior users
$S_{\mathrm{M}}^{\mathrm{E}}$	Capacity with user grouping probability for macro edge users
$v_{x.y}$	Lagrangian multiplier y defined in chapter x

$\mathcal{X}$	Bandwidth usage ratio of base station
z_{xy}	Tier selection coefficient for x and y tiers
α	Pathloss exponent
β_t	Power coefficient of SFR for base station tier t
γ_{M}	Threshold of user grouping for macro users
γ_{P}	Threshold of user grouping for pico users
γ_t	Threshold of user grouping for tier t
$\delta_{i,s}$	Interfering indicator of base station i for tier s
Δ_t	Frequency reuse factor for tier t
$\epsilon_{x.y}$	Optimization constraint y defined in chapter x
$\kappa_i(\cdot)$	Coverage probability of user i
$\kappa^{\mathrm{I}}(\cdot)$	Coverage probability of an interior user
$\kappa_t^{\mathrm{N}}(\cdot)$	Coverage probability of a near user of tier t
$\kappa_t^{\text{F-I}}(\cdot)$	Coverage probability of a far-interior user of tier t
$\kappa_t^{\text{F-E}}(\cdot)$	Coverage probability of a far-edge user of tier t
$\kappa_{\mathrm{P}}(\cdot)$	Coverage probability of a pico user
$\kappa_{\mathrm{P}}^{\mathrm{I}}(\cdot)$	Coverage probability of a pico interior user
$\kappa_{\mathrm{P}}^{\mathrm{E}}(\cdot)$	Coverage probability of a pico edge user
λ_{M}	Density of macro base station deployment
λ_{P}	Density of macro base station deployment
λ_t	Density of tier t base station deployment
$\mu_{\mathrm{M}}^{\Delta\mathrm{P}}$	Energy consumption power factor for macro base station
$\mu_{\mathrm{M}}^{\Delta\mathrm{N}}$	Energy consumption resource usage factor for macro base station
$\mu_{\mathrm{M}}^{\mathrm{const}}$	Energy consumption constant for macro base station
$\mu_{\mathrm{P}}^{\mathrm{const}}$	Energy consumption constant for pico base station
$\mu_{\mathrm{M}}^{\Delta}$	Simplified energy consumption power factor for macro base station
$\mu_{\mathrm{P}}^{\Delta}$	Simplified energy consumption power factor for pico base station
φ_t	Threshold of power level selection for tier t

σ^2	Noise power
$\Phi_i^{i \to j}$	Uplink SINR of user i for decode order $(i \to j)$
Ψ	Downlink SINR
Ψ_{M}	SINR of macro user
$\Psi_{\mathrm{M}}^{\mathrm{I}}$	SINR of macro interior user
$\Psi_{\mathrm{M}}^{\mathrm{E}}$	SINR of macro edge user
Ψ_{P}	SINR of pico user
$\Psi_{\mathrm{P}}^{\mathrm{I}}$	SINR of pico interior user
$\Psi_{\mathrm{P}}^{\mathrm{E}}$	SINR of pico edge user
Ψ_t^{N}	SINR of near user for base station tier t
$\Psi_t^{\mathrm{N\text{-}I}}$	SINR for near-interior user in base station tier t
$\Psi_{t,s}^{\mathrm{N\text{-}E}}$	SINR for near-edge user for base station tier t in edge-s frequency part
$\Psi_t^{\mathrm{N(F)}}$	SINR of far users signal measured by near user for base station tier t
Ψ_t^{F}	SINR for far user for base station tier t
$\Psi_t^{\mathrm{F\text{-}I}}$	SINR for far-interior user for base station tier t
$\Psi_{t,s}^{\mathrm{F\text{-}E}}$	SINR for far-edge user for base station tier t in edge-s frequency part
ω_{M}	Threshold of the worst region for macro base stations
ω_{P}	Threshold of the worst region for pico base stations

LIST OF ACRONYMS/ABBREVIATIONS

2D	Two Dimensional
3GPP	The 3rd Generation Partnership Project
4G	The 4th Generation
5G	The 5th Generation
6G	The 6th Generation
ABS	Almost Blank Sub-Frame
AEC	Area Energy Consumption
ASE	Area Spectral Efficiency
BS	Base Station
CDF	Cumulative Distribution Function
CoMP	Coordinated Multi-point
CSI	Channel State Information
CRE	Cell Range Extention
DC	Direct Current
EC	Energy Consumption
EE	Energy Efficiency
F-OFDM	Filtered Orthogonal Frequency Division Multiplexing
FFR	Fractional Frequency Reuse
ICIC	Inter-Cell Interference Coordination
IoT	Internet of Things
KKT	Karush-Kuhn-Tucker
KPI	Key Performance Indicator
LTE	Long Term Evolution
LPS	Low Power Sub-frame
MATLAB	Matrix Laboratory
MIMO	Multiple Input Multiple Output
MMTC	Massive Machine Type Communication
NF	Near-to-Far

NOMA	Non-Orthogonal Multiple Access
NOO	No-Optimal-Order
NN	Near-to-Near
OFDM	Orthogonal Frequency Division Multiplexing
OFDMA	Orthogonal Frequency Division Multiple Access
OMA	Orthogonal Multiple Access
PDF	Probability Density Function
PPP	Poisson Point Process
QoS	Quality of Service
RSRP	Reference Signal Received Power
RA	Resource Allocation
RB	Resource Block
SFR	Soft Frequency Reuse
SINR	Signal to Interference and Noise Ratio
SIC	Successive Interference Cancellation
SIR	Signal to Interference Ratio
SNR	Signal to Noise Ratio

1. INTRODUCTION

The cellular networks face increasing bandwidth demand by data-hungry applications in every succeeding generation. The 5th generation (5G) cellular networks had around 660 million subscribers by the end of 2021 and are expected to have 4.4 billion subscribers by 2027 [1]. The telecommunication industry adopts new technologies ever so quickly to meet increasing demands. To meet the traffic requirements, the standards from 4G to 6G include improved multiple access techniques, while introducing new wider bandwidth frequency bands [2]. Beside the advances on link level aspects, the densification of cellular deployment is a significant solution to meet the high data rate demand.

The densification is usually provided by the deployment of different tiers of base stations (BS) in the so called heterogeneous network architecture. Heterogeneous networks include at least two tiers of BS's; the ones with high transmit power are called the macro tier, and the ones with lower transmit powers are called the micro, pico, or femto tiers. While macro BS's provide extensive coverage, micro, pico, or femto BS's provide higher bandwidth by the more frequent reuse of frequency band [3]. The heterogeneous networks can be further divided to two types; open and closed access. Mobile devices connect to the tier with the strongest received signal power in open access, while they connect to only a pre-defined tier of BS's in closed access. The closed access networks, which are implemented by femto BS's, are expected to be an important use-case in 5G networks [4, 5]. However, the performance of the dense in-band heterogeneous networks is limited by interference of the neighboring BS's.

For the downlink, the user's signal is affected by the signals of other BS's which are utilizing the same frequency band. The interference damages especially the performance of the users, which are close to the boundary of the BS coverage. By heterogeneity of the network, the user experiences a superposition of interference from BS's in the same tier with serving BS (intra-tier interference) and interference from the BS's

of the other tiers (inter-tier interference). The severity of the inter-tier interference changes by the access type of the network. In closed access networks, the users can be located so close to the BS's of other tiers. Therefore, the users of a closed access tier experience severe inter-tier interference as they can get closer to interfering BS's.

The requirement of high data rate increases the eligibility of alternative spectrum access methods to conventional orthogonal multiple access (OMA). Non-orthogonal multiple access (NOMA) technology is a promising alternative, which provides around 30% data-rate gain over conventional OMA [6]. To provide increased bandwidth, the standardization efforts of both 4G and 5G networks include various downlink and uplink NOMA deployment scenarios [7, 8]. For 6G and beyond, NOMA promises performance advantage for multi-antenna scenarios [9], while channel estimation plays an important role to achieve such performance gain. Fortunately, more advanced channel models are recently studied [10,11] to assist further performance improvements for new technologies such as NOMA.

Interference management gains great importance in terms of providing fair performance to the distant users due to non-orthogonal signals of the users of the same BS. By employing NOMA, a third kind of interference, called intra-cell interference, is superposed on the user's signal. The intra-cell interference is eliminated by successive interference cancellation (SIC) technique for the users close to the BS [12]. However, NOMA users experience the intra-cell interference in addition to the intra-tier and inter-tier interference. Especially, the inter-tier interference by the macro BS's severely affects the edge user performance of pico or femto cells [13].

The densification of the BS deployment and employing SIC receiver promises high data rate by causing higher energy consumption (EC) of the network. As a consequence, the design of the wireless networks is required to include the energy efficiency (EE) of the network as another design metric. According to [14], the average EC in cellular BS's can reach up to 60% of the network EC. The next-generation cellular networks boost denser deployments in order to fulfill the high throughput and low delay

requirements. The densification of BS's is considered to meet these requirements especially at the busiest hours of the day. However, such a dense deployment would create a huge redundancy of the capacity at the off-peek times, where EE design becomes an important issue.

Heterogeneity of the BS's is provided for denser BS deployments. Even though pico and femto BS's have lower transmit power, frequent reuse of the same bandwidth increases area energy consumption (AEC) by denser BS deployment. The increased AEC causes the engineers to approach to wireless communication problems with EE goal to reduce operating expense. Interference coordination is one such problem, where the BS's idle some of the bandwidth usage. The idle bandwidth decreases interference to neighboring cell users, and also potentially decreases the EC. Instead of maximizing the bit-rate related metrics alone, the maximization of EE provides more practical results for both bit-rate and EC.

Beside downlink, NOMA promises efficiency for uplink use-cases. Uplink NOMA is considered as a good candidate to serve massive number of devices simultaneously for internet of things (IoT) applications in 6G [15]. The uplink performance of grant-based and grant-free machine type communication is already investigated for feasibility in 3GPP standards [8]. Moreover, EC of the connected devices is another key performance indicator (KPI) as most of IoT devices are battery powered. Ensuring lower EC for user devices and less signaling overhead has paramount importance for IoT use-cases [16].

1.1. Related Background

1.1.1. Inter-cell Interference Coordination (ICIC)

A widely studied solution to the interference problem in the literature is inter-cell interference coordination (ICIC) technique. ICIC techniques include modifications in spectrum usage and transmit power by coordination among neighboring BS's to suppress interference. ICIC is generally used to increase the performance of the users,

who experience severe interference due to their closer position to coverage boundaries.

ICIC solutions based on resource allocation (RA) and transmit power adjustment promise short-term spectral efficiency and EE gains. In long term evolution (LTE) networks, coordination of BS's is achieved by a control interface called X2, which is formed between neighboring BS's. An example of distributed ICIC algorithm utilizing X2 interface is proposed in [17], which is based on sharing information of interference-vulnerable users between neighboring BS's. A more advanced ICIC approach is given in [18] where a throughput and user traffic demand based utility function is optimized by dual decomposition.

A well-known approach for ICIC is the use of the fractional frequency reuse (FFR), which is based on statically idling or transmitting with different power levels in some part of the frequency band with a reuse factor [19]. In FFR-based methods, the users are grouped as interior and edge users to provide differentiated service. The outage probability and average rate of conventional ICIC schemes, strict FFR and soft frequency reuse (SFR), are analyzed in [20] using the stochastic geometry approach. In contrast to the wide usage of FFR, an alternative stochastic geometry analysis of ICIC is presented in [21], which is based on the dominant interferer suppression. In [22], the authors optimize the bandwidth assignment regarding the user traffic demands under the aggregate interference derived by stochastic geometry. An FFR parameter optimization problem is solved in [23] where the total capacity, worst region capacity and EC are formulated for finite number of BS's and solved by a generic Pareto optimization algorithm. However, stochastic geometry based analysis provides capability to optimize the parameters regarding the random behavior of channel and position of interfering BS's over infinite 2D plane.

The interference avoidance problem becomes more difficult with the inclusion of the inter-tier interference. Stochastic geometry analysis for FFR-based techniques in a heterogeneous network is presented in [24, 25], where the frequency reuse factor is increased by the number of BS tiers. Large number of frequency reuse factor increases

the idle part of the spectrum and reduces the overall sum-rate of the network. A more specialized technique between macro and pico tiers is proposed as almost blank sub-frames (ABS) which can be used in orthogonal frequency division multiple access (OFDMA)-based as well as other multi-carrier systems. ABS is a time-based interference coordination technique, where the BS's of a tier do not transmit data signals on pre-determined sub-frames, while the other tier schedules interference-vulnerable users to that sub-frame. The sub-frames, which do not transmit data, are called *almost* blank, since control and reference signals are still transmitted. In 3GPP standards, two use-cases are introduced for open and closed access [26]. In the closed access use-case, the femto BS uses ABS to decrease interference on macro user, which is positioned close to the femto BS. In the open access use-case, the macro BS uses ABS to increase performance of distant users of pico BS. These use-cases inevitably maintain their importance, since the technologies such as 5G and its successors are still expected to use heterogeneous networks [27].

In 4G networks, ABS is employed to avoid inter-tier interference as shown in [26]. A dynamically decision making power saving framework for ABS is presented in [28] depending on the user traffic. A modified version of ABS is referred to low power sub-frame (LPS), which is used to serve close users and to avoid interference to other tiers [29]. Aggregate and per user spectral efficiency analysis of ABS and LPS are presented in [30]. An extended coverage probability analysis of LPS is introduced in [31], where the results indicate ABS superiority for optimal cell range extension (CRE) bias. Another stochastic geometry analysis is presented in [32] where EE for different CRE bias, BS density, and LPS power parameters are presented. Compared to LPS, ABS does not transmit data for a group sub-frames, so a certain level of BS EC is potentially saved as shown in [33].

Beyond the analysis, optimization modelling is an important task for ensuring service quality of ABS technique. A joint optimization of RA and ABS ratio is presented in [34] where a utility function comprised of macro and pico user bit-rate is maximized. User association and ABS configuration are optimized for maximum EE and maximum

throughput of the user with the worst service in [35, 36]. A more extensive optimization problem that maximizes EE with respect to user association, ABS ratio, RA, and macro power allocation is introduced and solved in [37] where the original non-convex mixed integer problem is decomposed into 4 sub-problems. For LPS, numerical results of maximized EE by user grouping thresholds and sub-frame configuration are presented in [38].

All referred works present theoretical analysis and parameter optimization problems distinctly for the wireless networks. Considering stochastic geometry and optimization together, an optimization model is proposed in [39] for multi-antenna BS's. In this work, the optimal number of active users is derived as a ratio of number of antennas. Both area spectral efficiency (ASE) and network EC are optimized for the number of users, number of antennas, and BS density jointly. The minimum number of macro ABS's is derived to satisfy the service quality of the users with the worst capacity in [40], where the capacity is derived for irregularly deployed BS's by the stochastic geometry under round-robin scheduler assumption. Consideration of irregular BS deployment promises more realistic solutions. A more practical parameter optimization problem is proposed in [41], where the BS's are irregularly distributed and their locations are known prior to the optimization.

1.1.2. Non-Orthogonal Multiple Access (NOMA)

While dense deployment of heterogeneous networks provides better spectral efficiency by more frequent reuse of the frequency resource blocks (RB's), the spectral efficiency of the network can still be enhanced by the choice of multiple access technique. By the introduction of NOMA to heterogeneous networks, different kinds of non-orthogonal signals can co-exist in the same spectrum bands due to further increase spectral efficiency. As stated in [42], there are two alternative prominent NOMA types, power-domain and code-domain. The system model of this thesis includes the power-domain NOMA where the non-orthogonal signals of more than one user are transmitted in the same RB by different power levels.

The superposition coding in NOMA provides opportunity for a more flexible RA than conventional OMA. This flexibility allows the engineers to provide more sophisticated approaches to general cellular network problems. While the design problems such as RA, multiple input multiple output (MIMO), coordinated multi-point (CoMP), or ICIC become more complex in NOMA, new design problems such as power allocation and user pairing are introduced to the literature as shown in [43].

Power allocation and user pairing are important design aspects, which significantly contribute to the performance of NOMA. The allocation problem with power minimization objective is shown to be NP-hard in [44], where an algorithm is proposed to solve the problem after relaxation. A closed-form solution of power allocation for maximum sum-rate is given in [45] with respect to the quality of service (QoS) requirements of the users. In addition to the maximization the sum-rate, fairness of user capacities is another important criterion. A detailed evaluation of power allocation for maximum sum-rate and fairness is presented in [46]. To illustrate the theoretical limits of NOMA, a rule is introduced in [47] that defines the number of users to satisfy minimum bit-rate requirements of users. Moreover, a MIMO system is proposed in [48] where intra-cell interference is minimized by pre-equalization of the power levels. User pairing is another important design problem that affects the performance vitally. The optimal pairing for maximum sum-rate is shown to be pairing the nearest and the furthest users together in [49]. However, the choice of pairing and power allocation algorithms affects each other's performance, so they are usually considered together, as done in [50] for weighted sum-rate. With an optimization perspective, a power minimization and scheduling problem is formulated and solved in [51] for multi-band and multi-user wireless environment.

Beyond the link level, system level analysis also has a significance to better evaluate the characteristics of the NOMA wireless environment. An early work [52] presents closed-form results for outage probability and ergodic capacity with channel approximation for irregularly distributed users. Stochastic geometry analysis is presented in [53] where both instantaneous and averaged signal to interference and noise ratio

(SINR) based user ordering methods are covered and a feasible power allocation algorithm is proposed. In [54], coverage probability and ergodic capacity is analyzed under heterogeneous network interference. Another work provides the stochastic geometry analysis of a two tier network [55], which includes multi-antenna macro cells and NOMA small cells. The authors of [56] address this power allocation problem and propose a solution based on a cooperation scheme that meets the desired signal to interference ratio (SIR). Moreover, different multi-cell downlink cooperation schemes are proposed in [57] without providing extensive theoretical background. However, to the best of our knowledge, the literature still lacks interference coordination schemes suitable for NOMA networks. Energy and spectral efficiency of NOMA in heterogeneous networks are presented in [58], where the other design problems such as MIMO, cognitive radio, device-to-device, cooperation, etc. are discussed for a NOMA system. Another use case of NOMA is analyzed in [59], where the re-configurable intelligent surfaces are shown to alter SIC demodulation order by improved user performance. However, the system level performance is highly dependent on the power levels and the pairing strategy as in the link level.

Inter-cell interference should be included to the signal model of NOMA for a more realistic system level analysis. However, the inclusion of inter-cell interference complicates NOMA design by improving the variety of interference types experienced by the users. Some complicated design problems such as user clustering, BS selection for silencing are discussed in [60]. By including inter-cell interference to the system model, algorithms are proposed for distributed clustering/power allocation and centralized frequency allocation in [61]. A femto-cell network where the users are served by NOMA on cognitive radio with guaranteed QoS definitions is presented in [62]. In this work, transmit power optimization problem to optimize femto-BS sum-rate is proposed along with a pairing method. For interference mitigation, user selection and pre-coding methods are proposed in [63], where intra-cell interference is eliminated and inter-cell interference leakage suppressed. A earlier work [64] presents edge and average user performance improvements by simulation of FFR method on a NOMA network. Moreover, a stochastic geometry model which models interference suppres-

sion as Bernolli random variable is presented in [65]. In this model, aerial/terrestrial users, minimum distance or maximum SINR based user association, and directional antennas are included to extend the analysis.

Even though NOMA provides better sum-rates with a more flexible spectrum usage, the usage of NOMA and OMA together is also desirable to benefit from the advantages of both spectrum access techniques. Hybrid use of NOMA and OMA is discussed as a research challenge in [66], where the user pairs with high channel state information (CSI) difference are considered as being suitable for NOMA. Users are grouped as either NOMA or OMA users in the pairing phase in [67], where the proposed algorithm adjusts pairing and modulation coding scheme (MCS) together. Besides, the capability of users can be limited in a practical environment. In [68], a practical algorithm is proposed for the optimization of user selection, power allocation, and MCS where receivers of the users differ as OMA and NOMA with varying SIC levels. However, inter-cell interference may be an important factor for the selection of the multiple access scheme. In [69], the size of NOMA cluster is limited and edge users are served by CoMP to increase their performance. A previously referred work [53] also assumes edge users should be served with OMA and considers them out of its scope. Therefore, the employment of OMA along with NOMA to increase the edge user performance still requires a deeper examination.

For uplink NOMA, the spectrum efficiency relies on diversity gain in SIC receiver of the BS. For most of the literature, the superposed uplink NOMA signals of users are decoded by the order of their received powers [70]. However, this scheme is found to be sub-optimal regarding user bit-rate demands [71]. Simply put, the firstly decoded signal suffers from interference of others and decoding low bit-rate user first may be optimal on some instances. Therefore, the channel and bit-rate demand of users affect the optimal decoding order together. In [71], a hybrid decoding order method between channel and bit-rate demand based ordering schemes is introduced along with explanatory discussion on the subject. If grant-based and grant-free users' signals are considered in the same RB, only one of them can have bit-rate requirement. In such

scenario, decoding order is selected by a threshold, which is the function of grant-based user's channel, is proposed in [72]. This ordering method is further improved in [73] by adjusting grant-free user's power to reduce interference on grant-based user. For joint optimization of transmit power and decoding order, a deep neural network algorithm is proposed to maximize number of users with satisfied QoS requirement in [74]. Similarly, decoding order is optimized under energy constraints in [75] by maximizing user fairness. Another work for maximization of fairness is presented in [76] where the optimal solution is obtained by proposed algorithm. A closed-form solution is presented for optimal decoding order in [77] by a simple rule including both user channels and bit-rate demands.

1.1.3. Energy Efficiency

The literature contains a great variety of methods to increase the EE of cellular networks, which are summarized in [78]. One common approach to reduce the EC of the wireless network is adjust some of the cells to sleep mode when the network is less active. A case study where femto BS's are switching to fixed time sleeping in user inactivity is presented in [79], where the results for actual wait duration for users are shown. A stochastic geometry analysis for sleeping BS's is presented in [80] for a heterogeneous network, where macro BS power control is evaluated for compensation of coverage holes due to sleeping lower tier BS's. Beside sleep mode in calm hours, power control and RA promises potential energy saving for a wireless network. With this regard, a power saving optimization is presented by [81] for antenna adaptation, power control, and discontinuous transmission.

Energy-aware design for heterogeneous networks is generally considered with two metrics, spectral and energy efficiencies. Spectral efficiency measures the amount of data traffic per unit of spectrum bandwidth, while EE measures the amount of data traffic per unit of energy consumed by the network. The maximization of EE is usually considered together with the spectral efficiency to evaluate actual service quality. One such problem is modelled and solved in [22] for transmit power and RA first for a

single BS and then generalized to multi-cell homogeneous networks with the help of stochastic geometry. Compared to the single cell solution, the analysis of a multi-cell environment is more practical as the interference effect is included. The BS deployment density is also an important factor, which has a slight effect on EC and bit-rate. In [82], Pareto optimal operational region of a heterogeneous network is presented by deployment density for maximum spectral and EE. The analytical results indicate that a low amount of degradation in spectral efficiency (around %4), achieves maximum EE. An alternative approach for energy efficient design is the minimization of EC. In [83], EC minimization of a heterogeneous network is studied with deployment density and transmit power optimization parameters under coverage probability constraint. While minimizing the EC, it is critical to employ a signal related constraint, such as the coverage probability, to ensure QoS. Especially in heterogeneous networks, inter-tier interference (included in [82, 83]) has vital effect on the received signal at the user. A practical ICIC problem is presented for optimization of EE in [84], by adding the number of dominant interferers as a new parameter into utility function. As the size of dominant interferer set gets higher, more BS's are silenced to decrease the interference and less energy is consumed. Energy and spectral efficiency of FFR methods are analyzed in [85] for the hexagonal BS deployment.

1.2. Research Motivation and Contributions

Heterogeneous networks maintain their importance from 4G to later generations, because of their practical use [86]. Beside proposing solutions to engineering problems, this thesis contains theoretical analysis for different heterogeneous wireless environments to reveal the feasibility of the commonly used solutions and the performance trade-offs. However, theoretically modeling signals coming from different kinds of BS's is not a straight-forward task. To cope with this problem, theoretical results are derived for randomly located BS's and users by the help of stochastic geometry [87, 88]. All of the numerical results in Chapters 3, 4, 5, and 7 are obtained by calculating mathematical expressions, instead of Monte-Carlo simulations. In following sub-sections, the motivations and the contributions are summarized for different topics.

1.2.1. Energy Efficient ICIC

Conventional ICIC techniques include either idling or adjusting transmit power for some part of the RB's. These changes in spectrum usage results in changed EC of BS's. By the parameterized EC model of BS's in [33], maximum transmit power and RB usage percentage have affect on BS EC. Moreover, the densification of the BS deployment increases EC of the network by increasing number of BS per unit area. Hence, a system level analysis of a heterogeneous network, employing ICIC, is required to indicate the potential bit-rate gains with the cost of network level EC. The analysis is also beneficial to obtain plausible design parameters for ICIC. ICIC design parameters are dependent on the network, whose every alternative deployment is taken into account by stochastic geometry analysis. Therefore, stochastic geometry provides suitable framework to obtain the optimal design parameters for a given BS densities with regard of every instance of irregular deployments. In this thesis, we combine stochastic geometry and maximization of EE objective by ICIC design parameters. For energy efficient ICIC design, following contributions are presented in later chapters.

- For homogeneous networks of macro BS's, a stochastic geometry based capacity analysis and parameter optimization framework are presented in Chapter 3. The analysis includes capacity derivations for single BS and the worst-region, where the users experience the worst signal quality due to their distance to serving and interfering BS's. The capacity derivations utilize the coverage probability results from [20]. Moreover, the EE constrained optimization problems are formulated by using the capacity derivations. EC of BS's are taken into account for EE concern. Two parameter optimization problems are presented with the objectives of maximizing base station capacity and minimizing EC. Beside providing the optimal values to design parameters, the results indicate that optimally allocated RB's result into a more energy efficient network, compared to adjusting only the transmit power.
- For heterogeneous networks, the literature on the suppression of inter-tier interference is mostly about analysis or optimization of ABS implementation on macro

BS's ([30–32, 34–38, 40, 89]). However, 3GPP standards define use cases for ABS implementation in both macro and pico BS's [26]. Chapter 4 presents stochastic geometry analysis for a two tier heterogeneous network where the potential energy saving gains by macro and pico tier BS's are indicated. The system model also includes CRE bias to show its effect on the ABS implementation. By extending the system model to both open and closed access, this chapter provides insight on meeting service requirements of a worst-region user and AEC with comparison between the access types.

- After the presentation of a stochastic geometry analysis for two tier heterogeneous network, an optimization problem with maximization of the derived EE objective is presented with the worst-region user capacity and AEC constraints in Chapter 4. The derived EE objective includes ASE, which is based on ergodic capacity derivations by stochastic geometry, and AEC, which includes BS power consumption models and deployment densities. Unlike similar studies [22, 32, 35–37], this optimization model includes actual BS EC model for more practical evaluation of network operation expenditure. Moreover, randomly located BS assumption in the derivation of ASE metric provides opportunity to use a more realistic model as shown in [90].
- The numerical results in Chapter 4 indicate valuable insight on the heterogeneous network with ABS. For certain system configuration and constraints, the results provide design guidelines whether to utilize macro ABS, pico ABS, or no ABS for a heterogeneous network. In general, the implementation of macro ABS provides better EE, while the implementation of pico ABS provides more flexibility to meet the worst-user constraints. Compared with the open access, satisfying the constraints in closed access networks is observed to be more difficult, where macro ABS has more vital impact on the performance. Moreover, the performance of optimal ABS under different CRE bias is observed for macro and pico ABS implementation. The results provide an intuition for CRE bias value choice, where some values provide numerically optimal points.

1.2.2. Interference Mitigation for NOMA

Employing NOMA in heterogeneous networks complicates the downlink interference model. The user signal is superposed with three types of distorting signals; inter-tier, intra-tier, and intra-cell interference. The statistical behavior of these interference signals is dependent on the channel conditions, the deployment positions, access type of the network, multiple access method, and many other aspects. For an extended modeling for these aspects, the performance of the user is analyzed with the help of stochastic geometry. When an ICIC function is employed, statistical behavior of interference also changes as some part of it is suppressed. Most of the existing work in the literature [60–63, 65] either discusses the potential benefits of ICIC or covers it with very simple model as an auxiliary functionality to their original objectives. One early work [64] presents simulations for coexistence of FFR with NOMA. However, the literature still lacks of detailed analysis of complicated interference model of NOMA deployed heterogeneous network and the numerically obtained outcomes for already discussed ICIC alternatives [60]. In this thesis, we present stochastic geometry analysis for NOMA deployed heterogeneous network. The detailed contributions as analysis and interference mitigation techniques for NOMA are listed below.

- A stochastic geometry based coverage analysis of NOMA and FFR coexistence is presented in Chapter 5. The analysis include coexistence of NOMA with strict FFR and SFR techniques in open and closed access heterogeneous network of K tier of base stations. The purpose of strict FFR and SFR is to lower intra-tier and inter-tier interference and provide a better service to the users who are closer to the edges of the serving BS coverage. Our analysis results reveal that FFR techniques provide certain level of coverage probability increase to edge users of NOMA by improving their signal quality. Besides, NOMA with strict FFR outperforms NOMA with SFR as the BS deployment density of the network increases.
- A similar stochastic geometry analysis is also presented for a 2-tier heterogeneous network in 6 including open and closed access alternatives. Beside access

type, the stochastic geometry analysis in Chapter 6 includes power level optimization and user pairing for NOMA in order to present more realistic performance comparison. Two power level optimization methods for the maximization of sum-rate and fairness are presented. For power optimization, the literature offers a variety of solutions, but few works include power level optimization along with stochastic geometry analysis. In [56], power levels of users are optimized for maximum throughput using the stochastic geometry analysis outcomes. In contrast, stochastic geometry based comparison of optimal sum-rate and fairness is presented together. For pairing part, two generic pairing methods are included from literature; near-to-near (NN) [58] and near-to-far (NF) [49] pairing. A stochastic geometry based comparison for these pairing methods is presented for user-specific and system level performance values.

- A hybrid multiple access model, where NOMA and OMA serve in the same spectrum band for interference mitigation, is presented in Chapter 6. In power-domain NOMA, the distant users treat the paired near user's signal as intra-cell interference [43]. In the proposed hybrid model by serving edge users with OMA, intra-cell interference is avoided in the edge user's signal which results in a performance improvement. The performance of the hybrid model is evaluated using the stochastic geometry analysis tools. The analysis covers power optimization and pairing for NOMA users to provide a fair comparison of hybrid usage to conventional NOMA. The numerical results indicate that the hybrid model provides good performance for BS sum-rate and edge user capacity together, while conventional NOMA can achieve the best performance in only one of those metrics.

1.2.3. Uplink Decode Order Optimization

In uplink NOMA, intra-cell interference is the dominant interference among the all of the interference types. As SIC receiver is deployed in BS, intra-cell interference is experienced in only first decoded users's signal in the sequence of decoding. Therefore, the choice of the decoding order in BS also selects the user whose signal will be decoded under intra-cell interference. The literature contains various works [71–75, 77], where

the decoding order is selected by the received signal power and bit-rate requirements of the users. However, the user devices are expected to vary in power capabilities in a practical system. Among paired users, if the user with the worst channel power will be firstly decoded under intra-cell interference, its transmit power should be above a certain level to ensure its bit-rate demand. This contradicts with low EC KPI for uplink NOMA in [16]. Therefore, decoding low channel power user first is feasible under certain conditions of its bit-rate demand and power budget together.

- The relationship between decoding order and bit-rate and power constraints of the users is investigated in Chapter 7. Firstly, a joint optimization problem of the decoding order and transmit powers for users with different bit-rate demand and power constraint is solved. Comparing to the existing work in the literature, different power capabilities of the devices are included in the optimization problem. By the solution to this problem, thresholds on bit-rate and power constraints of the user is derived for the feasibility of switching decoding order.

1.3. Organization of Dissertation

The rest of the dissertation is organized as mentioned in this section. Chapter 2 presents a preliminary system model including signal models, user grouping probabilities, and EC model. Chapter 5 presents a stochastic geometry analysis for homogeneous network and energy efficient parameter optimization problems for FFR. Similarly, Chapter 4 presents a stochastic geometry analysis for heterogeneous network and energy efficient parameter optimization for ABS. In Chapter 5, coverage probability of strict FFR and SFR is shown for NOMA-employed heterogeneous networks. In Chapter 6, the performance of a proposed method, hybrid NOMA, is presented with extensive analysis of NOMA including power levels optimization and pairing. Chapter 7 shows a decode order optimization solution for uplink NOMA under user power constraints. Finally, conclusions and future directions for the dissertation is presented in Chapter 8.

2. GENERAL SYSTEM MODEL

This thesis presents a variation of interference mitigation techniques under different wireless environments. Before going into details of these techniques, this chapter presents a generalized system model for interference types and their mathematical formulations. Moreover, EC models for BS's and user equipment are also presented as reference to EE work of later chapters.

Most of the analytical work considers a heterogeneous network, where BS's with different coverage capacities are present. Figure 2.1 presents a wireless network consists of two base-station tiers. The user whose performance is analyzed is referred as *typical user*. In the illustrated topology, the typical user gets service from Pico BS. For downlink, the typical user experiences three types of interference, intra-tier interference from other pico BS's, inter-tier interference from macro BS's, and intra-cell interference from its own service BS.

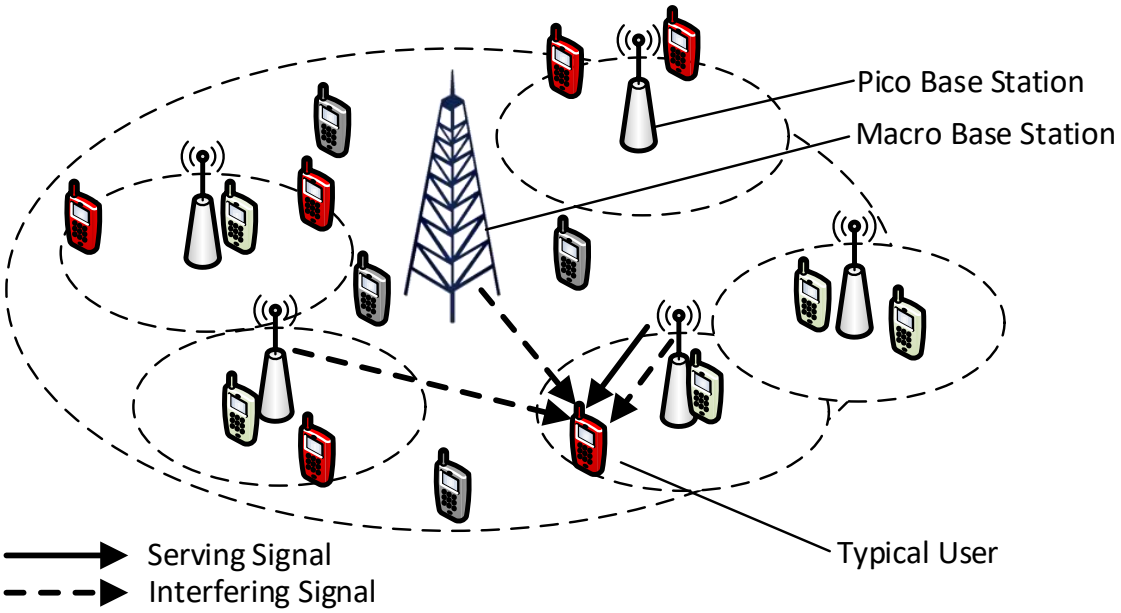

Figure 2.1. A topology of a 2-tier heterogeneous network.

2.1. Downlink Signal Model

The downlink performance of the users is mathematically analyzed by the stochastic geometry assumptions. These assumptions are required for mathematically modeling different types of interference. For the downlink analysis, the BS's are assumed to be randomly located as a Poisson point process (PPP) on an infinite 2D plane. The density of BS deployments is parameterized as λ_t with the unit of $1/m^2$. The t index is used for base-station tier, which takes values M and P for macro and pico tiers of 2-tier wireless network or takes $1, 2, \ldots, T$ values for T-tier wireless network. The typical user is assumed to be located at the origin of the 2D plane. The analysis of the typical user in this thesis is applicable to all users by Slivnyak's theorem [88].

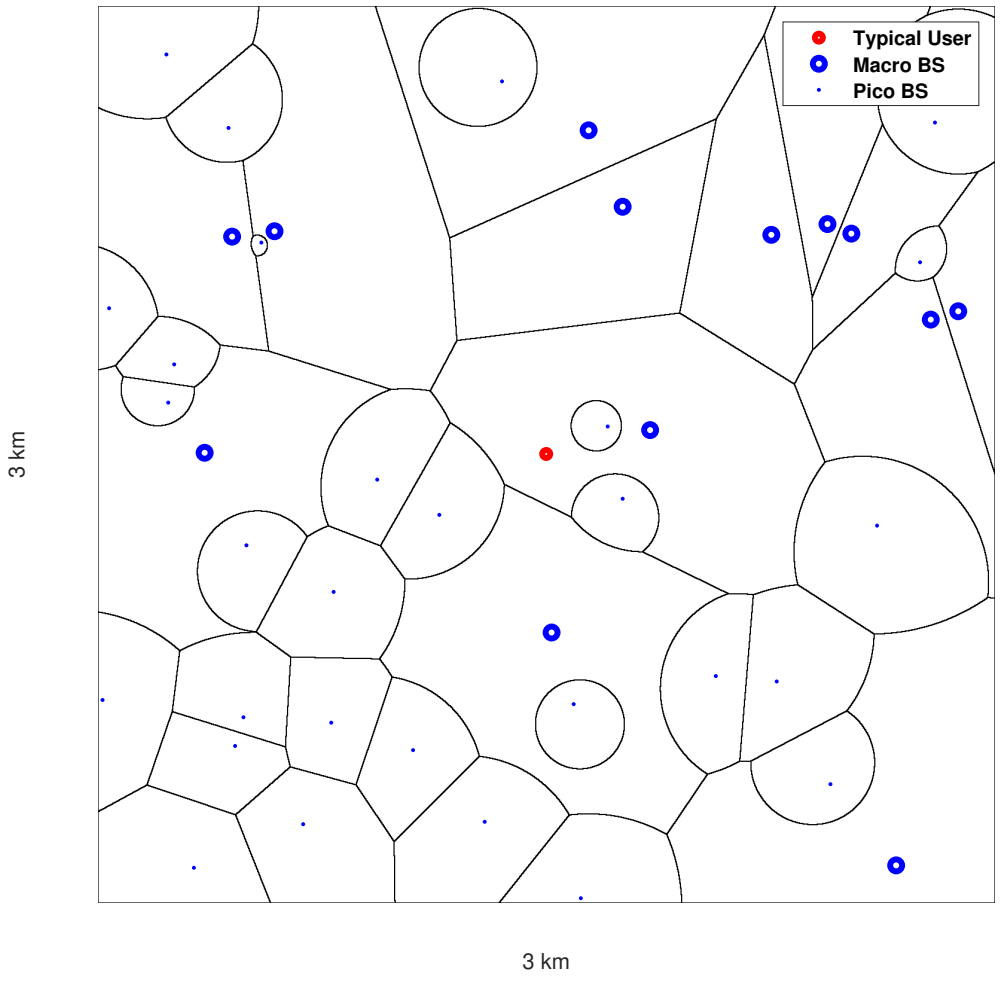

Figure 2.2. Voronoi diagram for a 2-tier heterogeneous network.

Figure 2.2 presents an example Voronoi diagram to illustrate coverage areas of randomly distributed BS's of a 2-tier heterogeneous network. By the randomness of the deployment, macro BS deployment can be so dense as in the north-east of the diagram or can be so sparse as in the south-west of the diagram. The diagram also shows the coverage in the sparse macro BS deployment regions are compensated with pico BS's. The typical user in the diagram gets service from the closest macro BS. This user is subject to interference from other macro BS's and all pico BS's.

Under these assumptions, a generalized SINR definition experienced by the typical user is given as

$$\Psi_t = \frac{P_t h r^{-\alpha}}{\sigma^2 + I_{t|t} + \sum\limits_{s \in \mathcal{I}(t)} I_{s|t} + I_{\text{NOMA}}}, \tag{2.1}$$

where Ψ_t is the instantaneous received SINR of a user of BS tier t, P_t is transmit power of tier t BS's, h is small-scale channel power gain, r is the euclidean distance between the user and serving BS, α is the pathloss exponent, and σ^2 is the noise power. The small-scale channel is assumed to be Rayleigh fading, because of its common use. Therefore, the channel power gain, h, is exponentially distributed. The rate parameter of h equals to 1. Moreover, the denominator of equation (2.1) contains the summation of received powers of three different types of interference signals. The definitions of different interference signals are presented in the following subsections.

2.1.1. Intra-tier Interference

Intra-tier interference is the superposition of the interfering signals coming from the BS's, which are in the same tier with the serving BS. The received power of intra-tier interference is given as

$$I_{t|t} = \sum_{r_i > q_{t|t}} P_t h_i r_i^{-\alpha}, \tag{2.2}$$

where $I_{t|t}$ is the total power of interference from tier t BS's, $q_{t|t}$ is the minimum distance between the typical user and the same tier interfering BS's, P_t is the transmit power of

interfering BS, h_i is the small-scale channel power for i-th interfering BS, and r_i is the distance from i-th interfering BS to the typical user. h_i is exponentially distributed, similar to h.

Equation (2.2) presents the summation of infinite number of interferers, which are distributed in 2D infinite plane with homogeneous PPP with the density of λ_t. The typical user is assumed to be getting service from the closest BS among all randomly distributed BS's. The interfering BS's of the same tier cannot be closer than the serving BS. Therefore, the interfering BS's are assumed to be randomly distributed outside a disc, which is centered to the typical user and has radios of r. In other words, the distance to interfering BS's, r_i, cannot be lower than the distance to serving BS, r. In equation (2.2), the minimum distance, $q_{t|t}$, takes value as $q_{t|t} = r$ for intra-tier interference.

2.1.2. Inter-tier Interference

Inter-tier interference is the superposition of signal coming from the BS's of other tiers. The received power of inter-tier interference is given as

$$\sum_{s\in\mathcal{I}(t)} I_{s|t} = \sum_{s\in\mathcal{I}(t)} \sum_{r_i>q_{s|t}} P_s h_i r_i^{-\alpha}, \tag{2.3}$$

where $I_{s|t}$ is the total power of interference from tier s to the user of tier t, $\mathcal{I}(t)$ is the set of tiers interfering to tier t users, and $q_{s|t}$ is the minimum distance between a user of tier t and interfering BS's of tier s. In contrast to intra-tier interference, $q_{s|t}$ value is determined regarding the method of BS tier selection by the user.

Equation (2.3) includes the summation of infinite number of interfering signals per BS tier. For 2-tier heterogeneous network, the set of interfering tiers is defined as $\mathcal{I}(\mathrm{P}) = \{\mathrm{M}\}$ or $\mathcal{I}(\mathrm{M}) = \{\mathrm{P}\}$. For T-tier heterogeneous network, the set of interfering tiers is defined as $\mathcal{I}(t) = \{s|s \neq t, s \in \{1, 2, \ldots, T\}\}$ where the interferer index s is an integer different than t.

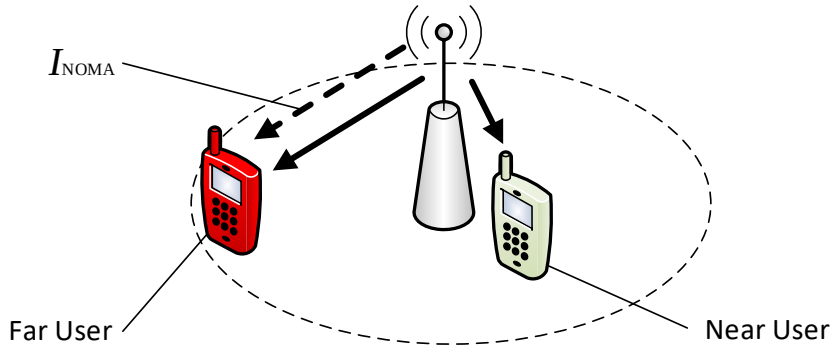

Figure 2.3. A BS serving two users with non-orthogonal signals.

2.1.3. Intra-cell Interference

Intra-cell interference is experienced by the user when NOMA is employed. In this thesis, power domain NOMA is employed where the non-orthogonal signals of paired users are scheduled to the same RB with different power levels. These paired users are named as *near* and *far* users. In most of the cases, BS serves to far user with higher transmit power, since its channel conditions are worse. SIC technique is employed in the receivers of these users [12]. By employing SIC, near user first decodes far user's signal, and then decodes its own signal by subtracting decoded signal of far user from the received signal. Far user treats near user's signal as noise. This additional noise is considered as intra-cell interference, I_{NOMA}, in this thesis. As illustrated in Figure 2.3, only far user experiences the intra-cell interference.

The transmit powers for near and far users' signals are formulated with a^{near} and a^{far} power coefficients, where they have unit sum, $a^{\text{near}} + a^{\text{far}} = 1$. The intra-cell interference experienced by far user is given as

$$I_{\text{NOMA}} = a^{\text{near}} P_t h r^{-\alpha}, \tag{2.4}$$

which is the received power of near user's signal by far user. Comparing to other interference types, intra-cell interference has the same channel and BS distance conditions with serving signal.

2.2. Uplink Signal Model

The source of uplink interference is caused by the other users, who transmits in the same RB with the typical user. Similar to downlink model, intra-cell interference is caused by other users of the same BS, intra-tier interference is caused by the users of other BS's of the same tier, and inter-tier interference is caused by the users of the BS's of other tiers. However, the interference coming from the users of other BS's is not affecting the uplink signal as much as downlink, since the users are only transmitting on their own allocated RB's [69]. With this regard, we include only intra-cell interference in uplink signal model in this thesis.

For this thesis, the number of scheduled uplink users to the same RB is limited to 2. The receiver of the BS employs SIC technique for uplink. The firstly decoded signal is subtracted from the received signal for decoding the other user's signal. When the signal of user i is decoded prior to the signal of user j, their respective received SINRs in BS are given as

$$\Phi_i^{i\to j} = \frac{p_i g_i}{\sigma^2 + p_j g_j}, \qquad \Phi_j^{i\to j} = \frac{p_j g_j}{\sigma^2}, \tag{2.5}$$

where p_i and p_j are respective uplink transmit powers of user i and j, g_i and g_j are respective uplink channel powers of i and j including pathloss and small-scale fading. In equation (2.5), only first decoded user i experiences intra-cell experience, which is in the denominator as $p_j g_j$. Therefore, the selection of the decode order changes the user, who experiences the inter-cell interference.

2.3. Selection of Base Station Tier

Two types of access methods, which are open and closed access [26] are covered in analysis. In open access, the user can connect to any BS tier depending on the received power measurements. In the closed access, the serving tier is already pre-configured for the user. In practice, open access environments include pico and micro cells, while closed access environments include femto cells. For this thesis, BS tiers are referred by

macro and pico for 2-tier network or by t index for T-tier network, regardless of tiers being open or closed access.

In open access networks, the user measures the average reference signal received powers (RSRP) from all the neighboring BS's as shown in [91]. After the average RSRP values are measured, the user compares and selects the best as serving BS. The mathematical derivations in this section utilizes the formulation from [92]. Mathematical formulations are separately presented for T-tier and 2-tier networks in following sub-sections.

2.3.1. T-tier Network

For the open access tier selection, the average RSRP of BS tier t, measured by the user, is given as

$$P_t r_t^{-\alpha}, \tag{2.6}$$

where r_t is the distance of the user to the closest BS of tier t. The user selects the highest average RSRP after measuring all BS tiers. In [92], the probability of selecting tier t is given as

$$\mathfrak{p}_t = \frac{\lambda_t P_t^{2/\alpha}}{\sum_{s=1}^{T} \lambda_s P_s^{2/\alpha}} \tag{2.7}$$

for open access networks. For closed access networks, the tier selection probability equals to 1 for pre-selected tier. For both access types, the probability density function (PDF) of the distance to serving BS is given as

$$f_{r_t}(r) = \begin{cases} \frac{2\pi\lambda_t r}{\Pr(t)} \exp\left(-\pi r^2 \sum_{s=1}^{T} \lambda_s \left(\frac{P_s}{P_t}\right)^{2/\alpha}\right), & \text{open access,} \\ 2\pi\lambda_t r \exp\left(-\lambda_t \pi r^2\right), & \text{closed access.} \end{cases} \tag{2.8}$$

The minimum distance of the user of tier t to interfering BS's of tier s is given as

$$q_{s|t} = \begin{cases} r_t, & t = s, \\ \left(\frac{P_s}{P_t}\right)^{\frac{1}{\alpha}} r_t, & t \neq s \text{ and open access}, \\ 0, & t \neq s \text{ and closed access}. \end{cases} \tag{2.9}$$

As the closed access user selects always the same tier, the distance to interfering BS's of other tiers are not lower bounded. This property of closed access networks improves severity of inter-tier interference, since interfering BS's can located so close to the user.

2.3.2. 2-tier Network

Tier selection for 2-tier heterogeneous networks contains extra parameter of tier selection bias, $\mathfrak{b}$ and presented with a simpler formulation. By including $\mathfrak{b}$, the user connects to one of the BS tiers with the following criteria

$$P_{\mathrm{M}} r_{\mathrm{M}}^{-\alpha} \underset{\text{Macro}}{\overset{\text{Pico}}{\lessgtr}} \mathfrak{b} P_{\mathrm{P}} r_{\mathrm{P}}^{-\alpha}, \tag{2.10}$$

where P_{M} and P_{P} are respective transmit powers of macro and pico BS's, r_{M} and r_{P} are the distances to the closest macro and pico BS's, respectively. $\mathfrak{b}$ parameter is introduced to tier selection method to enhance general system capacity by CRE property in the pico cells.

By the randomness of r_{M} and r_{P} in equation (2.10), respective tier selection probabilities of a user are given as

$$\begin{aligned} \mathfrak{p}_{\mathrm{M}} &= \frac{\lambda_M}{\lambda_M + \lambda_P z_{\mathrm{PM}}}, \\ \mathfrak{p}_{\mathrm{P}} &= \frac{\lambda_P}{\lambda_P + \lambda_M z_{\mathrm{MP}}}, \end{aligned} \tag{2.11}$$

where z_{MP} and z_{PM} are tier coefficients depending on the access method [92]. These coefficients are defined as

$$(z_{\mathrm{PM}}, z_{\mathrm{MP}}) = \begin{cases} \left(\left(\frac{\mathfrak{b}P_{\mathrm{P}}}{P_{\mathrm{M}}}\right)^{2/\alpha}, \left(\frac{P_{\mathrm{M}}}{\mathfrak{b}P_{\mathrm{P}}}\right)^{2/\alpha}\right), & \text{open access}, \\ (0,0), & \text{closed access}. \end{cases} \tag{2.12}$$

As the BS's are distributed according to homogeneous PPP, the PDF of the distance

between the user and the serving BS is given as

$$\begin{aligned} f_{\mathrm{M}}(r) &= 2\pi r\left(\lambda_M + \lambda_P z_{\mathrm{PM}}\right) e^{-\pi r^2(\lambda_M+\lambda_P z_{\mathrm{PM}})}, \\ f_{\mathrm{P}}(r) &= 2\pi r\left(\lambda_P + \lambda_M z_{\mathrm{MP}}\right) e^{-\pi r^2(\lambda_P+\lambda_M z_{\mathrm{MP}})} \end{aligned} \tag{2.13}$$

for the macro and pico BS's, respectively [92]. Therefore, the minimum distances of pico interfering BS to macro user and macro interfering BS to pico user are given as

$$\begin{aligned} q_{P|M} &= \sqrt{z_{\mathrm{MP}}} r_M, \\ q_{M|P} &= \sqrt{z_{\mathrm{PM}}} r_P. \end{aligned} \tag{2.14}$$

2.4. Selection of Interior or Edge User Groups

In this thesis, all of the presented interference mitigation methods require user grouping as interior and edge to differentiate the service of the users which are closer to the edge of coverage boundaries. The grouping decision is made by the average RSRP or SINR measurements to qualify the signal quality of the user. While grouping decision by average RSRP is generally used for user grouping in practice [93], grouping decision by SINR provides better performance [20]. In the following sub-section, the grouping probabilities for two approaches are presented.

2.4.1. Decision by Reference Signal Received Power (RSRP)

As the serving BS obtains the average RSRP measurement of the user, the user is decided to be interior or edge by a threshold comparison as

$$P_t r_t^{-\alpha} \underset{\text{Interior}}{\overset{\text{Edge}}{\lessgtr}} \gamma_t, \tag{2.15}$$

where γ_t is threshold to group tier t users as edge or interior. t index becomes M or P for 2-tier network or takes an integer value for T-tier network.

For 2-tier network, the probability of getting service as an edge user can be expressed as the tail probability of equation (2.13) depending on the criteria in equa-

tion (2.15) and is given as

$$\begin{aligned} \mathcal{P}_{\mathrm{M}}^{\mathrm{E}} &= e^{-\pi\left(\frac{P_{\mathrm{M}}}{\gamma_{\mathrm{M}}}\right)^{\frac{2}{\alpha}}(\lambda_M+\lambda_P z_{\mathrm{PM}})}, \\ \mathcal{P}_{\mathrm{P}}^{\mathrm{E}} &= e^{-\pi\left(\frac{P_{\mathrm{P}}}{\gamma_{\mathrm{P}}}\right)^{\frac{2}{\alpha}}(\lambda_P+\lambda_M z_{\mathrm{MP}})} \end{aligned} \tag{2.16}$$

for macro and pico users, respectively. For t-tier network, the probability of getting service as an edge user is derived by the tail probability of equation (2.8) as

$$\mathcal{P}_t^{\mathrm{E}} = \begin{cases} e^{-\pi \sum\limits_{s=1}^{T} \lambda_s \left(\frac{P_s}{\gamma_t}\right)^{2/\alpha}}, & \text{open access,} \\ e^{-\pi\lambda_t\left(\frac{P_t}{\gamma_t}\right)^{2/\alpha}}, & \text{closed access.} \end{cases} \tag{2.17}$$

2.4.2. Decision by Signal to Interference and Noise Ratio (SINR)

For the SINR-based grouping decision, the measured received SINR of the user is compared with threshold as

$$\Psi_t \underset{\text{Interior}}{\overset{\text{Edge}}{\lessgtr}} \gamma_t. \tag{2.18}$$

Interference mitigation techniques suppresses interference components in equation (2.1), so changes the SINR definition. The compared definition, Ψ_t, differs for different interference mitigation techniques. Hence, the edge user selection probability is given in a generalized form as

$$\mathcal{P}_t^{\mathrm{E}} = 1 - \Pr(\Psi_t > \gamma_t) = 1 - \kappa_t(\gamma_t), \tag{2.19}$$

where $\kappa_t(\cdot)$ is the coverage probability of tier t.

2.5. Selection of Non-Orthogonal Signal Power Level

When NOMA is employed, the users can be scheduled to the same RB's with different non-orthogonal signals. Considering the users served in the same RB, far users are served with higher signal power level than near users ($a^{\mathrm{far}} > a^{\mathrm{near}}$). In this thesis, two different approaches are employed for the selection of near and far users.

2.5.1. RSRP-based

RSRP-based near/far user selection is similarly defined as RSRP-based interior/edge user grouping in Section 2.4.1. Measured average RSRP values is compared with a threshold as

$$P_t r_t^{-\alpha} \underset{\text{Near}}{\overset{\text{Far}}{\lessgtr}} \varphi_t, \tag{2.20}$$

where φ_t is power level selection threshold for tier t. As the average RSRP is lower than φ_t, the user is considered to be distant to the serving BS. The probability of selecting a user as far user is given as

$$\mathfrak{P}_t = \begin{cases} e^{-\pi \sum_{s=1}^{T} \lambda_s \left(\frac{P_s}{\varphi_t}\right)^{2/\alpha}}, & \text{open access,} \\ e^{-\pi \lambda_t \left(\frac{P_t}{\varphi_t}\right)^{2/\alpha}}, & \text{closed access,} \end{cases} \tag{2.21}$$

which is obtained similar to equation (2.17).

2.5.2. SINR-based

For SINR-based power level selection, the mathematical model is extended to cover signal conditions of all users differently. The BS is assumed to be gathering all received SINR measurements from the users. The users are ordered by their SINR values. By this SINR order, the user with lower index has higher SINR measurement ($i < j \Rightarrow \Psi_i > \Psi_j$). For each RB, the near and far users are selected by a pairing method considering the SINR order of the users. The pairing methods are presented by pairing sets, which is defined as

$$\mathbb{P}(n) = \{(i,j) | i,j \in \{1,2,\ldots,n\}\}, \tag{2.22}$$

where the argument n is the number of users. The pairing set, $\mathbb{P}(n)$, consists of $\frac{n}{2}$ integer pairs, where each pair represents scheduled near and far user to a RB. For an example of $n = 50$ users, having pair $(2, 49)$ in $\mathbb{P}(n)$ means that the users 2 and 49 are scheduled to the same RB.

2.6. Energy Consumption

Macro and pico BS EC amounts differ due to their coverage capabilities. A linear EC model is adapted by the parameterized model in [33]. For simplicity, the adapted model assumes that the BS's transmit by single antenna with 10MHz bandwidth. For the efficiency calculation of power amplifier of macro BS's, the maximal output of power amplifier is assumed as 80 Watts, while maximum transmit power is 40 Watts. Based on these assumptions, hourly EC of a macro BS is given as

$$\mathrm{EC}'_{\mathrm{M}} = \mu_{\mathrm{M}}^{\mathrm{const}} + P_{\mathrm{M}} \left(\mu_{\mathrm{M}}^{\Delta \mathrm{P}} + \mu_{\mathrm{M}}^{\Delta \mathrm{N}} \mathcal{X} \right), \tag{2.23}$$

where P_{M} is the transmit power macro BS, $\mathcal{X}$ is active load ratio, and $\mu_{\mathrm{M}}^{\mathrm{const}}$, $\mu_{\mathrm{M}}^{\Delta \mathrm{P}}$, $\mu_{\mathrm{M}}^{\Delta \mathrm{N}}$ values are constants. The unit in equation (2.23) is $Watt \times h$. The constants in this model include power consumption of base-band processing, radio frequency small signal transceiver, power amplifier gain, power loss of DC-DC converter, main supply, cooling, and feeder cable. In this work, we neglect non-linearity of the power amplifier by taking its gain constant for $P_{\mathrm{M}} = 40$, which causes very small deviation on EC values. For the analysis on heterogeneous network, a more simplified model is employed. Simplified EC models for macro and pico BS's are respectively given as

$$\mathrm{EC}_{\mathrm{M}} = \mu_{\mathrm{M}}^{\mathrm{const}} + \mu_{\mathrm{M}}^{\Delta} P_{\mathrm{M}} \mathcal{X}, \tag{2.24}$$

$$\mathrm{EC}_{\mathrm{P}} = \mu_{\mathrm{P}}^{\mathrm{const}} + \mu_{\mathrm{P}}^{\Delta} P_{\mathrm{P}} \mathcal{X}, \tag{2.25}$$

where the maximum and minimum values of EC is ensured to be the same with equation (2.23). The values for constants and factors are presented in Table 2.1. The analysis of heterogeneous networks includes a more general metric, which defines network EC per unit environment area. This metric is called AEC and it is defined as

$$\mathrm{AEC} = \lambda_M \mathrm{EC}_{\mathrm{M}} + \lambda_P \mathrm{EC}_{\mathrm{P}} \tag{2.26}$$

with unit of $Watt \times h/m^2$.

Table 2.1. BS EC model constants and factors.

Parameters	$\mu_{\mathrm{M}}^{\mathrm{const}}$	$\mu_{\mathrm{P}}^{\mathrm{const}}$	$\mu_{\mathrm{M}}^{\Delta}$	$\mu_{\mathrm{M}}^{\Delta \mathrm{P}}$	$\mu_{\mathrm{M}}^{\Delta \mathrm{N}}$	$\mu_{\mathrm{P}}^{\Delta}$
Values	55.8361	6.4205	8.6275	4.4275	4.200	15.4340

2.7. Conclusion

The generalized system model in this chapter includes preliminary definitions for latter chapters. Each chapter contains its own system model section which is extension from the SINR definitions in this chapter. Furthermore, tier selection and user grouping related probabilities are introduced to be used in stochastic geometry analysis. Finally, two alternative BS EC models are presented.

3. ENERGY EFFICIENT FRACTIONAL FREQUENCY REUSE

Conventional ICIC techniques improve edge user performance by idling RB's or adjusting transmit power of the signals serving to a group of users. These improvements in the spectrum usage changes in EC of the BS. Design of ICIC techniques in EC constraint potentially provide network level energy saving and decrease in operating expenses. Strict FFR is commonly used ICIC technique, which includes idling some part of the RB's with a reuse factor to prevent interference to the edge users of neighboring BS's. In this chapter, we present derivations on macro BS and the worst region capacity for strict FFR technique with the help of stochastic geometry techniques. By utilizing these derivations, two optimization problems are presented to obtain the best design parameters for strict FFR for different BS densities and EC constraints.

The rest of the chapter is organized as follows. The stochastic geometry model and strict FFR method are presented in Section 3.1. Then, the capacity analysis is presented in Section 3.2 and the parameter optimization problems are presented in Section 3.3. The numerical results of optimized strict FFR system is presented in Section 3.4 and conclusions are presented in Section 3.5.

3.1. System Model

3.1.1. Base Station Deployment

Each Macro BS location is assumed to follow independent and identical uniform distribution on an infinite 2D plane. Therefore, the BS locations are distributed by a homogeneous PPP, with macro BS density of λ_{M} $(1/m^2)$. The users are assumed to be connected to the closest BS by the Euclidean distance. For all of the analysis, the typical user is centered in the origin of 2D plane. All of the BS's are randomly deployed according to their PPP and the typical user is connected to the one that is

closest to the origin.

The SINR of the typical user, used as the principal metric in the analytical derivations, is given as

$$\Psi_{\mathrm{M}} = \frac{P_{\mathrm{M}} h r^{-\alpha}}{\sigma^2 + \sum\limits_{r_i > q_{\mathrm{M|M}}} P_{\mathrm{M}} h_i r_i^{-\alpha}}, \tag{3.1}$$

where r and r_i are the distances of the serving and i-th interfering BS's to the typical user, h and h_i are channel gain powers of the received signals of serving and i-th interfering BS's, $q_{\mathrm{M|M}}$ is the minimum distance to interfering BS's, P_{M} is transmit power of macro BS, α is pathloss exponent, and σ^2 is the noise power. By homogeneous PPP, there is only intra-tier interference, so $q_{\mathrm{M|M}}$ equals to r as shown in Section 2.1.1. In this model, all channel gains and distances are assumed to be random. The channels of serving and interfering BS's are assumed to be Rayleigh fading. Hence, the channel gain powers, h and h_i, are exponentially distributed where rate parameter equals to 1.

3.1.2. Fractional Frequency Reuse

FFR approaches are based on grouping the users as edge and interior. In this chapter, the users are grouped by their SINR measurements as in Section 2.4.2 by

$$\Psi_{\mathrm{M}}^{\mathrm{I}} \underset{\text{Edge}}{\overset{\text{Interior}}{\gtrless}} \gamma_{\mathrm{M}}, \tag{3.2}$$

which is based on instantaneous SINR of an interior RB ($\Psi_{\mathrm{M}}^{\mathrm{I}}$). We only consider $\Psi_{\mathrm{M}}^{\mathrm{I}}$ for user grouping as the definition of $\Psi_{\mathrm{M}}^{\mathrm{E}}$ differs for different FFR techniques. The user grouping threshold, γ_{M}, is one of the important design parameters for all FFR techniques. For discriminating the interior and edge user services, the available RB's are divided into groups depending on reuse factor Δ, as shown in Figure 3.1.

Strict FFR is widely used FFR technique that is based on frequency reuse for edge users by suppressing some of the RB's to increase edge performance. As presented in Figure 3.1, the spectrum is divided into $\Delta + 1$ frequency groups. Beside the reuse

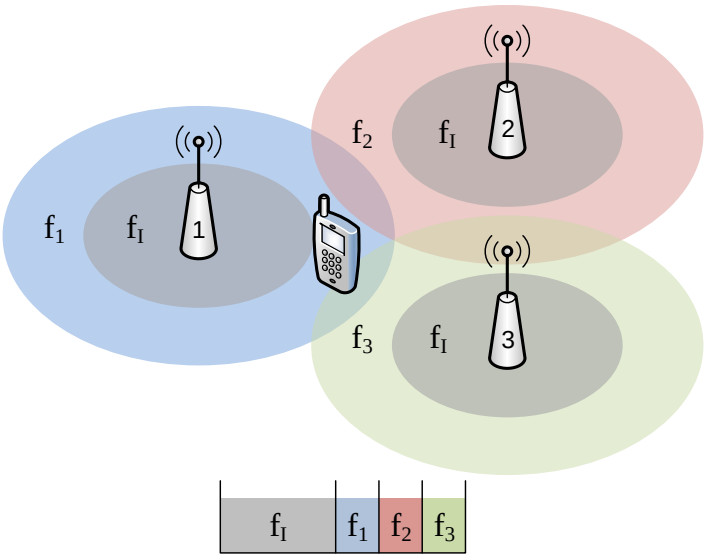

Figure 3.1. Frequency assignment of strict FFR technique ($\Delta = 3$).

factor Δ, a special design parameter of strict FFR is $\mathrm{F_I}$, which is the number of RB's in the interior frequency group $|\mathrm{f_I}| = \mathrm{F_I}$. For the edge users, frequency reuse is deployed by Δ groups $(\mathrm{f}_j; 1, 2, \ldots, \Delta)$. Each edge frequency group is comprises $|\mathrm{f}_j| = \frac{\mathrm{F}-\mathrm{F_I}}{\Delta}$ RB's where F is total number of RB's. For frequency reuse of edge users, each BS has been assigned to transmit at one of the f_j RB sets for edge users. The SINR for interior and edge users for strict FFR technique are

$$\begin{aligned} \Psi_{\mathrm{M}}^{\mathrm{I}} &= \frac{P_{\mathrm{M}} h r^{-\alpha}}{\sigma^2 + \sum\limits_{r_i > r} P_{\mathrm{M}} h_i r_i^{-\alpha}}, \\ \Psi_{\mathrm{M}}^{\mathrm{E}} &= \frac{P_{\mathrm{M}} h r^{-\alpha}}{\sigma^2 + \sum\limits_{r_i > r} P_{\mathrm{M}} h_i r_i^{-\alpha} \delta_i}, \end{aligned} \tag{3.3}$$

where δ_i is a Bernoulli random variable which becomes 1 with probability $1/\Delta$. δ_i random variable indicates that i-th interfering BS uses the same edge frequency group f_j with the serving BS.

3.2. Capacity Analysis

3.2.1. Average Total Capacity

Average total capacity is defined as average capacity of a BS with regard of its own coverage. This metric is also explained as the average capacity of a single user

which is the only user getting service from BS. Therefore, the average total capacity is defined as

$$\mathbb{C}_{\text{M.BS}} = \left(\frac{\text{F} - \text{F}_\text{I}}{\Delta}\right) \mathcal{B}_{\text{RB}} S_{\text{M}}^{\text{E}} + \text{F}_\text{I} \mathcal{B}_{\text{RB}} S_{\text{M}}^{\text{I}}, \tag{3.4}$$

where

$$\begin{aligned} S_{\text{M}}^{\text{E}} &= \text{E}\left[\ln(1+\Psi_{\text{M}}^{\text{E}}) | \Psi_{\text{M}}^{\text{I}} < \gamma_{\text{M}}\right] \Pr\left(\Psi_{\text{M}}^{\text{I}} < \gamma_{\text{M}}\right), \\ S_{\text{M}}^{\text{I}} &= \text{E}\left[\ln(1+\Psi_{\text{M}}^{\text{I}}) | \Psi_{\text{M}}^{\text{I}} > \gamma_{\text{M}}\right] \Pr\left(\Psi_{\text{M}}^{\text{I}} > \gamma_{\text{M}}\right). \end{aligned} \tag{3.5}$$

As each user is either interior or edge, the average total capacity comprises total capacity of all attached edge and interior users of the BS. $\frac{\text{F}-\text{F}_\text{I}}{\Delta}$ and F_I are the total number of RB's that are assigned to edge and interior users, respectively. $\mathcal{B}_{\text{RB}}$ denotes the conversion factor for the capacity of 1 RB, such that $\mathcal{B}_{\text{RB}} = \log_2(e) \times [180 \times 10^3 \text{ Hertz}] \cong 259.7 \times 10^3$ for long-term evolution (LTE) networks. S_{M}^{E} and S_{M}^{I} are the partial components of average total capacity for edge and interior users, respectively. Both are defined as the multiplication of the conditional capacity and the user grouping probability.

The capacity values is derived by making use of a relationship between expected value and tail probability in this chapter. As defined in [94], expected value of non-negative random variables can be obtained by its tail probability. Hence, the relationship between coverage probability of Ψ and expected value of capacity is

$$\text{E}\left[\ln\left(1+\Psi\right)\right] = \int_0^\infty \Pr(\Psi > e^t - 1) dt = \int_0^\infty \frac{\Pr(\Psi > \tau)}{\tau + 1} d\tau. \tag{3.6}$$

By the help of relationship in equation (3.6), the edge capacity component of total capacity becomes

$$\begin{aligned} S_{\text{M}}^{\text{E}} &= \text{E}\left[\ln\left(1+\Psi_{\text{M}}^{\text{E}}\right) | \Psi_{\text{M}}^{\text{I}} < \gamma_{\text{M}}\right] \Pr\left(\Psi_{\text{M}}^{\text{I}} < \gamma_{\text{M}}\right) \\ &= \int_0^\infty \frac{\Pr\left(\Psi_{\text{M}}^{\text{E}} > \tau | \Psi_{\text{M}}^{\text{I}} < \gamma_{\text{M}}\right)}{\tau+1} d\tau P\left(\Psi_{\text{M}}^{\text{I}} < \gamma_{\text{M}}\right) \\ &= \int_0^\infty \frac{\Pr\left(\Psi_{\text{M}}^{\text{E}} > \tau, \Psi_{\text{M}}^{\text{I}} < \gamma_{\text{M}}\right)}{\tau+1} d\tau \end{aligned} \tag{3.7}$$

$$= \int_0^{\infty} \frac{\Pr\left(\Psi_{\mathrm{M}}^{\mathrm{E}}>\tau\right)-\Pr\left(\Psi_{\mathrm{M}}^{\mathrm{E}}>\tau,\Psi_{\mathrm{M}}^{\mathrm{I}}>\gamma_{\mathrm{M}}\right)}{\tau+1} d\tau \ ,$$

where the second line is obtained by inserting the relationship from equation (3.6) and the third line is obtained by extending $\Pr\left(\Psi_{\mathrm{M}}^{\mathrm{E}} > \tau | \Psi_{\mathrm{M}}^{\mathrm{I}} < \gamma_{\mathrm{M}}\right)$ with Bayes' rule. By inserting already defined coverage probabilities $\Pr\left(\Psi_{\mathrm{M}}^{\mathrm{E}} > \tau\right)$ and $\Pr\left(\Psi_{\mathrm{M}}^{\mathrm{E}} > \tau, \Psi_{\mathrm{M}}^{\mathrm{I}} > \gamma_{\mathrm{M}}\right)$ from [20], $S_{\mathrm{M}}^{\mathrm{E}}$ is obtained as

$$\begin{aligned} S_{\mathrm{M}}^{\mathrm{E}} &= \pi\lambda \int_0^{\infty}\int_0^{\infty} \frac{1}{\tau+1} \mathrm{e}^{-\frac{u^{\alpha/2}\sigma^2\tau}{P_{\mathrm{M}}} - \pi\lambda u\left(1+\frac{1}{\Delta}\rho(\tau)\right)} du d\tau \\ &\quad -\pi\lambda \int_0^{\infty}\int_0^{\infty} \frac{1}{\tau+1} \mathrm{e}^{-\frac{u^{\alpha/2}\sigma^2}{P_{\mathrm{M}}}(\tau+\gamma_{\mathrm{M}}) - \pi\lambda u\left(1+\frac{1}{\Delta}\xi(\tau,\gamma_{\mathrm{M}})+\frac{\Delta-1}{\Delta}\rho_1(\gamma_{\mathrm{M}})\right)} du d\tau \ , \end{aligned} \tag{3.8}$$

where

$$\rho_x(y) = \int_x^{\infty} \frac{1}{1+\frac{v^{\alpha/2}}{y}} dv \tag{3.9}$$

and

$$\xi(x,y) = \int_1^{\infty} \left[1 - \frac{1}{1+xv^{-\frac{\alpha}{2}}} \frac{1}{1+yv^{-\frac{\alpha}{2}}}\right] dv. \tag{3.10}$$

By following similar steps, interior capacity part $S_{\mathrm{M}}^{\mathrm{I}}$ of $\mathbb{C}_{\mathrm{M.BS}}$ becomes

$$\begin{aligned} S_{\mathrm{M}}^{\mathrm{I}} &= \mathrm{E}\left[\ln(1+\Psi_{\mathrm{M}}^{\mathrm{I}}) | \Psi_{\mathrm{M}}^{\mathrm{I}} > \gamma_{\mathrm{M}}\right] \Pr\left(\Psi_{\mathrm{M}}^{\mathrm{I}} > \gamma_{\mathrm{M}}\right) \\ &= \int_0^{\infty} \frac{\Pr\left(\Psi_{\mathrm{M}}^{\mathrm{I}}>\tau | \Psi_{\mathrm{M}}^{\mathrm{I}}>\gamma_{\mathrm{M}}\right)}{\tau+1} d\tau \Pr\left(\Psi_{\mathrm{M}}^{\mathrm{I}} > \gamma_{\mathrm{M}}\right) = \int_0^{\infty} \frac{\Pr\left(\Psi_{\mathrm{M}}^{\mathrm{I}}>\tau,\Psi_{\mathrm{M}}^{\mathrm{I}}>\gamma_{\mathrm{M}}\right)}{\tau+1} d\tau \\ &= \int_{\gamma_{\mathrm{M}}}^{\infty} \frac{\Pr\left(\Psi_{\mathrm{M}}^{\mathrm{I}}>\tau\right)}{\tau+1} d\tau + \int_0^{\gamma_{\mathrm{M}}} \frac{\Pr\left(\Psi_{\mathrm{M}}^{\mathrm{I}}>\gamma_{\mathrm{M}}\right)}{\tau+1} d\tau \\ &= \int_{\gamma_{\mathrm{M}}}^{\infty} \frac{\Pr\left(\Psi_{\mathrm{M}}^{\mathrm{I}}>\tau\right)}{\tau+1} d\tau + \Pr\left(\Psi_{\mathrm{M}}^{\mathrm{I}} > \gamma_{\mathrm{M}}\right) \ln\left(1+\gamma_{\mathrm{M}}\right) \ , \end{aligned} \tag{3.11}$$

where the third line is obtained by considering

$$\Pr\left(\Psi_{\mathrm{M}}^{\mathrm{I}} > \tau, \Psi_{\mathrm{M}}^{\mathrm{I}} > \gamma_{\mathrm{M}}\right) = \Pr\left(\Psi_{\mathrm{M}}^{\mathrm{I}} > \max\left\{\tau, \gamma_{\mathrm{M}}\right\}\right)$$

relationship. By inserting already defined probability $\Pr\left(\Psi_{\mathrm{M}}^{\mathrm{I}} > \tau\right)$ from [20], $S_{\mathrm{M}}^{\mathrm{I}}$ is

obtained as

$$\begin{aligned} S_{\mathrm{M}}^{\mathrm{I}} &= \pi\lambda \int_0^{\infty}\int_0^{\infty} \tfrac{1}{\tau+1} \mathrm{e}^{-\frac{u^{\alpha/2}\sigma^2\tau}{P_{\mathrm{M}}} - \pi\lambda u(1+\rho_1(\tau))} du d\tau \\ &\quad + \pi\lambda \int_{\gamma_{\mathrm{M}}}^{\infty} \mathrm{e}^{-\frac{u^{\alpha/2}\sigma^2\tau}{P_{\mathrm{M}}} - \pi\lambda u(1+\rho_1(\tau))} du \ln(1+\tau) \ , \end{aligned} \tag{3.12}$$

where $\rho_1(y)$ function is defined in equation (3.9).

3.2.2. Average Worst-Region Capacity

The maximization of the average total capacity alone provides high throughput while causing the users close to the coverage boundaries to get poor service quality. Therefore, the capacity analysis are extended with the coverage region that gets the worst service quality. The worst quality region is defined by Ψ_{M} being below a threshold, ω_{M}. In this chapter, the users in the worst quality region are assumed to be only edge users. By this assumption, ω_{M} threshold should be chosen as $\gamma_{\mathrm{M}} > \omega_{\mathrm{M}} > 0$. Before introducing $\Psi_{\mathrm{M}}^{\mathrm{E}}$ and $\Psi_{\mathrm{M}}^{\mathrm{I}}$, the average worst-region capacity of a macro BS is given as

$$\begin{aligned} \mathcal{C}_{\mathrm{M}}^{\mathrm{Worst}} &= \mathrm{E}\left[\ln(1+\Psi_{\mathrm{M}}) \,|\, \Psi_{\mathrm{M}} < \omega_{\mathrm{M}}\right] \\ &= \tfrac{1}{\Pr(\Psi_{\mathrm{M}}<\omega_{\mathrm{M}})} \int_0^{\omega_{\mathrm{M}}} \ln(1+x) f_{\Psi_{\mathrm{M}}}(x) dx \\ &= \tfrac{1}{\Pr(\Psi_{\mathrm{M}}<\omega_{\mathrm{M}})} \int_0^{\omega_{\mathrm{M}}} \int_0^{\ln(1+x)} f_{\Psi_{\mathrm{M}}}(x) dt dx \\ &= \tfrac{1}{\Pr(\Psi_{\mathrm{M}}<\omega_{\mathrm{M}})} \int_0^{\ln(1+\omega_{\mathrm{M}})} \int_{e^t-1}^{\omega_{\mathrm{M}}} f_{\Psi_{\mathrm{M}}}(x) dx dt \\ &= \tfrac{1}{\Pr(\Psi_{\mathrm{M}}<\omega_{\mathrm{M}})} \int_0^{\ln(1+\omega_{\mathrm{M}})} \left[\Pr\left(\Psi_{\mathrm{M}} < \omega_{\mathrm{M}}\right) - \Pr\left(\Psi_{\mathrm{M}} < e^t - 1\right)\right] dt \\ &= \ln(1+\omega_{\mathrm{M}}) - \tfrac{1}{\Pr(\Psi_{\mathrm{M}}<\omega_{\mathrm{M}})} \int_0^{\omega_{\mathrm{M}}} \tfrac{\Pr(\Psi_{\mathrm{M}}<\tau)}{\tau+1} d\tau. \end{aligned} \tag{3.13}$$

To introduce user grouping, the Ψ_{M} is considered to be covering both edge and interior users by their grouping probabilities with γ_{M} threshold. Namely, the CDF of Ψ_{M} is given as

$$\Pr\left(\Psi_{\mathrm{M}} < \omega_{\mathrm{M}}\right) = \Pr\left(\Psi_{\mathrm{M}}^{\mathrm{I}} < \omega_{\mathrm{M}} | \Psi_{\mathrm{M}}^{\mathrm{I}} > \gamma_{\mathrm{M}}\right) \Pr\left(\Psi_{\mathrm{M}}^{\mathrm{I}} > \gamma_{\mathrm{M}}\right) \tag{3.14}$$

$$
\begin{aligned}
&+ \Pr\left(\Psi_{\mathrm{M}}^{\mathrm{E}} < \omega_{\mathrm{M}} | \Psi_{\mathrm{M}}^{\mathrm{I}} < \gamma_{\mathrm{M}}\right) \Pr\left(\Psi_{\mathrm{M}}^{\mathrm{I}} < \gamma_{\mathrm{M}}\right) \\
= \quad & \Pr\left(\omega_{\mathrm{M}} > \Psi_{\mathrm{M}}^{\mathrm{I}} > \gamma_{\mathrm{M}}\right) + \Pr\left(\Psi_{\mathrm{M}}^{\mathrm{E}} < \omega_{\mathrm{M}}, \Psi_{\mathrm{M}}^{\mathrm{I}} < \gamma_{\mathrm{M}}\right) \\
= \quad & \Pr\left(\Psi_{\mathrm{M}}^{\mathrm{E}} < \omega_{\mathrm{M}}, \Psi_{\mathrm{M}}^{\mathrm{I}} < \gamma_{\mathrm{M}}\right) \ ,
\end{aligned}
$$

where the last step is obtained by the assumption $\omega_{\mathrm{M}} < \gamma_{\mathrm{M}}$. By the assumption, the replacement of $\Pr\left(\Psi_{\mathrm{M}} < \tau\right)$ with $\Pr\left(\Psi_{\mathrm{M}}^{\mathrm{E}} < \omega_{\mathrm{M}}, \Psi_{\mathrm{M}}^{\mathrm{I}} < \gamma_{\mathrm{M}}\right)$ in equation (3.13), the average capacity of the users in worst Ψ_{M} region is given as

$$
\mathrm{E}\left[\ln\left(1+\Psi_{\mathrm{M}}\right) | \Psi_{\mathrm{M}} < \omega_{\mathrm{M}}\right] \overset{\gamma_{\mathrm{M}} \geq \omega_{\mathrm{M}}}{=} \ln\left(1+\omega_{\mathrm{M}}\right) - \frac{1}{\Pr\left(\Psi_{\mathrm{M}}^{\mathrm{E}} < \omega_{\mathrm{M}}, \Psi_{\mathrm{M}}^{\mathrm{I}} < \gamma_{\mathrm{M}}\right)} \int_{0}^{\omega_{\mathrm{M}}} \frac{\Pr\left(\Psi_{\mathrm{M}}^{\mathrm{E}} < \tau, \Psi_{\mathrm{M}}^{\mathrm{I}} < \gamma_{\mathrm{M}}\right)}{\tau+1} d\tau, \tag{3.15}
$$

where $\Pr\left(\Psi_{\mathrm{M}}^{\mathrm{E}} < \omega_{\mathrm{M}}, \Psi_{\mathrm{M}}^{\mathrm{I}} < \gamma_{\mathrm{M}}\right)$ is numerically calculated by Bayes' rule as

$$
\begin{aligned}
&\Pr\left(\Psi_{\mathrm{M}}^{\mathrm{E}} < \omega_{\mathrm{M}}, \Psi_{\mathrm{M}}^{\mathrm{I}} < \gamma_{\mathrm{M}}\right) = \\
&\quad 1 - \Pr\left(\Psi_{\mathrm{M}}^{\mathrm{E}} > \omega_{\mathrm{M}}\right) - \Pr\left(\Psi_{\mathrm{M}}^{\mathrm{I}} > \gamma_{\mathrm{M}}\right) + \Pr\left(\Psi_{\mathrm{M}}^{\mathrm{E}} > \omega_{\mathrm{M}}, \Psi_{\mathrm{M}}^{\mathrm{I}} > \gamma_{\mathrm{M}}\right).
\end{aligned} \tag{3.16}
$$

The definitions of $\Pr\left(\Psi_{\mathrm{M}}^{\mathrm{E}} > \omega_{\mathrm{M}}\right)$, $\Pr\left(\Psi_{\mathrm{M}}^{\mathrm{I}} > \gamma_{\mathrm{M}}\right)$, $\Pr\left(\Psi_{\mathrm{M}}^{\mathrm{E}} > \omega_{\mathrm{M}}, \Psi_{\mathrm{M}}^{\mathrm{I}} > \gamma_{\mathrm{M}}\right)$ are present in [20].

For the performance analysis, ω_{M} parameter may be hard to define due to lack of knowledge about the tail distribution of the Ψ_{M}. As an alternative, a worst region probability p_{worst}, is used to define a more consistent worst service quality region. For further analysis, $\mathcal{C}_{\mathrm{M}}^{\mathrm{Worst}}$ metric is always used with the worst-region probability p_{worst}. The p_{worst} parameter is introduced to formulation by replacing ω_{M} constant in equation (3.15) with the inverse of the CDF of the Ψ_{M}, which is given as

$$
\mathcal{F}_{\Psi_{\mathrm{M}}^{\mathrm{E}}, \Psi_{\mathrm{M}}^{\mathrm{I}}}(\tau) \overset{\gamma_{\mathrm{M}} \geq \omega_{\mathrm{M}}}{=} \Pr\left(\Psi_{\mathrm{M}}^{\mathrm{E}} < \tau, \Psi_{\mathrm{M}}^{\mathrm{I}} < \gamma_{\mathrm{M}}\right). \tag{3.17}
$$

The inverse of $\mathcal{F}_{\Psi_{\mathrm{M}}^{\mathrm{E}}, \Psi_{\mathrm{M}}^{\mathrm{I}}}(\tau)$ function may not have a close-form solution, but it is invertible numerically due to its strictly monotone increasing behavior. The previously stated assumption $\gamma_{\mathrm{M}} > \omega_{\mathrm{M}}$ is updated to

$$
\Pr\left(\Psi_{\mathrm{M}}^{\mathrm{I}} < \gamma_{\mathrm{M}}\right) > \Pr\left(\Psi_{\mathrm{M}}^{\mathrm{I}} < \omega_{\mathrm{M}}\right) = p_{\mathrm{worst}}. \tag{3.18}
$$

Therefore, for any p_{worst} value smaller than $\Pr\left(\Psi_{\mathrm{M}}^{\mathrm{I}} < \gamma_{\mathrm{M}}\right)$, the average capacity of the

worst quality region is given as

$$\begin{aligned}\mathcal{C}_{\mathrm{M}}^{\mathrm{Worst}} &= \mathrm{E}\left[\ln\left(1+\Psi_{\mathrm{M}}\right)|\Psi_{\mathrm{M}} < \mathcal{F}^{-1}_{\Psi_{\mathrm{M}}^{\mathrm{E}},\Psi_{\mathrm{M}}^{\mathrm{I}}}\left(p_{\mathrm{worst}}\right)\right] \\ &= \ln\left(1+\mathcal{F}^{-1}_{\Psi_{\mathrm{M}}^{\mathrm{E}},\Psi_{\mathrm{M}}^{\mathrm{I}}}\left(p_{\mathrm{worst}}\right)\right) - \frac{1}{p_{\mathrm{worst}}}\int_{0}^{\mathcal{F}^{-1}_{\Psi_{\mathrm{M}}^{\mathrm{E}},\Psi_{\mathrm{M}}^{\mathrm{I}}}(p_{\mathrm{worst}})} \frac{\mathcal{F}_{\Psi_{\mathrm{M}}^{\mathrm{E}},\Psi_{\mathrm{M}}^{\mathrm{I}}}(\tau)}{\tau+1}d\tau.\end{aligned} \tag{3.19}$$

3.3. Parameter Optimization

Regarding analytical results on the capacity by stochastic geometry, it is imperative to define a FFR parameter optimization problem that includes probabilistic behavior of the environment. The general scope of the earlier works on FFR is to provide fair performance to the users which are close to the cell boundary. Therefore, an FFR parameter optimization problem has to include minimum capacity constraint for the worst service quality region of the coverage.

Strict FFR has three important design parameters that have effect on capacity and EC; number of interior users $\mathrm{F_I}$, user grouping threshold γ_{M}, and transmit power P_{M}. Considering these parameters, two different optimization problems are defined to achieve EE. The first problem depends on the maximization of average total capacity such that

$$\max_{\mathrm{F_I},\gamma_{\mathrm{M}},P_{\mathrm{M}}} \ \mathrm{F_I}S_{\mathrm{M}}^{\mathrm{I}} + \tfrac{\mathrm{F}-\mathrm{F_I}}{\Delta}S_{\mathrm{M}}^{\mathrm{E}} \tag{3.20a}$$

$$\text{subject to } \epsilon_{3.1} \leq \tfrac{\mathrm{F}-\mathrm{F_I}}{\Delta}\mathcal{B}_{\mathrm{RB}}\mathcal{C}_{\mathrm{M}}^{\mathrm{Worst}} \tag{3.20b}$$

$$\epsilon_{3.2} \geq \mu_{\mathrm{M}}^{\mathrm{const}} + P_{\mathrm{M}}\left(\mu_{\mathrm{M}}^{\Delta\mathrm{P}} + \tfrac{\mu_{\mathrm{M}}^{\Delta\mathrm{N}}}{\mathrm{F}}\left(\mathrm{F_I} + \tfrac{\mathrm{F}-\mathrm{F_I}}{\Delta}\right)\right) \tag{3.20c}$$

$$\mathrm{F} \geq \mathrm{F_I} \geq 0 \tag{3.20d}$$

$$\gamma_{\mathrm{M}} \geq \gamma_{\mathrm{min}} \tag{3.20e}$$

$$P_{\mathrm{M}}^{\mathrm{max}} \geq P_{\mathrm{M}} \geq 0 \ , \tag{3.20f}$$

where $\epsilon_{3.1}$ is the minimum average capacity of worst-region (bits/sec) and $\epsilon_{3.2}$ is maximum EC of one BS ($Watt{\times}h$). Constraint (3.20b) is a condition on non-linear function, the worst-region capacity, and Constraint (3.20c) is based on the EC model in

equation (2.23). While integrating EC model, the spectrum usage of Strict FFR, $\frac{1}{\mathrm{F}}\left(\mathrm{F_I}+\frac{\mathrm{F}-\mathrm{F_I}}{\Delta}\right)$, is inserted into $\mathcal{X}$ value. In this problem, parameter $\mathrm{F_I}$ is assumed to be continuous instead of discrete for simplification. Another simplification is done by introducing a minimum value to γ_{M} as $\gamma_{\min}$. This minimum value is chosen as $\gamma_{\min}=\omega_{\mathrm{M}}$ where $p_{\mathrm{worst}}=P\left(\Psi_{\mathrm{M}}^{\mathrm{I}}<\omega_{\mathrm{M}}\right)$.

The second parameter optimization problem of Strict FFR is an alteration of Problem (3.20). Swapping the EC and average total capacity measures, the second problem focuses on minimization of EC, while average total capacity is maintained over a level such that

$$\min_{\mathrm{F_I},\gamma_{\mathrm{M}},P_{\mathrm{M}}} \; P_{\mathrm{M}}\left(\mu_{\mathrm{M}}^{\Delta\mathrm{P}}+\frac{\mu_{\mathrm{M}}^{\Delta\mathrm{N}}}{\mathrm{F}}\left(\mathrm{F_I}+\frac{\mathrm{F}-\mathrm{F_I}}{\Delta}\right)\right) \tag{3.21a}$$

$$\text{subject to } \epsilon_{3.1}\leq\frac{\mathrm{F}-\mathrm{F_I}}{\Delta}\mathcal{B}_{\mathrm{RB}}\mathcal{C}_{\mathrm{M}}^{\mathrm{Worst}} \tag{3.21b}$$

$$\epsilon_{3.3}\leq\mathrm{F_I}\mathcal{B}_{\mathrm{RB}}S_{\mathrm{M}}^{\mathrm{I}}+\frac{\mathrm{F}-\mathrm{F_I}}{\Delta}\mathcal{B}_{\mathrm{RB}}S_{\mathrm{M}}^{\mathrm{E}} \tag{3.21c}$$

$$\mathrm{F}\geq\mathrm{F_I}\geq 0 \tag{3.21d}$$

$$\gamma_{\mathrm{M}}\geq\gamma_{\min} \tag{3.21e}$$

$$P_{\mathrm{M}}^{\max}\geq P_{\mathrm{M}}\geq 0\ , \tag{3.21f}$$

where $\epsilon_{3.3}$ in this problem is minimum average total capacity (bits/sec).

3.4. Numerical Results

Most of the environment parameters of optimization are presented in Tables 2.1 and 3.1. Besides, for both problems, minimum average worst-case region capacity, $\epsilon_{3.1}$ is chosen 50 kbits/sec and number of total RB's, F, is chosen 50 (in LTE, F = 50 scenario is valid in 10 MHz downlink bandwidth). For both of the problems, we have used the non-linear constrained optimization problem solver in MATLAB. This solver makes use of a pre-optimized combination of the trust-region and inner point methods [95].

Figure 3.2 shows the optimization results of Problem (3.20) for varying maximum EC limits and BS densities. The first Figure 3.2(a) presents comparison of the

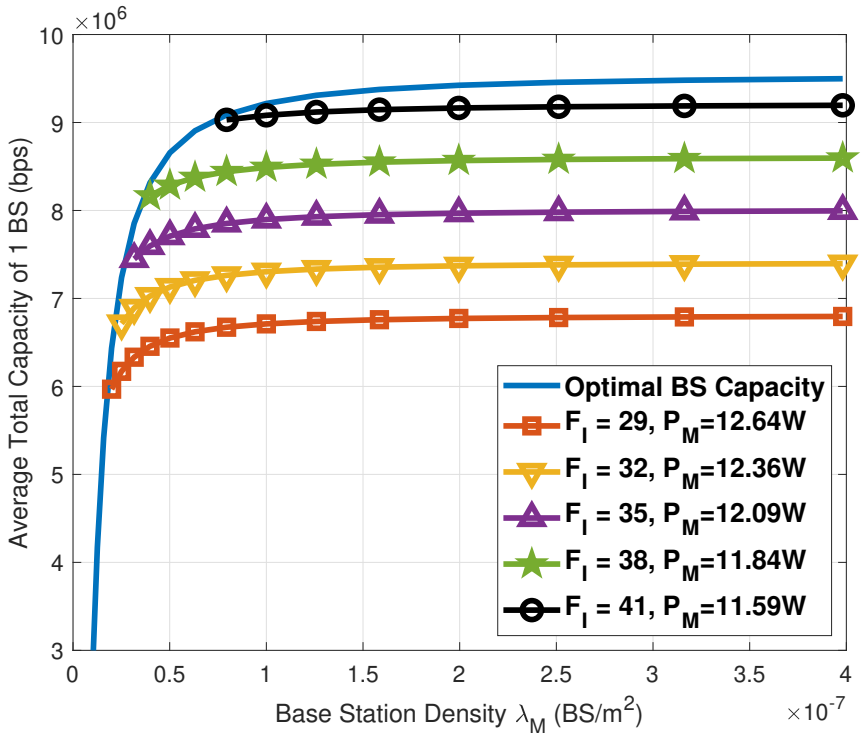

(a) Optimal vs. constant parameters for the same EC.

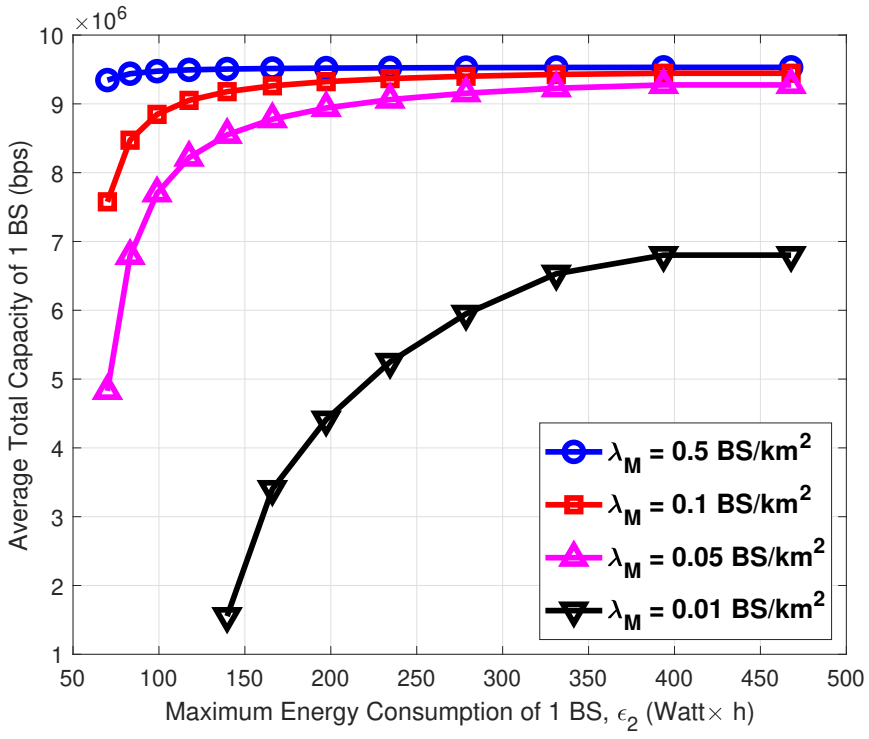

(b) All optimal parameters.

Figure 3.2. Numerical results for maximizing average total capacity by Problem (3.20).

Table 3.1. General parameters for numerical results.

Parameter	**Value**
α	3
σ^2	-100 dB
Δ	3
p_{worst}	0.05
F	50
$\epsilon_{3.1}$	50 kbits/sec

optimal and constant FFR parameters, where all of the BS's operate with fixed power consumption, 150 $Watt \times h$ ($\gamma_{\text{M}} = 0.2$). The curves of the constant parameters have interrupted where they cannot fulfill the worst-region constraint ($\epsilon_{3.1}$). Hence, the constant design parameter curves cannot provide higher worst-region capacity than $\epsilon_{3.1}$ for low BS densities. Moreover, average total capacity of the optimal parameters provides the upper bound to other possible outcomes. In Figure 3.2(b), there are four curves for four different BS densities. All of the curves converge as EC. From the analysis, F_I has direct linear relation to the total capacity. For lower values of EC, average total capacity is maximized by increasing F_I. From this relationship, we can conclude that optimization of RB's is more energy efficient than optimization of only transmit power of BS.

The Figure 3.3(a) presents comparison of EC for non-optimal FFR parameters and optimal FFR parameters by Problem (3.21). In the non-optimal curves, γ_{M} parameter equals to 0.2 and F_I parameters are calculated as integer to get closest average total capacity to 7 Mbit/sec. The EC of BS does not change drastically for different BS densities, while the optimal curve forms a lower bound of EC. As Problems (3.20) and (3.21) are optimized for the same environment parameter sets, F_I value similarly converges to the same level due to maintain worst-region average capacity constraint in Figure 3.3(b). As the objective of Problem (3.21) is to minimize EC, it is likely to lower F_I to decrease active number of RB's. Similar to the results of Problem (3.21), a joint

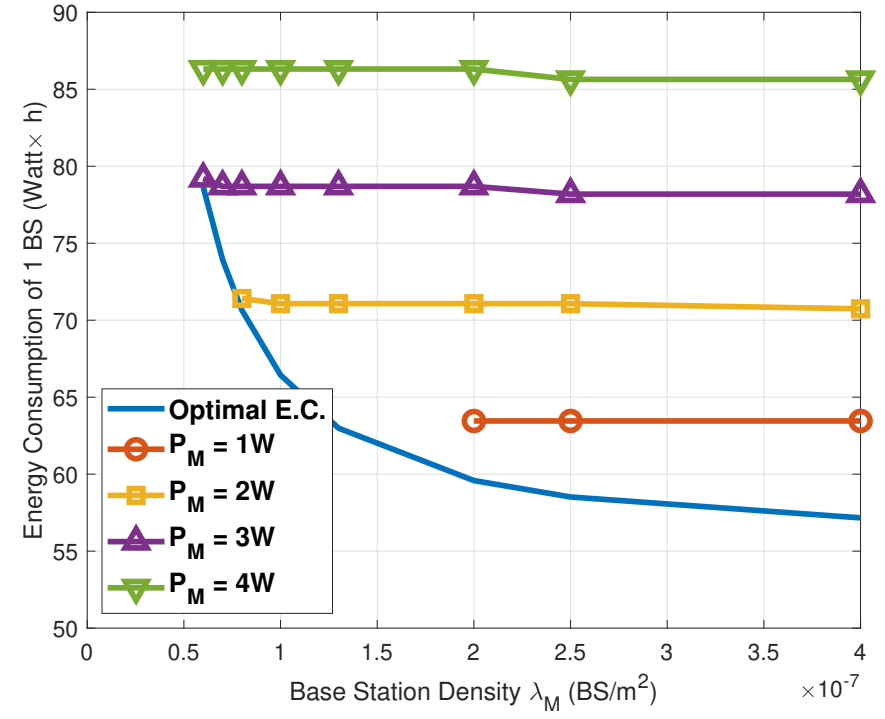

(a) Optimal vs. constant parameters for similar total capacity.

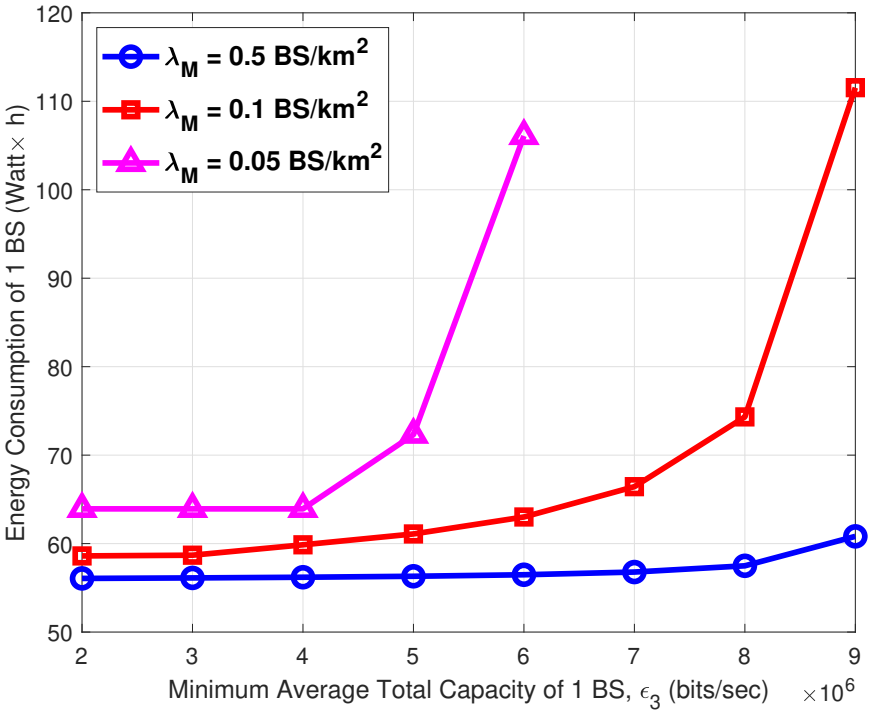

(b) All optimal parameters.

Figure 3.3. Numerical results for minimizing EC by Problem (3.21).

optimizer of transmit power and RB's firstly fulfills constraints with RB adjustments (parameter F_I), because it is more energy efficient.

3.5. Conclusion

In this chapter, we have considered on the stochastic geometry analysis and parameter optimization of one of the widely implemented methods; strict FFR. The stochastic geometry analysis of average total capacity and worst-region capacity have studied and two different parameter optimization problems are solved. The numerical results indicate that increasing transmit power provide slight capacity increase with high EC cost. However, well-optimized RB allocation promises decent capacity without causing much EC. Therefore, the results of this chapter indicates significance of RB allocation to provide EE.

4. ENERGY EFFICIENT ALMOST BLANK SUB-FRAME

Inter-tier interference has significant effect on the performance of the users in heterogeneous networks. Depending on the access type of the network, the BS's of the other tier can reside very close to the user and decrease the signal quality vitally. To avoid this problem, ABS method is standardized by 3GPP [26]. In ABS, a BS does not transmit data in certain sub-frames to decrease the interference to edge users of the other tiers. This sub-frame is called as almost blank, as the control related signals are still transmitted. When a BS deploys ABS, it's EC is also reduced for a certain level. Similar to the parameter optimization formulation in Chapter 3, the optimization of number of ABS's per BS tier with EE perspective promises network level energy saving. In this chapter, an analysis, including ASE and the worst-region capacity, is presented. By the derivations from this analysis, an optimization problem with EE objective for choice of ABS's per BS tier is modelled and a solving algorithm is proposed. The proposed algorithm finds whether it is feasible or not to deploy ABS for a BS tier and the optimal number of ABS's by network level constraints.

In the rest of the chapter, SINR definitions for ABS-deployed 2-tier heterogeneous network are presented in Section 4.1. ASE and the worst-region capacity models are presented in Section 4.2. The parameter optimization problem and solver algorithm are presented in Section 4.3. The numerical results are presented in Section 4.4 and the conclusion for the chapter is presented in Section 4.5.

4.1. System Model

A heterogeneous network environment containing two tiers of BS's, macro and pico tiers, is considered. The users are select the BS tier by their RSRP measurements. After the serving BS tier is selected, the serving BS groups the users as interior and edge users depending on their average RSRP measurements. As macro and pico users are further grouped into interior and edge categories, there are 4 different user types.

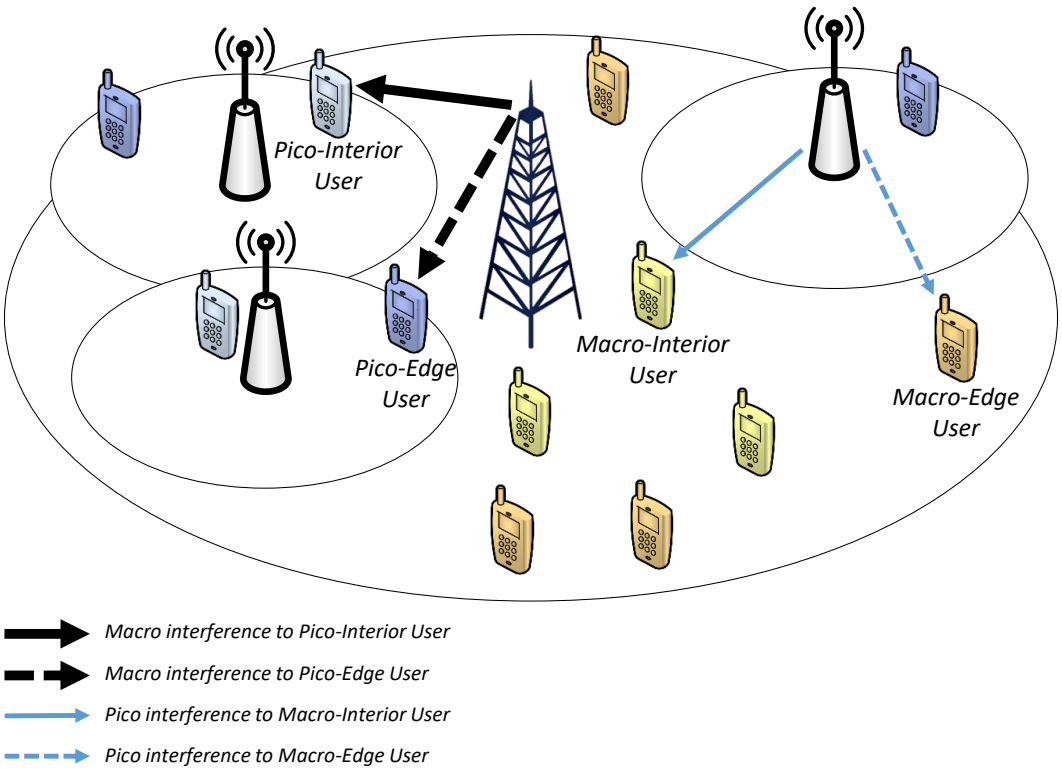

Figure 4.1. A network topology example for inter-tier interference.

The network topology with the specified user groups and inter-tier interference types is shown in Figure 4.1. As the users are grouped differently, the interference coming from the other tier is also illustrated differently (as straight and dashed lines). This chapter presents ABS method to minimize the interference experienced by the edge users, illustrated as dashed lines.

Before moving with the mathematical definitions and derivations, probabilistic definitions for BS tier selection is as presented in Section 2.3.2, interior and edge user grouping probabilities are as presented in Section 2.4.1, and the BS EC model is the simplified model presented in Section 2.6 for this chapter.

4.1.1. Almost Blank Sub-Frame

ABS technique reduces the inter-tier interference by suppressing data transmission in certain sub-frames. Figure 4.2 shows the macro and pico cell frame structure, where both tiers make use of the ABS's. k_M and k_P are respectively defined as the

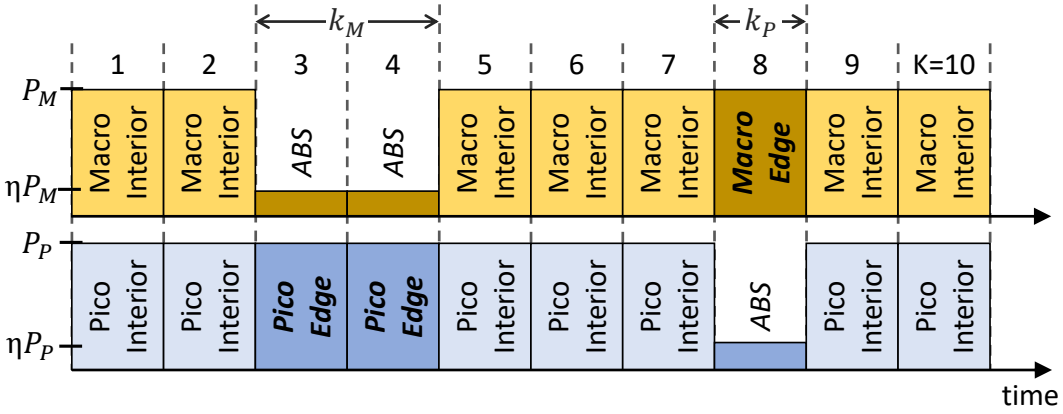

Figure 4.2. $K = 10$ frame structure and sub-frame transmission powers ($k_M = 2$ and $k_P = 1$).

numbers of ABS's in macro and pico tiers. As only the control and the reference signals are transmitted, ABS transmit power is reduced by a factor of η. Assuming that macro and pico BS's share their ABS occupation with each other, they schedule their edge users to the sub-frames corresponding to the other tiers ABS's.

We consider randomly located macro and pico BS's on an unbounded 2D plane with PPP having λ_M and λ_P $(1/\mathrm{m}^2)$ densities, respectively, while the typical user is assumed to be at the origin of the 2D plane. The analysis of the typical user in this work is applicable to all users by Slivnyak's theorem [88]. In this configuration, macro BS's utilize $(K - k_P - k_M)$ of their sub-frames for interior user transmissions and k_P of their sub-frames for edge user transmissions. Hence, the SINR values of interior and edge macro cell users are respectively given as

$$\begin{aligned} \Psi_{\mathrm{M}}^{\mathrm{I}} &= \frac{P_{\mathrm{M}} h r^{-\alpha}}{\sigma^2 + I_{\mathrm{M|M}} + I_{\mathrm{P|M}}}, \\ \Psi_{\mathrm{M}}^{\mathrm{E}} &= \frac{P_{\mathrm{M}} h r^{-\alpha}}{\sigma^2 + I_{\mathrm{M|M}} + \eta I_{\mathrm{P|M}}}, \end{aligned} \tag{4.1}$$

where P_{M} is the transmit power of the macro BS, h is the power gain of the small scale channel, r is the distance between the serving BS and the user, α is the pathloss exponent, σ^2 is the noise power. The definitions of the power of small-scale fading (h), intra-tier and inter-tier interference values $(I_{t|t}, I_{s|t})$ are as defined in Section 2.1.

For the pico cells, interior and edge users are scheduled to $(K - k_P - k_M)$ interior sub-frames, and k_M edge sub-frames corresponding to macro ABS's. Hence, the interior and edge SINR definitions for pico users are respectively given as

$$\begin{aligned} \Psi_{\mathrm{P}}^{\mathrm{I}} &= \frac{P_{\mathrm{P}} h r^{-\alpha}}{\sigma^2 + I_{\mathrm{M|P}} + I_{\mathrm{P|P}}}, \\ \Psi_{\mathrm{P}}^{\mathrm{E}} &= \frac{P_{\mathrm{P}} h r^{-\alpha}}{\sigma^2 + \eta I_{\mathrm{M|P}} + I_{\mathrm{P|P}}}, \end{aligned} \tag{4.2}$$

where P_{P} is the pico BS transmit power.

4.2. Capacity Analysis

In this section, we briefly introduce the analysis for the ASE and the worst-region capacity whose mathematical derivations are presented in Appendices A and B, respectively.

4.2.1. Area Spectral Efficiency

The ASE is defined as the Shannon capacity per square meter. This quantity comprises the total capacity of different types of BS's in the wireless environment such that

$$\mathrm{ASE} = \lambda_M \left(\mathbb{C}_{\mathrm{M.BS}}^{\mathrm{I}} + \mathbb{C}_{\mathrm{M.BS}}^{\mathrm{E}} \right) + \lambda_P \left(\mathbb{C}_{\mathrm{P.BS}}^{\mathrm{I}} + \mathbb{C}_{\mathrm{P.BS}}^{\mathrm{E}} \right), \tag{4.3}$$

where $\mathbb{C}_{\mathrm{M.BS}}^{\mathrm{I}}$ and $\mathbb{C}_{\mathrm{M.BS}}^{\mathrm{E}}$ are the respective total capacities of the interior and edge sub-frames of a macro BS, and $\mathbb{C}_{\mathrm{P.BS}}^{\mathrm{I}}$ and $\mathbb{C}_{\mathrm{P.BS}}^{\mathrm{E}}$ are the respective total capacities of the interior and edge sub-frames of a pico BS.

The edge users of macro BS gets service by k_P sub-frames corresponding to the pico BS ABS's. The interior users of both tiers gets service by non-ABS $(K - k_P - k_M)$ sub-frames as shown in Figure 4.2. Hence, the respective total capacities of the interior and edge sub-frames of a single macro BS are given as

$$\mathbb{C}_{\mathrm{M.BS}}^{\mathrm{I}} = \mathcal{B} \tfrac{K - k_P - k_M}{K} \mathrm{E} \left[\ln \left(1 + \Psi_{\mathrm{M}}^{\mathrm{I}} \right) \right] \tag{4.4}$$

$$= \mathcal{B}\frac{K-k_P-k_M}{K}\frac{2\pi(\lambda_M+\lambda_P z_{\mathrm{PM}})}{1-e^{-\pi(P_{\mathrm{M}}/\gamma_{\mathrm{M}})^{2/\alpha}(\lambda_M+\lambda_P z_{\mathrm{PM}})}} \cdot \int_0^{\infty}\int_0^{(P_{\mathrm{M}}/\gamma_{\mathrm{M}})^{1/\alpha}} \frac{r}{\tau+1}\; e^{-\frac{r^{\alpha}\sigma^2\tau}{P_{\mathrm{M}}}-\pi r^2\left(\lambda_M+\lambda_P z_{\mathrm{PM}}+\lambda_M\rho_1(\tau)+\lambda_P\rho_{z_{\mathrm{PM}}}\left(\frac{P_\tau}{P_{\mathrm{M}}}\right)\right)} dr d\tau,$$

$$\mathbb{C}^{\mathrm{E}}_{\mathrm{M.BS}} = \mathcal{B}\frac{k_P}{K}\mathrm{E}\left[\ln\left(1+\Psi^{\mathrm{E}}_{\mathrm{M}}\right)\right] \tag{4.5}$$

$$= \mathcal{B}\frac{k_P}{K}\frac{2\pi(\lambda_M+\lambda_P z_{\mathrm{PM}})}{e^{-\pi(P_{\mathrm{M}}/\gamma_{\mathrm{M}})^{2/\alpha}(\lambda_M+\lambda_P z_{\mathrm{PM}})}} \cdot \int_0^{\infty}\int_{(P_{\mathrm{M}}/\gamma_{\mathrm{M}})^{1/\alpha}}^{\infty} \frac{r}{\tau+1}\; e^{-\frac{r^{\alpha}\sigma^2\tau}{P_{\mathrm{M}}}-\pi r^2\left(\lambda_M+\lambda_P z_{\mathrm{PM}}+\lambda_M\rho_1(\tau)+\lambda_P\rho_{z_{\mathrm{PM}}}\left(\frac{\eta P_{\mathrm{P}}\tau}{P_{\mathrm{M}}}\right)\right)} dr d\tau,$$

where $\mathcal{B}$ equals to $B\log_2(e)$, B is the bandwidth in Hertz, and $\rho_x(y)$ function is defined as equation (3.9).

The capacity of a pico BS is also interpreted as summation of the sub-frames which serve to edge or interior users. The edge users of macro BS gets service by k_P sub-frames, while the interior users gets service by $(K-k_P-k_M)$ sub-frames. The total capacity values of pico BS's are respectively given as

$$\mathbb{C}^{\mathrm{I}}_{\mathrm{P.BS}} = \mathcal{B}\frac{K-k_P-k_M}{K}\mathrm{E}\left[\ln\left(1+\Psi^{\mathrm{I}}_{\mathrm{P}}\right)\right] \tag{4.6}$$

$$= \mathcal{B}\frac{K-k_P-k_M}{K}\frac{2\pi(\lambda_P+\lambda_M z_{\mathrm{MP}})}{1-e^{-\pi(P_{\mathrm{P}}/\gamma_{\mathrm{P}})^{2/\alpha}(\lambda_P+\lambda_M z_{\mathrm{MP}})}} \cdot \int_0^{\infty}\int_0^{(P_{\mathrm{P}}/\gamma_{\mathrm{P}})^{1/\alpha}} \frac{r}{\tau+1}\; e^{-\frac{r^{\alpha}\sigma^2\tau}{P_{\mathrm{P}}}-\pi r^2\left(\lambda_P+\lambda_M z_{\mathrm{MP}}+\lambda_P\rho_1(\tau)+\lambda_M\rho_{z_{\mathrm{MP}}}\left(\frac{P_{\mathrm{M}}\tau}{P_{\mathrm{P}}}\right)\right)} dr d\tau,$$

$$\mathbb{C}^{\mathrm{E}}_{\mathrm{P.BS}} = \mathcal{B}\frac{k_M}{K}\mathrm{E}\left[\ln\left(1+\Psi^{\mathrm{E}}_{\mathrm{P}}\right)\right] \tag{4.7}$$

$$= \mathcal{B}\frac{k_M}{K}\frac{2\pi(\lambda_P+\lambda_M z_{\mathrm{MP}})}{e^{-\pi(P_{\mathrm{P}}/\gamma_{\mathrm{P}})^{2/\alpha}(\lambda_P+\lambda_M z_{\mathrm{MP}})}} \cdot \int_0^{\infty}\int_{(P_{\mathrm{P}}/\gamma_{\mathrm{P}})^{1/\alpha}}^{\infty} \frac{r}{\tau+1}\; e^{-\frac{r^{\alpha}\sigma^2\tau}{P_{\mathrm{P}}}-\pi r^2\left(\lambda_P+\lambda_M z_{\mathrm{MP}}+\lambda_P\rho_1(\tau)+\lambda_M\rho_{z_{\mathrm{MP}}}\left(\frac{\eta P_{\mathrm{M}}\tau}{P_{\mathrm{P}}}\right)\right)} dr d\tau.$$

The detailed derivations for the analytical equations (4.4), (4.5), (4.6), and (4.7) are presented in Appendix A.

4.2.2. The Worst-Region Capacity

In this chapter, the worst-region is an area where the users are further than a pre-defined distance to the serving BS. The pre-defined distance may be different for the

macro and pico cells; so we denote ω_{M} and ω_{P} as the respective distances for macro and pico cells. We define ω_{M} and ω_{P} as the thresholds which has the same tail probability for the PDFs of r in equation (2.13) such that

$$\begin{aligned}\omega_{\mathrm{M}} &= \sqrt{\frac{-\ln(p_{\mathrm{worst}})}{\pi\big(\lambda_M + \lambda_P z_{\mathrm{PM}}\big)}},\\ \omega_{\mathrm{P}} &= \sqrt{\frac{-\ln(p_{\mathrm{worst}})}{\pi\big(\lambda_P + \lambda_M z_{\mathrm{MP}}\big)}},\end{aligned} \tag{4.8}$$

where p_{worst} is the tail probability of the shortest distance between the serving BS and the worst-region users.

The worst-region capacity definition changes by the existence of ABS. The worst-region users are considered as the edge users as they get service from sub-frames corresponding to ABS's of the other tier. However, when there is no ABS, the worst-region users gets service as the interior user. With this condition, the worst region capacities of the macro and pico users are given as

$$\mathbb{C}^{\mathrm{W}}_{\mathrm{M.User}} = \begin{cases} \mathbb{C}^{\mathrm{E\text{-}W}}_{\mathrm{M.User}}, & k_P > 0,\\ \mathbb{C}^{\mathrm{I\text{-}W}}_{\mathrm{M.User}}, & k_P = 0,\end{cases} \tag{4.9}$$

$$\mathbb{C}^{\mathrm{W}}_{\mathrm{P.User}} = \begin{cases} \mathbb{C}^{\mathrm{E\text{-}W}}_{\mathrm{P.User}}, & k_M > 0,\\ \mathbb{C}^{\mathrm{I\text{-}W}}_{\mathrm{P.User}}, & k_M = 0,\end{cases} \tag{4.10}$$

where the respective capacities for the interior and the edge worst-region macro users are given as

$$\begin{aligned}\mathbb{C}^{\mathrm{I\text{-}W}}_{\mathrm{M.User}} &= \mathrm{E}\left[\mathcal{B}\frac{K-k_M}{K}\frac{\ln\big(1+\Psi^{\mathrm{I}}_{\mathrm{M}}\big)}{N_{\mathrm{M}}}\middle| r > \omega_{\mathrm{M}}\right] \qquad (4.11)\\ &\approx \mathcal{B}\frac{K-k_M}{K}\frac{2\pi(\lambda_M+\lambda_P z_{\mathrm{PM}})^2}{\lambda_u p_{\mathrm{worst}}}\\ &\quad \cdot\int_0^{\infty}\int_{\omega_{\mathrm{M}}}^{\infty}\frac{r}{\tau+1}\; e^{-\frac{r^\alpha\sigma^2\tau}{P_{\mathrm{M}}}-\pi r^2\left(\lambda_M+\lambda_P z_{\mathrm{PM}}+\lambda_M\rho_1(\tau)+\lambda_P\rho_{z_{\mathrm{PM}}}\left(\frac{P_{\mathrm{P}}\tau}{P_{\mathrm{M}}}\right)\right)}dr d\tau\\ \mathbb{C}^{\mathrm{E\text{-}W}}_{\mathrm{M.User}} &= \mathrm{E}\left[\mathcal{B}\frac{k_P}{K}\frac{\ln\big(1+\Psi^{\mathrm{E}}_{\mathrm{M}}\big)}{N^{\mathrm{E}}_{\mathrm{M}}}\middle| r > \omega_{\mathrm{M}}\right] \qquad (4.12)\\ &\approx \mathcal{B}\frac{k_P}{K}\frac{2\pi(\lambda_M+\lambda_P z_{\mathrm{PM}})^2}{\lambda_u p_{\mathrm{worst}} e^{-\pi(P_{\mathrm{M}}/\gamma_{\mathrm{M}})^{2/\alpha}(\lambda_M+\lambda_P z_{\mathrm{PM}})}}\end{aligned}$$

$$\cdot \int_0^{\infty} \int_{\omega_{\mathrm{M}}}^{\infty} \frac{r}{\tau+1}\ e^{-\frac{r^{\alpha}\sigma^2\tau}{P_{\mathrm{M}}} - \pi r^2 \left(\lambda_M + \lambda_P z_{\mathrm{PM}} + \lambda_M \rho_1(\tau) + \lambda_P \rho_{z_{\mathrm{PM}}}\left(\frac{\eta P_{\mathrm{P}} \tau}{P_{\mathrm{M}}}\right)\right)} dr d\tau$$

and the respective capacities for the interior and the edge worst-region pico users are given as

$$\begin{aligned} \mathbb{C}^{\text{I-W}}_{\text{P.User}} &= \mathrm{E}\left[\mathcal{B}\frac{K-k_P}{K}\frac{\ln\left(1+\Psi^{\mathrm{I}}_{\mathrm{P}}\right)}{N_{\mathrm{P}}}\middle| r > \omega_{\mathrm{P}}\right] \qquad (4.13) \\ &\approx \mathcal{B}\frac{K-k_P}{K}\frac{2\pi(\lambda_P+\lambda_M z_{\mathrm{MP}})^2}{\lambda_u p_{\text{worst}}} \\ &\quad \cdot \int_0^{\infty} \int_{\omega_{\mathrm{P}}}^{\infty} \frac{r}{\tau+1}\ e^{-\frac{r^{\alpha}\sigma^2\tau}{P_{\mathrm{P}}} - \pi r^2 \left(\lambda_P + \lambda_M z_{\mathrm{MP}} + \lambda_P \rho_1(\tau) + \lambda_M \rho_{z_{\mathrm{MP}}}\left(\frac{P_{\mathrm{M}} \tau}{P_{\mathrm{P}}}\right)\right)} dr d\tau \\ \mathbb{C}^{\text{E-W}}_{\text{P.User}} &= \mathrm{E}\left[\mathcal{B}\frac{k_M}{K}\frac{\ln\left(1+\Psi^{\mathrm{E}}_{\mathrm{P}}\right)}{N^{\mathrm{E}}_{\mathrm{P}}}\middle| r > \omega_{\mathrm{P}}\right] \qquad (4.14) \\ &\approx \mathcal{B}\frac{k_M}{K}\frac{2\pi(\lambda_P+\lambda_M z_{\mathrm{MP}})^2}{\lambda_u p_{\text{worst}} e^{-\pi(P_{\mathrm{P}}/\gamma_{\mathrm{P}})^{2/\alpha}(\lambda_P+\lambda_M z_{\mathrm{MP}})}} \\ &\quad \cdot \int_0^{\infty} \int_{\omega_{\mathrm{P}}}^{\infty} \frac{r}{\tau+1}\ e^{-\frac{r^{\alpha}\sigma^2\tau}{P_{\mathrm{P}}} - \pi r^2 \left(\lambda_P + \lambda_M z_{\mathrm{MP}} + \lambda_P \rho_1(\tau) + \lambda_M \rho_{z_{\mathrm{MP}}}\left(\frac{\eta P_{\mathrm{M}} \tau}{P_{\mathrm{P}}}\right)\right)} dr d\tau, \end{aligned}$$

where N_{M} and N_{P} are the total number of users connected to macro and pico BS's, $N^{\mathrm{E}}_{\mathrm{M}}$ and $N^{\mathrm{E}}_{\mathrm{P}}$ are the number of edge users connected to macro and pico BS's, and λ_u defines density of users. When no ABS is employed in a tier ($k_P = 0$ or $k_P = 0$), all of the users of the other tier becomes interior users as there is no remaining bandwidth for edge (Figure 4.2). When the worst-region users are edge users, we assume that $\gamma_{\mathrm{P}} \geq P_{\mathrm{P}}\omega_{\mathrm{P}}^{-\alpha}$ for the pico worst-region users and $\gamma_{\mathrm{M}} \geq P_{\mathrm{M}}\omega_{\mathrm{M}}^{-\alpha}$ for the macro worst-region users. These assumptions are non-trivial as ω_{P} and ω_{M} are assumed to be large enough to represent the worst performance.

The derivation of the worst-region capacities of macro and pico BS's are presented in Appendix B.

4.3. Optimization of Energy Efficiency

The number of ABS's, k_P and k_M, affect both the capacity and the EC. With the inclusion of the worst-region capacity and EC constraints, the optimization problem

can be formulated as

$$\max_{k_P,k_M,\gamma_{\rm P},\gamma_{\rm M}} \ {\rm EE} = \frac{\rm ASE}{\rm AEC} \tag{4.15a}$$

$$\text{subject to } \mathbb{C}^{\rm W}_{\rm M.User} \geq \epsilon_{4.1} \tag{4.15b}$$

$$\mathbb{C}^{\rm W}_{\rm P.User} \geq \epsilon_{4.1} \tag{4.15c}$$

$${\rm AEC} \leq \epsilon_{4.2} \tag{4.15d}$$

$$p^{\rm min}_{\rm edge} \leq \mathcal{P}^{\rm E}_{\rm M} \leq p^{\rm max}_{\rm edge} \tag{4.15e}$$

$$p^{\rm min}_{\rm edge} \leq \mathcal{P}^{\rm E}_{\rm P} \leq p^{\rm max}_{\rm edge} \tag{4.15f}$$

$$k_P + k_m \leq K \tag{4.15g}$$

$$k_P, k_M, \gamma_{\rm P}, \gamma_{\rm M} \geq 0, \tag{4.15h}$$

where AEC is area energy consumption ($Watt \times h/m^2$) as defined in equation (2.26), $\epsilon_{4.1}$ (bps) represents a lower bound to the capacity of a worst-region user, $\epsilon_{4.2}$ ($Watt \times h/m^2$) denotes an upper bound to the AEC to restrict the EC, $\mathcal{P}^{\rm E}_{\rm M}$ and $\mathcal{P}^{\rm E}_{\rm P}$ are edge probabilities for macro and pico users defined in equation (2.16), and $p^{\rm min}_{\rm edge}$ and $p^{\rm max}_{\rm edge}$ are the edge probability lower and upper bounds, respectively. The solution set for the problem statement above includes *No-ABS* ($k_M = k_P = 0$), *Only-macro ABS* ($k_M > 0, k_P = 0$), *Only-Pico-ABS* ($k_M = 0, k_P > 0$), *Multi-Tier-ABS* ($k_M > 0, k_P > 0$) conditions. Constraints (4.15b) and (4.15c) differ from each other as shown in equations (4.9) and (4.10) based on the implementation of ABS.

To solve Problem (4.15), we first write the Lagrangian function with 12 multipliers as

$$\begin{aligned} L \ = \ & -{\rm EE} + v_{4.1}(\epsilon_{4.1} - \mathbb{C}^{\rm W}_{\rm M.User}) + v_{4.2}(\epsilon_{4.1} - \mathbb{C}^{\rm W}_{\rm P.User}) + v_{4.3}({\rm AEC} - \epsilon_{4.2}) \\ & + v_{4.4}(p^{\rm min}_{\rm edge} - \mathcal{P}^{\rm E}_{\rm M}) + v_{4.5}(\mathcal{P}^{\rm E}_{\rm M} - p^{\rm max}_{\rm edge}) \\ & + v_{4.6}(p^{\rm min}_{\rm edge} - \mathcal{P}^{\rm E}_{\rm P}) + v_{4.7}(\mathcal{P}^{\rm E}_{\rm P} - p^{\rm max}_{\rm edge}) \\ & + v_{4.8}(k_P + k_M - K) - v_{4.9}k_P - v_{4.10}k_M - v_{4.11}\gamma_{\rm P} - v_{4.12}\gamma_{\rm M}. \end{aligned} \tag{4.16}$$

The optimality for this problem can be achieved by the Karush-Kuhn-Tucker (KKT) conditions given in [96]. Instead of writing all conditions, we only focus on the equations

related to γ_{P} and γ_{M} to provide a partial closed-form solution. By assuming $k_M > 0$, the derivative of L with respect to γ_{P} is given as

$$-\frac{d\mathrm{EE}}{d\gamma_{\mathrm{P}}} - v_{4.2}\frac{d\mathbb{C}^{\text{E-W}}_{\text{P.User}}}{d\gamma_{\mathrm{P}}} + (v_{4.7} - v_{4.6})\frac{d\mathcal{P}^{\mathrm{E}}_{\mathrm{P}}}{d\gamma_{\mathrm{P}}} - v_{4.11} = 0 \ , \tag{4.17}$$

where $v_{4.2}$, $v_{4.6}$, $v_{4.7}$, and $v_{4.11}$ are non-negative Lagrangian multipliers. It is shown in Appendix C that the derivative, $\frac{dEE}{d\gamma_{\mathrm{P}}}$, is positive. By equations (4.14) and (2.16), it is also straight-forward to prove that $\frac{d\mathbb{C}^{\text{E-W}}_{\text{P.User}}}{d\gamma_{\mathrm{P}}}$ is negative and $\frac{d\mathcal{P}^{\mathrm{E}}_{\mathrm{P}}}{d\gamma_{\mathrm{P}}}$ is positive. At least one of the $v_{4.2}$ and $v_{4.7}$ should be positive in order to achieve equation (4.17). The inequalities related to $v_{4.2}$ and $v_{4.7}$ can be written as

$$\mathbb{C}^{\text{E-W}}_{\text{P.User}} \ \geq \ \epsilon_{4.1}, \tag{4.18}$$

$$e^{-\pi\left(\frac{P_{\mathrm{P}}}{\gamma_{\mathrm{P}}}\right)^{2/\alpha}(\lambda_P+\lambda_M z_{\mathrm{MP}})} \ \leq \ p^{\max}_{\text{edge}}, \tag{4.19}$$

where one of these inequalities should be an equality to satisfy the KKT conditions. With this proposition, the optimal γ_{P} and, similarly, the optimal γ_{M} are obtained by

$$\gamma^*_{\mathrm{P}}(k_M) = \ P_{\mathrm{P}}\left[\frac{\pi(\lambda_P+\lambda_M z_{\mathrm{MP}})}{-\ln\ \min\left\{p^{\max}_{\text{edge}}, \frac{\epsilon_{4.1}}{e^{-\pi\left(\frac{P_{\mathrm{P}}}{\gamma_{\mathrm{P}}}\right)^{2/\alpha}(\lambda_P+\lambda_M z_{\mathrm{MP}})}\mathbb{C}^{\text{E-W}}_{\text{P.User}}}\right\}}\right]^{\alpha/2}, \tag{4.20}$$

$$\gamma^*_{\mathrm{M}}(k_P) = \ P_{\mathrm{M}}\left[\frac{\pi(\lambda_M+\lambda_P z_{\mathrm{PM}})}{-\ln\ \min\left\{p^{\max}_{\text{edge}}, \frac{\epsilon_{4.1}}{e^{-\pi\left(\frac{P_{\mathrm{M}}}{\gamma_{\mathrm{M}}}\right)^{2/\alpha}(\lambda_M+\lambda_P z_{\mathrm{PM}})}\mathbb{C}^{\text{E-W}}_{\text{M.User}}}\right\}}\right]^{\alpha/2}. \tag{4.21}$$

Different cases related to Constraints (4.15b) and (4.15c) are important due to the feasible solution set definitions. ABS is used in macro BS's, Constraint (4.15b) can be reduced to

$$k_M \leq \ K\left(1 - \frac{K - k_M - k_P}{K}\frac{\epsilon_{4.1}}{\mathbb{C}^{\text{I-W}}_{\text{M.User}}}\right) \qquad \text{if } k_P = 0, \tag{4.22}$$

$$k_P \geq \ \frac{k_P\epsilon_{4.1}p^{\min}_{\text{edge}}}{e^{-\pi\left(\frac{P_{\mathrm{M}}}{\gamma_{\mathrm{M}}}\right)^{2/\alpha}(\lambda_M+\lambda_P z_{\mathrm{PM}})}\mathbb{C}^{\text{E-W}}_{\text{M.User}}} \qquad \text{if } k_P > 0. \tag{4.23}$$

Similarly, with the implementation of ABS in pico BS's, Constraint (4.15c) becomes

$$k_P \leq K\left(1-\frac{K-k_M-k_P}{K}\frac{\epsilon_{4.1}}{\mathbb{C}^{\text{I-W}}_{\text{P.User}}}\right) \qquad \text{if } k_M=0, \tag{4.24}$$

$$k_M \geq \frac{k_m\epsilon_{4.1}p^{\max}_{\text{edge}}}{e^{-\pi\left(\frac{P_{\text{P}}}{\gamma_{\text{P}}}\right)^{2/\alpha}(\lambda_P+\lambda_M z_{\text{MP}})}\mathbb{C}^{\text{E-W}}_{\text{P.User}}}nS^{\min}_{\text{P.user}} \qquad \text{if } k_M>0. \tag{4.25}$$

With all of these simplifications, we reduce the feasible set of the problem to 4 different sets as

$$\begin{aligned}
\mathbb{S}_0 &= \{\,(k_M,k_P,\gamma_{\text{M}},\gamma_{\text{P}})|k_M=k_P=\gamma_{\text{M}}=\gamma_{\text{P}}=0,\\
&\quad (4.22),(4.24),(4.15d)\,\}, &(4.26)\\
\mathbb{S}_M &= \{\,(k_M,k_P,\gamma_{\text{M}},\gamma_{\text{P}})|k_P=\gamma_{\text{M}}=0,\gamma_{\text{P}}=\gamma^*_{\text{P}}(k_M),k_M\in\mathbb{Z}^+,\\
&\quad (4.22),(4.25),(4.15d),(4.15g)\,\}, &(4.27)\\
\mathbb{S}_P &= \{\,(k_M,k_P,\gamma_{\text{M}},\gamma_{\text{P}})|k_M=\gamma_{\text{P}}=0,\gamma_{\text{M}}=\gamma^*_{\text{M}}(k_P),k_P\in\mathbb{Z}^+,\\
&\quad (4.23),(4.24),(4.15d),(4.15g)\,\}, &(4.28)\\
\mathbb{S}_{PM} &= \{\,(k_M,k_P,\gamma_{\text{M}},\gamma_{\text{P}})|\gamma_{\text{M}}=\gamma^*_{\text{M}}(k_P),\gamma_{\text{P}}=\gamma^*_{\text{P}}(k_M),(k_M,k_P)\in\mathbb{Z}^+,\\
&\quad (4.23),(4.25),(4.15d),(4.15g)\,\}, &(4.29)
\end{aligned}$$

where $\mathbb{S}_0$ is for the *No-ABS* case, $\mathbb{S}_M$ is for the *Only-Macro-ABS* case, $\mathbb{S}_P$ is for the *Only-Pico-ABS* case, and $\mathbb{S}_{MP}$ is for the *Multi-Tier-ABS* case. In all of these solution sets, γ_{P} and γ_{M} values are either constant or changing by discrete k_P and k_M values. Hence, finding a solution to the problem becomes finding an optimal value in a bounded 2D or 1D space as shown in Algorithm 1. The same algorithm can be implemented for the case where only Macro BS uses ABS by $\mathbb{S}_0\cup\mathbb{S}_M$ or for the case where only Pico BS uses ABS by $\mathbb{S}_0\cup\mathbb{S}_P$.

The complexity of Algorithm 1 depends on the size of the solution sets for combinations of k_M and k_P. When only one tier employs ABS, the solution is found with a complexity of $\mathcal{O}(K)$ by a search in $\mathbb{S}_M$ or $\mathbb{S}_P$. When both tiers employ ABS, the complexity of the algorithm becomes $\mathcal{O}\left(\frac{K^2}{2}\right)$ by $\mathbb{S}_{PM}$. The computation time of the algorithm is considered to be reasonable since the typical choice of K is not so high.

Algorithm 1 Algorithm for maximization of EE.

1: Initiate $\text{EE}_{\text{opt}} = k_{P,opt} = k_{M,opt} = \gamma_{P,opt} = \gamma_{M,opt} = 0$
2: Get the feasible solution set $\mathbb{S} = \mathbb{S}_0 \cup \mathbb{S}_P \cup \mathbb{S}_M \cup \mathbb{S}_{MP}$
3: **for each** $(k_M, k_P, \gamma_{\text{M}}, \gamma_{\text{P}}) \in \mathbb{S}$ **do**
4: Calculate $\text{EE} = \frac{\text{ASE}}{\text{AEC}}$
5: **if** $\text{EE} > \text{EE}_{\text{opt}}$ **then**
6: Found a better solution.
7: Update EE_{opt}, $k_{P,opt}$, $k_{M,opt}$, $\gamma_{P,opt}$, $\gamma_{M,opt}$
8: **end if**
9: **end for**

Table 4.1. General parameters for numerical results.

Parameters	Values
Density of Macro BS, λ_M	2×10^{-6} [BS/m^2]
Density of Pico BS, λ_P	10^{-5} [BS/m^2]
Density of users, λ_u	5×10^{-4} [user/m^2]
Transmit power, P_{M} / P_{P}	40 / 1 [Watts]
Edge prob. bounds, $p_{\text{edge}}^{\text{min}}$ / $p_{\text{edge}}^{\text{max}}$	0.1 / 0.5
Edge prob. for const. th., $p_{\text{edge}}^{\text{const}}$	0.25
Bias, $\mathfrak{b}$	4
Pathloss exponent, α	3
Noise power, σ^2	10^{-6} [Watts]
ABS power factor, η	0.01
Bandwidth, B	10 MHz
Num. of sub-frames in a frame, K	40
Tail prob. for the worst-region, p_{worst}	0.05
The worst-region bit-rate constraint, $\epsilon_{4.1}$	10^3 [bps]
AEC constraint, $\epsilon_{4.2}$	10^{-3} [Watt×hour/m^2]

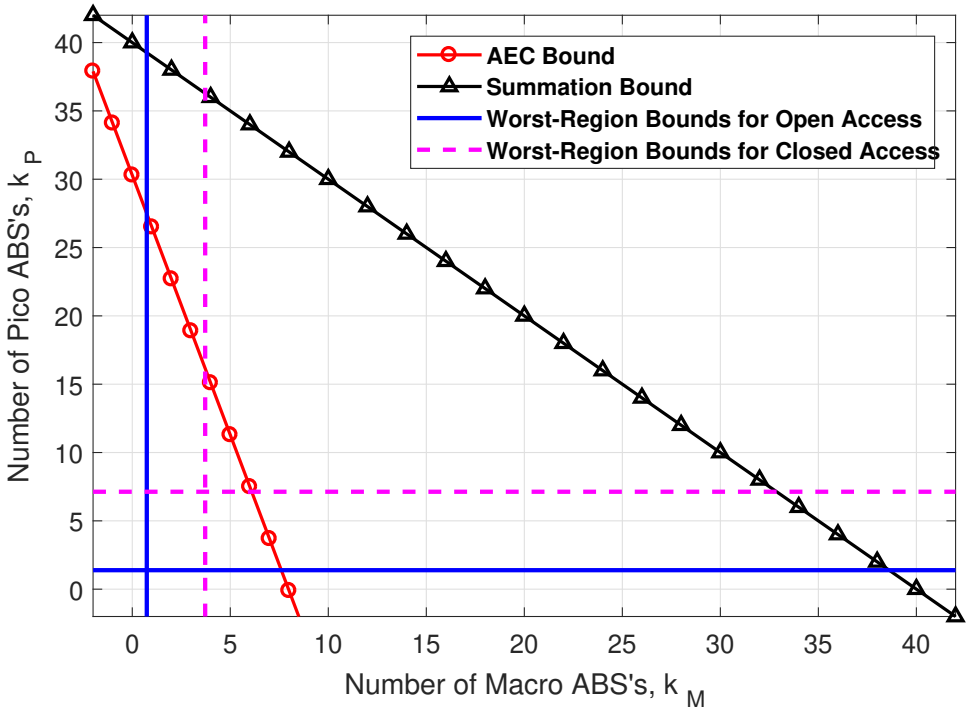

Figure 4.3. Feasible region for k_M and k_P for *Multi-Tier-ABS* case, $\mathbb{S}_{PM}$ ($\epsilon_{4.1} = 5 \times 10^3$ bps, $\epsilon_{4.2} = 0.8 \times 10^{-3}$ Watt×hour/m^2).

4.4. Numerical Results

In this section, we present numerical results where different ABS schemes are compared with each other under a variety of parameter sets. Tables 2.1 and 4.1 shows the general parameters of the environment used in the analysis. Any environment parameter, which is not in the x-axis of the plots or is not exclusively stated differently, is the same as the presented in Table 4.1. Among these parameters, the $p_{\text{edge}}^{\text{const}}$ parameter is only used in the *Optimal* k_M and $k_M = 4$, $k_P = 0$ curves for calculation of constant γ_{P} and γ_{M} by equations in (2.16).

Figure 4.3 shows the *Multi-Tier-ABS* feasible region for k_M and k_P where both of the tiers are assumed to have at least one ABS ($k_M > 0$, $k_P > 0$). The worst-region bounds in the figure reveal how Constraints (4.15b) and (4.15c) make the feasible region smaller in closed access networks, compared to open access. The summation bound shows an upper limit provided by Constraint (4.15g). AEC bound by Con-

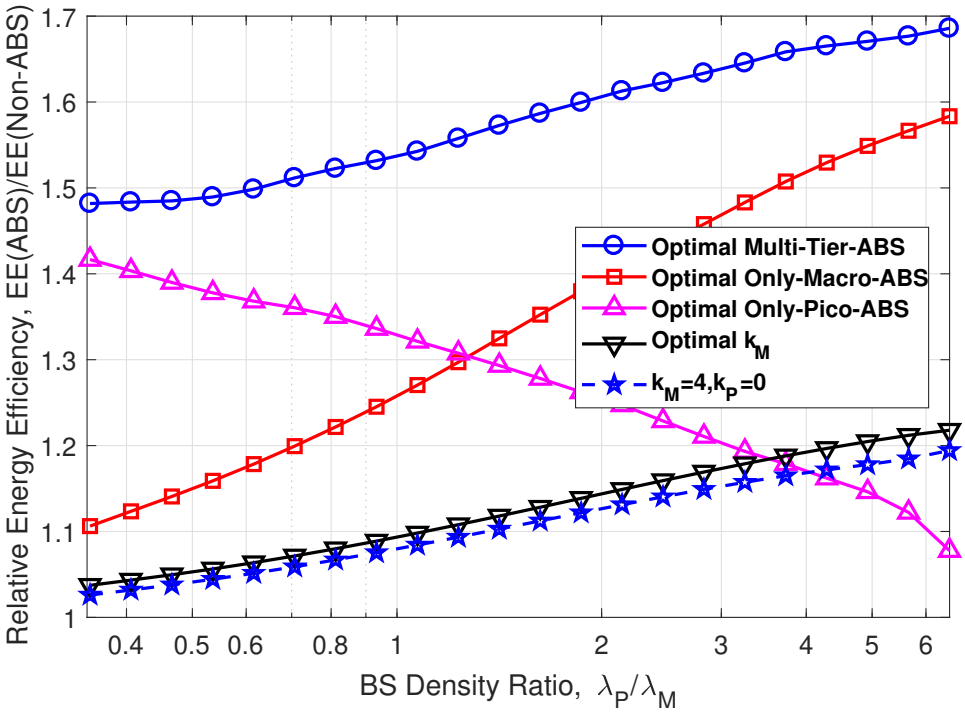

(a) Open access.

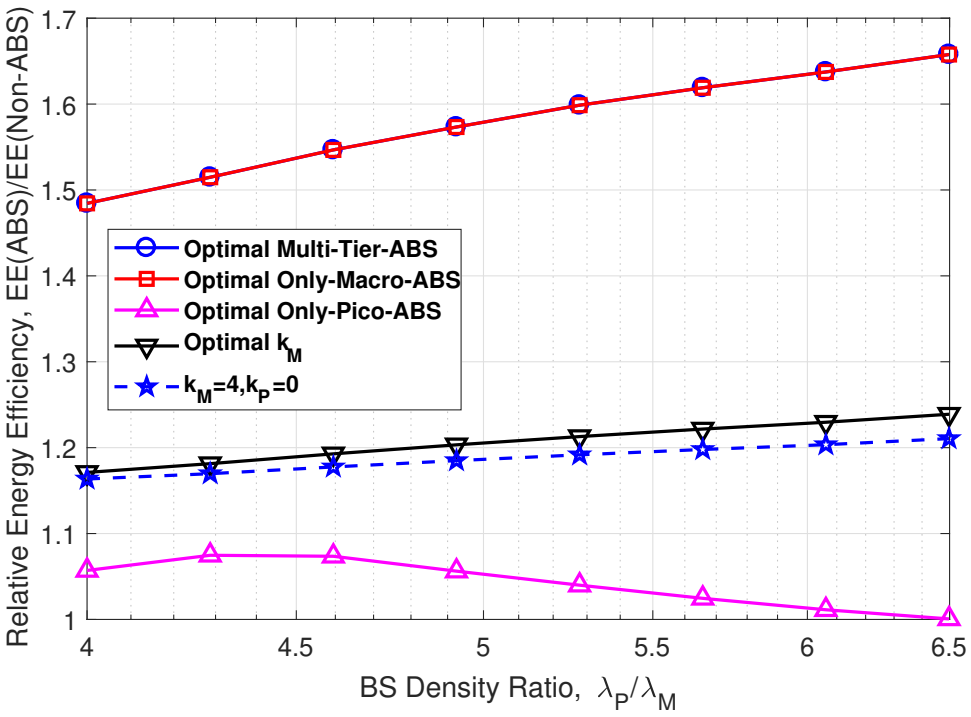

(b) Closed access.

Figure 4.4. Comparison of relative EE for changing BS density.

straint (4.15d) is a lower bound whose slope is mostly affected by the densities of two tiers and their power amplification gains. Macro BS power amplification consumes more energy due to high transmit power (40 W). Therefore, the use of ABS for Macro BS clearly saves more energy than Pico BS's for the same environment parameters.

Figure 4.4 shows the comparison between different ABS schemes for open and closed access. Relative EE metric is defined as the division of EE of given ABS scheme by EE of *No-ABS* scheme as

$$\text{Relative EE} = \frac{\text{EE(ABS is employed)}}{\text{EE(No ABS)}} \tag{4.30}$$

The x-axis (*BS Density Ratio*) is the division of varying Pico BS density values by constant Macro BS density from Table 4.1. In these plots, $k_M = 4, k_P = 0$ curve is drawn by all constant ABS parameters, while Optimal k_M curve is drawn by optimally selecting k_M alone (similar to [40]). Optimal *Only-Macro-ABS* curve is drawn by optimizing k_M and γ_{P} together by $\mathbb{S}_0$ and $\mathbb{S}_M$ solution sets. The big gap between Optimal *Only-Macro-ABS* curve and Optimal k_M curve in Figure 4.4(a) clearly shows that the optimization of γ_{P} and k_M together provides much better performance. Comparing to the others, Optimal *Only-Pico-ABS* curve is decreasing with BS Density Ratio. High pico BS density causes more pico ABS usage by Constraint (4.15b), so Optimal *Only-Pico-ABS* curve BS sum-rate and EE decreases. Moreover, Optimal *Multi-tier-ABS* curve provides the best performance in both plots. In closed access, inter-tier interference gets stronger and satisfying the worst-region constraints become more difficult. Under high pico BS density, Optimal *Multi-Tier-ABS* curve satisfies the pico worst-region Constraint (4.15c) with non-zero Macro ABS ($k_M > 0$), while satisfying the macro worst-region requirement in Constraint (4.15b) with no pico ABS's ($k_P = 0$). This behaviour causes Optimal *Multi-Tier-ABS* and Optimal *Only-Macro-ABS* curves to overlap under high interference.

Figure 4.5 shows the number of ABS's for several optimal ABS schemes from Figure 4.4(a). The optimal k_M and k_P values from Figure 4.5 indicate the effects of the worst-region and EC constraints distinctly. For the region where BS density

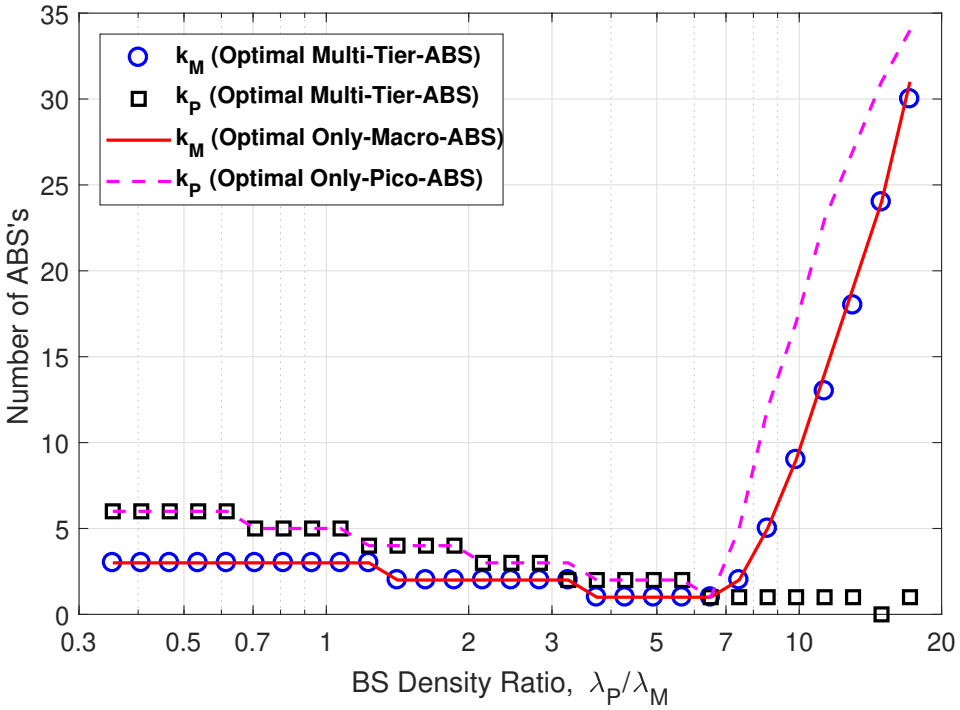

Figure 4.5. Number of optimal ABS's under different solution sets for open access.

ratio is lower than 6.5, the optimal k_M and k_P values are affected by the worst-region Constraints (4.23) and (4.25). In all 3 optimization schemes, k_M and k_P becomes equal to their lower bounds. However, higher values of BS density with large number of pico BS's cause EC to grow. As BS density surpasses 6.5, the k_M and k_P values should be much higher to satisfy the EC requirement in Constraint (4.15d). Comparing k_M and k_P of Optimal *Muti-Tier-ABS*, k_P stays low while k_M gets high to satisfy EC requirement. The macro BS typically consumes more energy, so the EC requirement can be met with lower k_M, comparing to k_P.

Figure 4.6 shows the ASE curves for varying AEC values. These plots are drawn by changing the density of the pico BS deployment, which directly affects the EC, for every adjacent point of the curves. *Multi-Tier-ABS* curves achieve the best spectral efficiency. In the closed access plot, *Multi-Tier-ABS* curve overlaps with *Only-Macro-ABS* similar to Figure 4.4(b). *No-ABS* curve of the closed access plot is shorter than the others, as they cannot satisfy the constraints for lower AEC values. Optimal *Only-Pico-ABS* curve also cannot cover the lower AEC values in closed access. Comparing Optimal *Only-Pico-ABS* and *No-ABS* to other curves with macro ABS's, we can con-

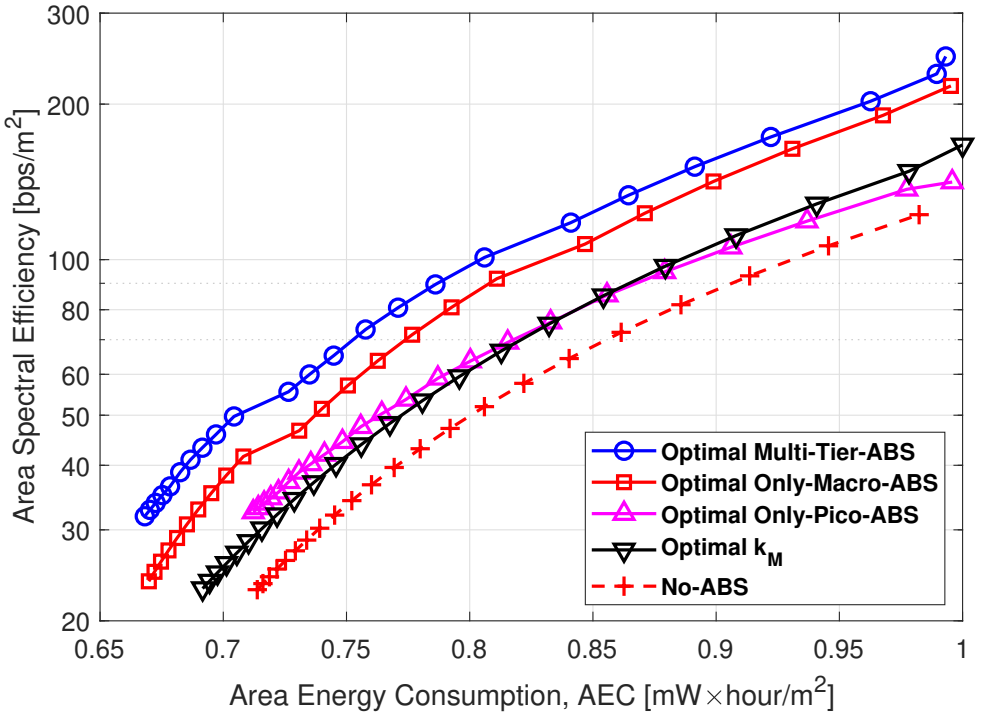

(a) Open access.

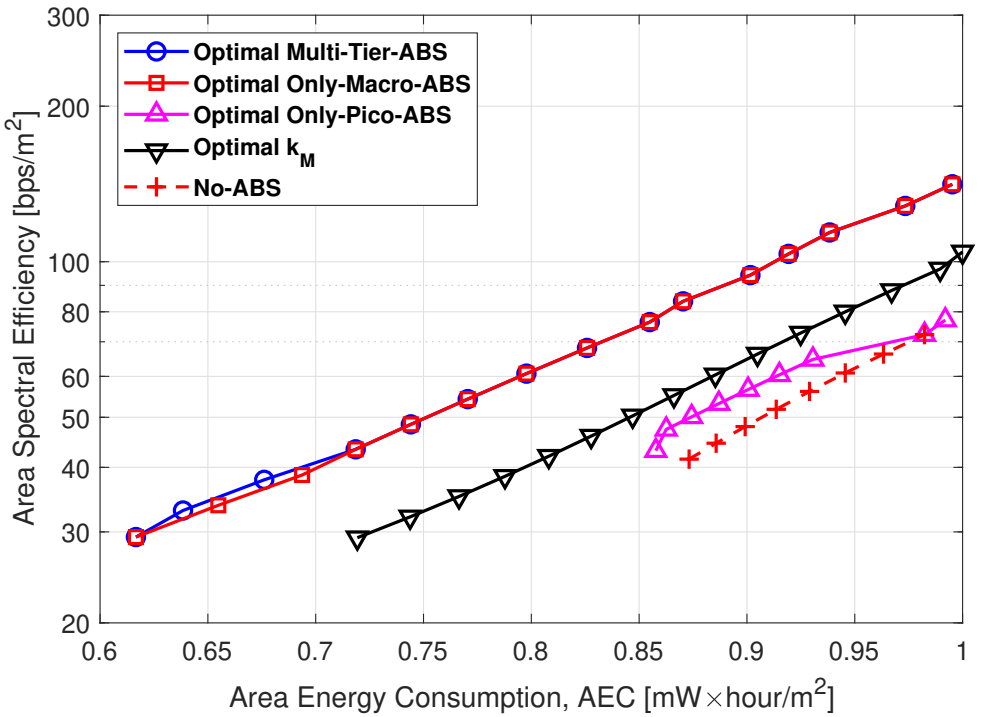

(b) Closed access.

Figure 4.6. Comparison of ASE of ABS schemes for EC variation.

clude that the optimization of the number of macro ABS's provides adaptability to tighter EC constraints. The ASE values of lower AEC levels are similar in both closed and open access, while open access curves provide better ASE for higher EC. This similarity caused by low AEC region to provide lower inter-tier interference in lower AEC region. In the low AEC region, the BS deployment is sparse and inter-tier interference is low, so the performance of open and closed access deployments gets closer to each other.

Figure 4.7 shows how EE diminishes as the average worst-region capacity constraint tightens. Relative EE metric (EE divided by EE of *No-ABS* case) is chosen as y-axis for better comparison. The behavior of the curves for open and closed access cases are pretty similar except the scale of x-axis. As the interference experienced by the worst-region users is higher in closed access, the closed access curves diminish earlier around $\epsilon_{4.1} = 1800$ bps. For lower $\epsilon_{4.1}$ region, Optimal *Multi-Tier-ABS* scheme can satisfy both macro and pico worst-region constraints with ABS's ($k_M > 0$, $k_P > 0$), so outperforms all other schemes. As $\epsilon_{4.1}$ gets higher, Optimal *Multi-Tier-ABS* scheme cannot satisfy the macro worst-region constraints with pico ABS's, and chooses $k_P = 0$. Hence, *Optimal Multi-Tier-ABS* and Optimal *Only-Macro-ABS* curves overlap. A similar behavior is also observed in Optimal *Only-Pico-ABS* curve, which provides the same performance with *No-ABS* scheme after a certain level of $\epsilon_{4.1}$ value. In the highest $\epsilon_{4.1}$ value of both open access and closed access curves, Optimal *Multi-Tier-ABS* curve provides higher EE than the others due to its adaptability to tighter constraints. After the highest $\epsilon_{4.1}$ values of the curves (12000 bps in open access and 1800 bps in closed access), all of the presented schemes fail to satisfy the worst-region constraints.

Figure 4.8 shows the relative EE results for varying tier selection bias values and the constant BS densities. Higher bias values cause the typical user to connect to the pico BS's more often than to the macro BS's and consequently reduces the macro BS coverage area. Smaller coverage area provides better signal quality to the macro users and better spectral efficiency to the macro BS. Optimal *Only-Pico-ABS* scheme takes advantage of the improved spectral efficiency of macro BS's as it lets them use all the

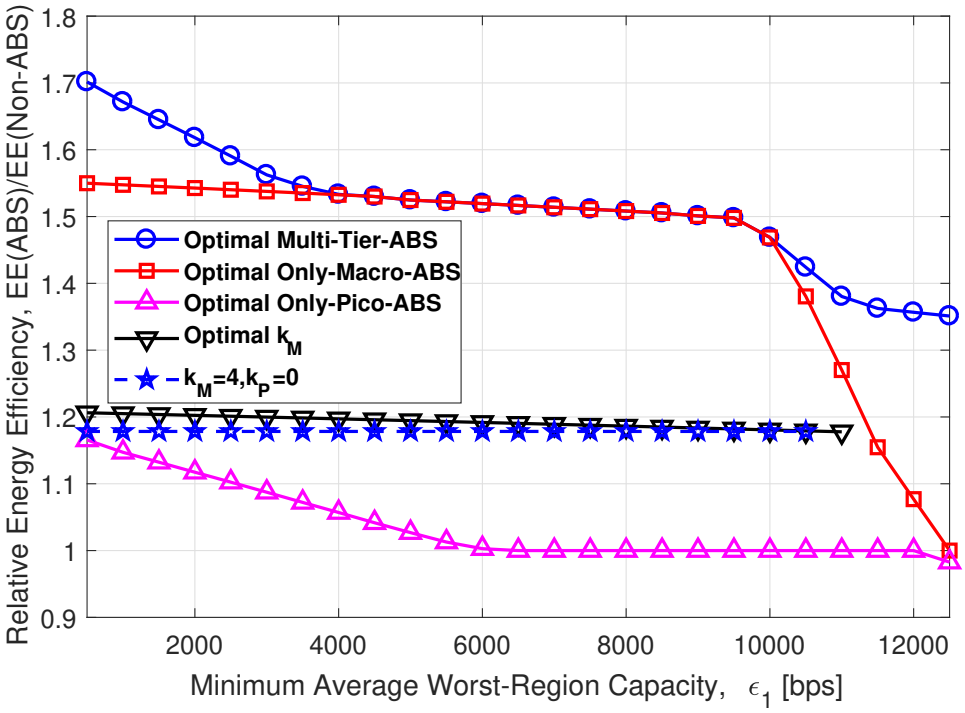

(a) Open access.

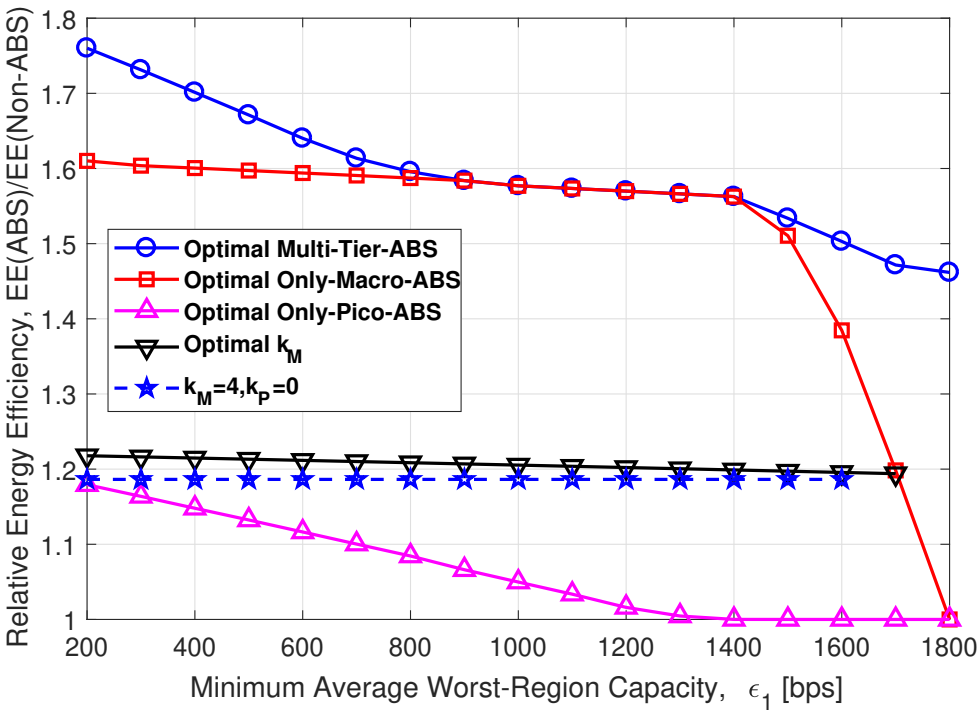

(b) Closed access.

Figure 4.7. EE comparison under the worst-region capacity constraint variation.

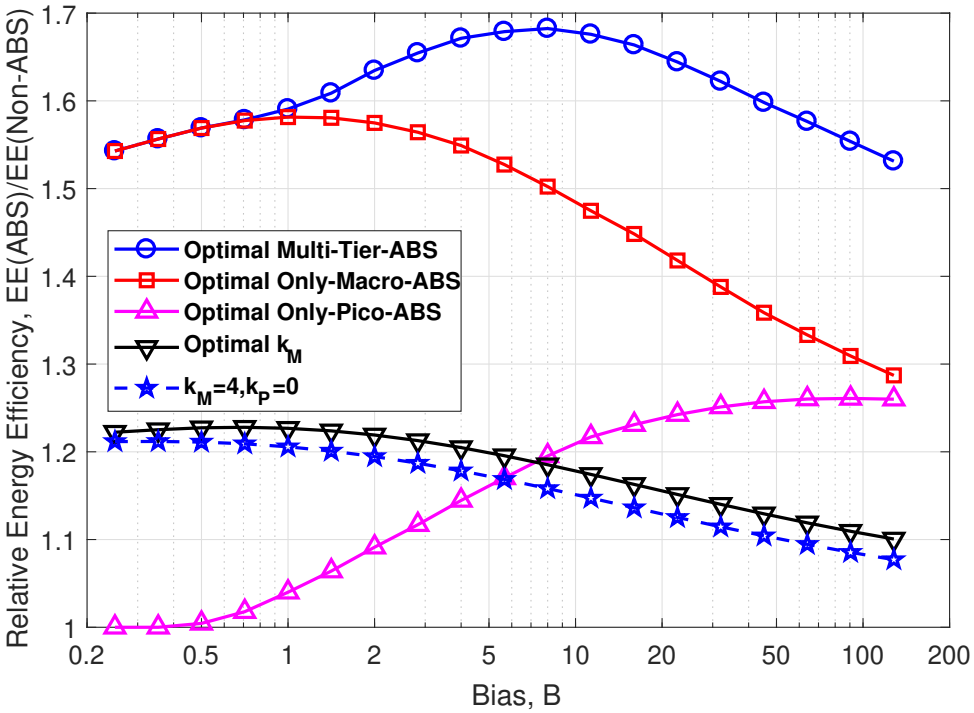

Figure 4.8. EE comparison under tier selection bias parameter variation.

bandwidth ($k_M = 0$). Therefore, the relative EE of Optimal *Only-Pico-ABS* curve increases with the bias. In contrast, macro ABS schemes cannot take advantage of the increasing macro BS spectral efficiency, as they limit macro bandwidth usage ($k_M > 0$). For increasing bias, Optimal *Only-Macro-ABS*, Optimal k_M, and $k_M = 4$,$k_P = 0$ schemes provide less ASE gain than *No-ABS* scheme, so their relative EE decreases. The plot also reveals that Optimal *Multi-Tier-ABS* scheme outperforms the others as it can take advantage of both low and high bias values.

4.5. Conclusion

In this chapter, stochastic geometry analysis of the spectral efficiency and worst-region capacity is presented for a heterogeneous network where both macro and pico BS's employ the ABS technique. The analytical framework is used to formulate and solve a constrained optimization problem that maximizes the EE. The numerical results indicate several implications on multi-tier ABS performance. Comparing macro and pico ABS, the results reveal that the macro ABS implementation provides better savings in network EC. Moreover, open and closed access options are compared for dif-

ferent EC requirements. Effect of CRE bias on ABS implementation is presented, and certain CRE bias values are observed to provide maximum EE for a certain wireless environment parameters.

5. FFR IN NOMA-BASED HETEROGENEOUS NETWORKS

NOMA provides network capacity gain comparing to conventional OMA networks. However, the statistical behavior of the interference experienced by the users becomes more complicated with the introduction of intra-cell interference. Conventional ICIC techniques, strict FFR and SFR, are designed to reduce intra-tier interference and often extended to reduce inter-tier interference, but their performance on intra-tier interference is not explored with detail through the literature. In this chapter, we present a coverage probability analysis with the help of stochastic geometry for strict FFR and SFR. The derivations are obtained for K-tier heterogeneous network with open and closed access options.

In the rest of the chapter, the mathematical model for the NOMA-FFR coexistence is presented in Section 5.1. Coverage probability analysis and the discussion of power rule are presented in Section 5.2. Numerical results are presented in Section 5.3 and conclusion is presented in Section 5.4.

5.1. System Model

We consider a T-tier heterogeneous cellular network. BS's of each tier are randomly located on a 2D infinite plane by homogeneous PPP with BS density of λ_t $(1/m^2)$ and transmit power of P_t, where t is index for BS tiers ($t \in \{1, 2, \ldots, T\}$).

In the coexistence of NOMA and FFR, every RB can be assigned to two different users. To take advantage of both techniques, every user is assigned to one of the three groups in this chapter; "near", "far-interior" and "far-edge". The near users are served with low power RB's, which are available for the entire spectrum. Each near user first demodulates the signal with stronger power, then demodulates its own signal with weaker power by subtracting previously demodulated high power signal as presented in

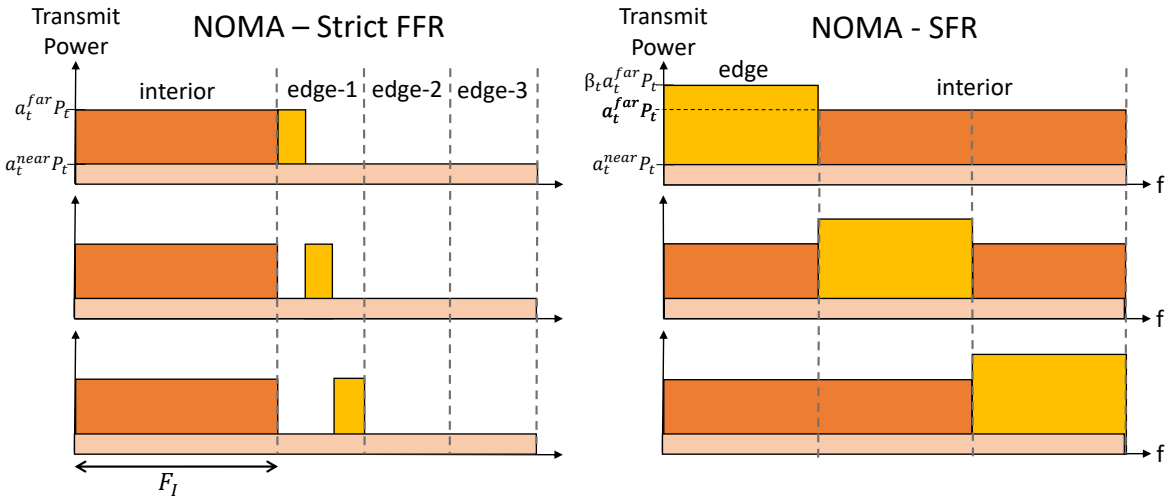

Figure 5.1. RB organization for NOMA-FFR coexistence.

Section 2.1.3. Far-interior users are served with higher power, while far-edge users uses the advantage of frequency reuse. The signal powers for near and far users of tier t are multiplied with a_t^{near} and a_t^{far} coefficients, whose summation equals to 1. Comparing NOMA-FFR with original FFR, only difference for far-interior and far-edge users is that they experience additional interference from low power signal of serving BS. In this work, two main FFR techniques, strict FFR and SFR, are considered. Their coexistence scenarios with NOMA are summarized in the following two subsections.

5.1.1. NOMA - Strict Fractional Frequency Reuse

Strict FFR aims to provide better service to the far-edge users by suppressing some of the RB with a reuse factor Δ_t. The coexistence scenario of NOMA and strict FFR is shown in Figure 5.1. In this scenario, the low power signal is transmitted through all of the available frequency RB's with transmit power $a_t^{\text{near}}P_t$ for the t-th tier. Moreover, the first F_I RB's are also used by the overlapping signal for the far-interior users with higher transmit power, $a_t^{\text{far}}P_t$. The remaining $(\text{F} - \text{F}_\text{I})$ RB's are divided into T groups and shared among the tiers. As presented in Figure 5.1, each tier t has its edge frequency resource group called as edge-s, which is further divided for intra-tier frequency reuse Δ_t ($\Delta_1 = 3$ in the figure). Every BS in tier t transmits its reference signal with the transmit power of P_t that is used for user grouping. The

relationship between downlink transmit powers is given by

$$P_t = a_t^{\text{near}} P_t + a_t^{\text{far}} P_t. \tag{5.1}$$

As there are more than one alternative to the downlink transmit powers, there exists different alternative SINR definitions. For near users, there are two different SINR definitions depending on the served frequency band in Figure 5.1. SINR values for tier t near users served in interior and edge-s frequency parts are respectively written as

$$\begin{aligned} \Psi_t^{\text{N-I}} &= \frac{a_t^{\text{near}} P_t h r^{-\alpha}}{\sigma^2 + I_t^{\text{sFFR-I}}}, \\ \Psi_{t,s}^{\text{N-E}} &= \frac{a_t^{\text{near}} P_t h r^{-\alpha}}{\sigma^2 + I_{t,s}^{\text{sFFR-E}}}, \end{aligned} \tag{5.2}$$

where $I_t^{\text{sFFR-I}}$ and $I_{t,s}^{\text{sFFR-E}}$ are interference experienced by tier t users under strict FFR in interior and edge-s frequency parts, h is the power of the fading channel gain of serving signal, r is distance to the serving BS, σ^2 is the noise power, α is the pathloss exponent. The interference components of strict FFR are defined as

$$\begin{aligned} I_t^{\text{sFFR-I}} &= \sum_{j=1}^{T} \sum_{r_i > q_{j|t}} P_j h_i r_i^{-\alpha}, \\ I_{t,s}^{\text{sFFR-E}} &= \sum_{r_i > q_{s|t}} \delta_{i,s} a_s^{\text{far}} P_s h_i r_i^{-\alpha} + \sum_{j=1}^{T} \sum_{r_i > q_{j|t}} a_j^{\text{near}} P_j h_i r_i^{-\alpha}, \end{aligned} \tag{5.3}$$

where $q_{x|y}$ is the minimum distance of tier x interferers to the typical user of tier y as defined in equation (2.9), $\delta_{i,s}$ is binary reuse random variable which becomes 1 when i-th interferer uses the same frequency with $1/\Delta_s$ probability, h_i is the power of the fading channel, and r_i is the distances to i-th interfering BS's of tier-j. The channel is considered to be Rayleigh fading for this chapter, so h and h_i random variables are exponentially distributed. Each of $I_t^{\text{sFFR-I}}$ and $I_{t,s}^{\text{sFFR-E}}$ consists of intra-tier and inter-tier interference values (Sections 2.1.1 and 2.1.2). While $I_t^{\text{sFFR-I}}$ includes all transmitted signals from all tiers, $I_{t,s}^{\text{sFFR-E}}$ includes near user signals from all tiers and far user signals only from its own tier with a reuse factor.

The SINR values for tier t far-interior and far-edge users are given as

$$\begin{aligned}\Psi_t^{\text{F-I}} =& \frac{a_t^{\text{far}} h r^{-\alpha}}{\sigma^2 + a_t^{\text{near}} h r^{-\alpha} + I_t^{\text{sFFR-I}}},\\ \Psi_t^{\text{F-E}} =& \frac{a_t^{\text{far}} h r^{-\alpha}}{\sigma^2 + a_t^{\text{near}} h r^{-\alpha} + I_{t,t}^{\text{sFFR-E}}},\end{aligned} \tag{5.4}$$

where the transmit power is multiplied with power multiplier of far users, a_t^{far}, and intra-cell interference term $a_t^{\text{near}} h r^{-\alpha}$ included in denominator (Section 2.1.3), comparing to near user SINR definitions in equation (5.2).

5.1.2. NOMA - Soft Frequency Reuse

In contrast to Strict FFR, SFR focuses on frequency reuse while all of the RB's are actively allocated to the near and far users. The downlink service quality of the far-edge users is enhanced by using higher transmit power, multiplied with SFR power factor, β_t, as shown in Figure 5.1. Similar to its general use, each BS tier makes intra-tier frequency reuse of far-edge user RB's, and there is no RB group that is dedicated for a tier. In other words, BS's of each tier can transmit with higher power, $\beta_t a_t^{\text{far}} P_t$, in any RB. Namely, the respective transmit powers of near, far-interior, and far-edge users are given as $a_t^{\text{near}} P_t$, $a_t^{\text{far}} P_t$, and $\beta_t a_t^{\text{far}} P_t$, where $a_t^{\text{near}} + a_t^{\text{far}} = 1$ and $\beta_k \geq 1$. In contrast to strict FFR, all of the user types served by SFR experiences the same type of interference. The SINR definition of near users served by SFR are given as

$$\Psi_t^{\text{N}} = \frac{a_t^{\text{near}} P_t h r^{-\alpha}}{\sigma^2 + I_t^{\text{SFR}}}, \tag{5.5}$$

where

$$I_t^{\text{SFR}} = \sum_{j=1}^{T} \sum_{r_i > q_{j|t}} \left(a_j^{\text{near}} P_j + (1 - \delta_{i,j}) a_j^{\text{far}} P_j + \delta_{i,j} \beta_j a_j^{\text{far}} P_j \right) h_i r_i^{-\alpha}, \tag{5.6}$$

which comprises intra-tier and inter-tier interference from serving signals of all of user types. Moreover, the SINR definitions of far-interior and far-edge users are given as

$$\begin{aligned}\Psi_t^{\text{F-I}} =& \frac{a_t^{\text{far}} P_t h r^{-\alpha}}{\sigma^2 + a_t^{\text{near}} P_t h r^{-\alpha} + I_t^{\text{SFR}}},\\ \Psi_t^{\text{F-E}} =& \frac{\beta_t a_t^{\text{far}} P_t h r^{-\alpha}}{\sigma^2 + a_t^{\text{near}} P_t h r^{-\alpha} + I_t^{\text{SFR}}},\end{aligned} \tag{5.7}$$

where the transmit powers are different and the denominator contains intra-cell interference $a_t^{\text{near}} P_t h r^{-\alpha}$ as defined in Section 2.1.3, comparing to near user SINR in equation (5.5).

5.2. Coverage Probability Analysis

The coverage probability analysis requires probability definitions for BS tier selection, interior or edge group selection, and power level selection. For this chapter, all of these selections are made based on average RSRP measurement of the user. The user is grouped by its RSRP measurement as

$$\text{User group} = \begin{cases} \text{Near} & \text{if} \quad P_t r^{-\alpha} > \varphi_t, \\ \text{Far-interior} & \text{if} \quad \varphi_t > P_t r^{-\alpha} > \gamma_t, \\ \text{Far-edge} & \text{if} \quad \gamma_t > P_t r^{-\alpha}, \end{cases} \tag{5.8}$$

where φ_t is the power level selection threshold for tier t, γ_t is interior/edge group selection threshold for tier t. These thresholds are always selected as $\varphi_t > \gamma_t$.

The coverage probability of NOMA-FFR coexistence comprises all different kinds of SINR cases from Section 5.1. Taking all these cases into account, the downlink coverage probability of a user can be written as

$$\kappa(\tau) = \sum_{t=1}^{T} \mathfrak{p}_t \left[(1 - \mathfrak{P}_t)\, \kappa_t^{\text{N}}(\tau) + \left(\mathfrak{P}_t - \mathcal{P}_t^{\text{E}} \right) \kappa_t^{\text{F-I}}(\tau) + \mathcal{P}_t^{\text{E}} \kappa_t^{\text{F-E}}(\tau) \right], \tag{5.9}$$

where $\kappa_t^{\text{N}}(\cdot)$, $\kappa_t^{\text{F-I}}(\cdot)$, and $\kappa_t^{\text{F-E}}(\cdot)$ are respective coverage probabilities of near, far-interior, and far-edge users for tier t. $\mathfrak{p}_t$ is the probability of the user to select tier t, as defined in equation (2.7). $\mathfrak{P}_t$ and $\mathcal{P}_t^{\text{E}}$ are respective probabilities to select the tier t users as far and edge as defined in equations (2.21) and (2.17).

$\kappa_t^{\text{N}}(\cdot)$, $\kappa_t^{\text{F-I}}(\cdot)$, and $\kappa_t^{\text{F-E}}(\cdot)$ are case-specific coverage probabilities and they differ depending on the FFR technique. All of the analytical expressions in this section are valid for both open and closed access by inserting appropriate $f_{r_t}(r)$ from equation (2.8) and $q_{x|y}$ from equation (2.9).

5.2.1. Strict Fractional Frequency Reuse

The case-specific coverage probability values of far-interior and far-edge users are similar to the only strict FFR case in [24] with the addition of near user's low power signal. The derivations of the analytical results in this section are presented in Appendix D. As shown in Figure 5.1, near users can get service from interior or edge-s frequency band parts. The user gets service from any RB, so the probability of getting service from interior part of frequency band is $\frac{\mathrm{F_I}}{\mathrm{F}}$ and the probability of getting service from edge-s part of frequency band is $\left(1-\frac{\mathrm{F_I}}{\mathrm{F}}\right)$. Therefore, the coverage probability of near users of the t-th tier BS, employing strict FFR and NOMA, is given as

$$\begin{aligned}\kappa_t^{\mathrm{N}}(\tau) &= \tfrac{\mathrm{F_I}}{\mathrm{F}}\Pr\left(\Psi_t^{\text{N-I}}>\tau,\Psi_t^{\text{F-I}}>\mathcal{T}\right)+\left(1-\tfrac{\mathrm{F_I}}{\mathrm{F}}\right)\Pr\left(\Psi_t^{\text{N-E}}>\tau,\Psi_t^{\text{F-E}}>\mathcal{T}\right) \quad (5.10)\\ &= \int_0^{(P_t/\varphi_t)^{1/\alpha}} \exp\left(-\tfrac{\tau r^\alpha\sigma^2}{a_t^{\text{near}}P_t}\right)\left[\tfrac{\mathrm{F_I}}{\mathrm{F}}\mathcal{L}_{I_t^{\text{sFFR-I}}}\left(\tfrac{\tau r^\alpha}{a_t^{\text{near}}P_t}\right)\right.\\ &\quad \left.+\left(1-\tfrac{\mathrm{F_I}}{\mathrm{F}}\right)\sum_{j=1}^{T}\tfrac{1}{T}\mathcal{L}_{I_{t,j}^{\text{sFFR-E}}}\left(\tfrac{\tau r^\alpha}{a_t^{\text{near}}P_t}\right)\right]\tfrac{f_{r_t}(r)}{1-\mathfrak{P}_t}dr\ ,\end{aligned}$$

where Laplace transform of interior frequency band interference, $\mathcal{L}_{I_t^{\text{sFFR-I}}}(\cdot)$, and Laplace transform of edge-s frequency band interference, $\mathcal{L}_{I_{t,s}^{\text{sFFR-E}}}(\cdot)$, are respectively given as

$$\mathcal{L}_{I_t^{\text{sFFR-I}}}(x)=\exp\left\{-2\pi\sum_{j=1}^{T}\lambda_j\int_{q_{j|t}}^{\infty}\frac{u}{1+\frac{u^\alpha}{x(a_j^{\text{near}}P_j+a_j^{\text{far}}P_j)}}du\right\} \quad (5.11)$$

and

$$\begin{aligned}\mathcal{L}_{I_{t,s}^{\text{sFFR-E}}}(x) &= \exp\left\{-2\pi\left(\tfrac{\lambda_s}{\Delta_s}\int_{q_{s|t}}^{\infty}\frac{u}{1+\frac{u^\alpha}{s(a_s^{\text{near}}P_s+a_s^{\text{far}}P_s)}}du\right.\right. \quad (5.12)\\ &\quad \left.\left.+\lambda_s\tfrac{\Delta_s-1}{\Delta_s}\int_{q_{s|t}}^{\infty}\frac{u}{1+\frac{u^\alpha}{xa_s^{\text{near}}P_s}}du+\sum_{\substack{j=1\\ j\neq s}}^{T}\lambda_j\int_{q_{j|t}}^{\infty}\frac{u}{1+\frac{u^\alpha}{xa_j^{\text{near}}P_j}}du\right)\right\}.\end{aligned}$$

$\mathcal{T}$ is threshold in near user to be able to decode far users signal for SIC implementation. Similarly, the coverage probabilities of far-interior and far-edge users of the t-th tier BS, employing strict FFR and NOMA, are respectively given as

$$\kappa_t^{\text{F-I}}(\tau) = \Pr\left(\Psi_t^{\text{F-I}}>\tau\right) \quad (5.13)$$

$$= \int_{(P_t/\varphi_t)^{1/\alpha}}^{(P_t/\gamma_t)^{1/\alpha}} \exp\left(-\frac{\tau r^\alpha \sigma^2}{a_t^{\text{far}} P_t - \tau a_t^{\text{near}} P_t}\right) \mathcal{L}_{I_t^{\text{sFFR-I}}}\left(\frac{\tau r^\alpha}{a_t^{\text{far}} P_t - \tau a_t^{\text{near}} P_t}\right) \frac{f_{r_t}(r)}{\mathfrak{P}_t - \mathcal{P}_t^{\text{E}}} dr,$$

$$\kappa_t^{\text{F-E}}(\tau) = \Pr\left(\Psi_t^{\text{F-E}} > \tau\right) \tag{5.14}$$
$$= \int_{(P_t/\gamma_t)^{1/\alpha}}^{\infty} \exp\left(-\frac{\tau r^\alpha \sigma^2}{a_t^{\text{far}} P_t - \tau a_t^{\text{near}} P_t}\right) \mathcal{L}_{I_{t,t}^{\text{sFFR-E}}}\left(\frac{\tau r^\alpha}{a_t^{\text{far}} P_t - \tau a_t^{\text{near}} P_t}\right) \frac{f_{r_t}(r)}{\mathcal{P}_t^{\text{E}}} dr.$$

5.2.2. Soft Frequency Reuse

For the SFR case, the interference model is the same for both the edge and interior RB's as given in Section 5.1.2. Hence, the coverage analysis of all groups include the same LT of interference. The derivations of the analytical results in this section are presented in Appendix E. Therefore, the coverage probabilities of near, far-interior, and far-edge users of the t-th tier BS, employing SFR and NOMA, are respectively given as

$$\kappa_t^{\text{N}}(\tau) = \int_{0}^{(P_t/\varphi_t)^{1/\alpha}} \exp\left(-\frac{\tau r^\alpha \sigma^2}{a_t^{\text{near}} P_t}\right) \mathcal{L}_{I_t^{\text{SFR}}}\left(\frac{\tau r^\alpha}{a_t^{\text{near}} P_t}\right) \frac{f_{r_t(r)}}{1 - \mathfrak{P}_t} dr, \tag{5.15}$$

$$\kappa_t^{\text{F-I}}(\tau) = \int_{(P_t/\varphi_t)^{1/\alpha}}^{(P_t/\gamma_t)^{1/\alpha}} \exp\left(-\frac{\tau r^\alpha \sigma^2}{a_t^{\text{far}} P_t - \tau a_t^{\text{near}} P_t}\right) \mathcal{L}_{I_t^{\text{SFR}}}\left(\frac{\tau r^\alpha}{a_t^{\text{far}} P_t - \tau a_t^{\text{near}} P_t}\right) \frac{f_{r_t}(r)}{\mathfrak{P}_t - \mathcal{P}_t^{\text{E}}} dr, \tag{5.16}$$

$$\kappa_t^{\text{F-E}}(\tau) = \int_{(P_t/\gamma_t)^{1/\alpha}}^{\infty} \exp\left(-\frac{\tau r^\alpha \sigma^2}{\beta_t a_t^{\text{far}} P_t - \tau a_t^{\text{near}} P_t}\right) \mathcal{L}_{I_t^{\text{SFR}}}\left(\frac{\tau r^\alpha}{\beta_t a_t^{\text{far}} P_t - \tau a_t^{\text{near}} P_t}\right) \frac{f_{r_t}(r)}{\mathcal{P}_t^{\text{E}}} dr, \tag{5.17}$$

where LT of SFR interference, $\mathcal{L}_{I_t^{\text{SFR}}}(\cdot)$, is given as

$$\mathcal{L}_{I_t^{\text{SFR}}}(x) = \exp\left\{-2\pi \sum_{j=1}^{T} \lambda_j \left(\frac{1}{\Delta_j} \int_{q_{j|t}}^{\infty} \frac{u}{1 + \frac{u^\alpha}{x(a_j^{\text{near}} P_j + \beta_j a_j^{\text{far}} P_j)}} du \right.\right. \tag{5.18}$$
$$\left.\left. + \frac{\Delta_j - 1}{\Delta_j} \int_{q_{j|t}}^{\infty} \frac{u}{1 + \frac{u^\alpha}{x(a_j^{\text{near}} P_j + a_j^{\text{far}} P_j)}} du \right)\right\}.$$

5.3. Numerical Results

For the numerical results, a heterogeneous cellular network with 2 BS tiers is considered ($T = 2$). The transmit powers of tier-1 and tier-2 BS's are $P_1 = 10$W and

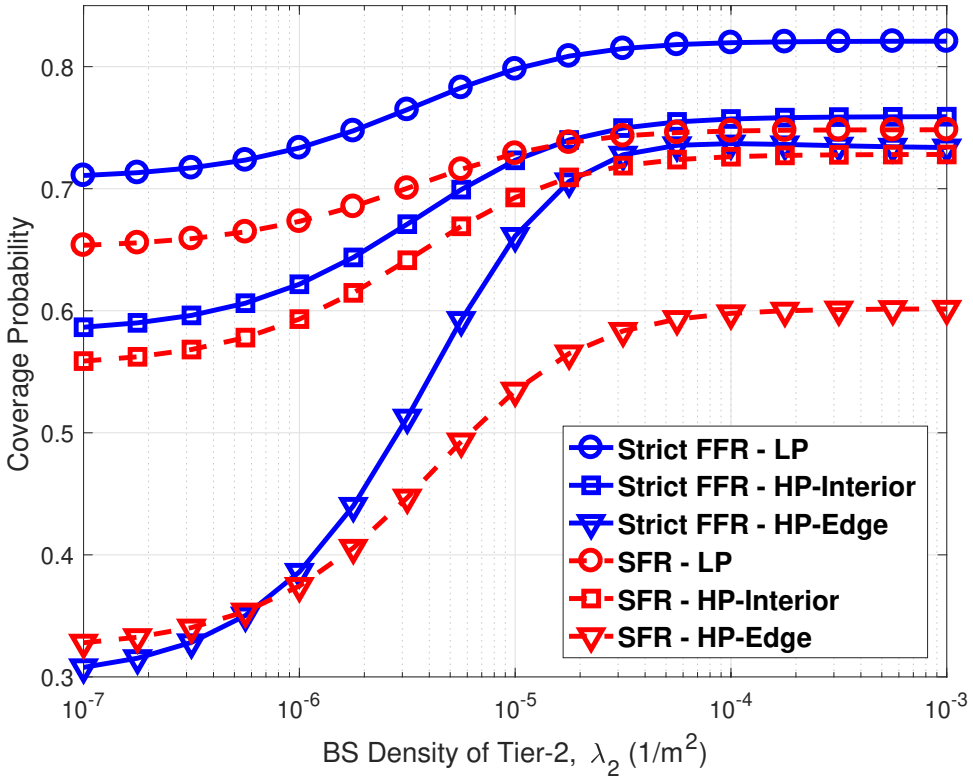

Figure 5.2. Coverage probabilities of near, far-interior, and far-edge users in open access.

$P_2 = 1$W. The power factors for both tiers are $a_t^{\text{near}} = 0.2$, $a_t^{\text{far}} = 0.8$, and $\beta_t = 0.5$. The BS density of tier-1 is 10^{-6} $1/m^2$, while tier 2 BS density varies in the x axis of the analysis figures. Besides, noise power is assumed to be $\sigma^2 = 10^{-7}$W, pathloss exponent is $\alpha = 3$, reuse factor is $\Delta_t = 3$, both of coverage thresholds are $\tau = \mathcal{T} = 0.1$, the number of interior and total RB's are $\mathrm{F_I} = 32$ and $\mathrm{F} = 50$, respectively. User grouping thresholds, φ_t and γ_t, are selected by ensuring $\mathfrak{P}_t = 0.5$ for all cases, $\mathcal{P}_t^{\mathrm{E}} = 0.5(1-\mathrm{F_I}/\mathrm{F})$ for Strict FFR, and $\mathcal{P}_t^{\mathrm{E}} = 0.5/\Delta_t$ for SFR.

Figure 5.2 shows a detailed comparison of coverage probabilities of near, far-interior, and far-edge users. For the open access, the coverage increase and converge to a level by the increased density of BS's. The convergence is obtained by the balance between increased interference and received power by high BS densities. Strict FFR/NOMA coexistence outperforms SFR/NOMA due to its suppression of interference.

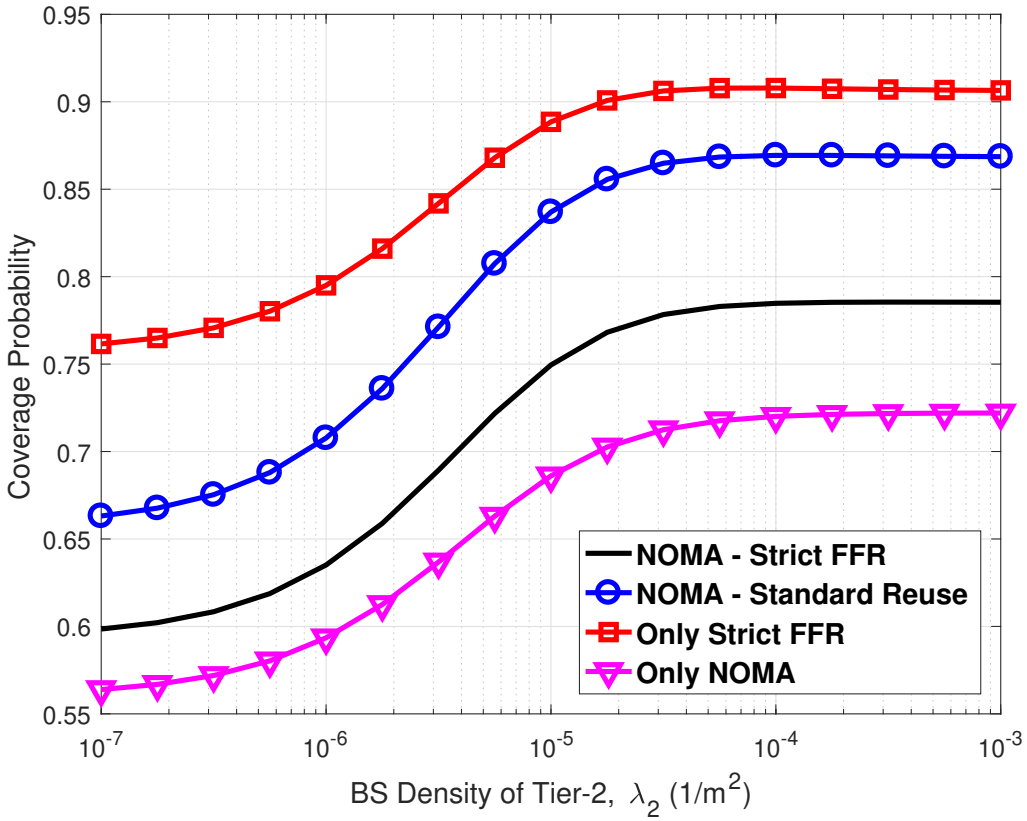

Figure 5.3. Coverage probability for strict FFR in open access NOMA network.

Figures 5.3 and 5.4 present coverage probabilities of different coexistence cases of NOMA with Strict FFR or SFR. The *NOMA-Strict FFR* and *NOMA-SFR* cases present all of user types. For the other cases, *NOMA-Standard Reuse* case only includes near and far-edge users, *Only Strict FFR* and *Only SFR* cases present original FFR without low power signal of near users, and *Only NOMA* case neglects any frequency reuse. One obvious fact is that coverage probability is better in *Only Strict FFR* and *Only SFR* cases, because this cases employ standard FFR without extra interference low power signal. *Only NOMA* case which represents NOMA scheme without edge frequency reuse, has poor performance due to the lack of inter-cell interference management. Comparing *NOMA-Standard Reuse* and *NOMA-Strict FFR* cases with *Only NOMA* case, we conclude that the coexistence of NOMA and FFR has potential coverage gains in denser networks of Strict FFR. However, NOMA-SFR coexistence provides poor coverage performance for denser networks, while it provides a performance peak for a BS density level. Both closed and open access NOMA-SFR results are observed

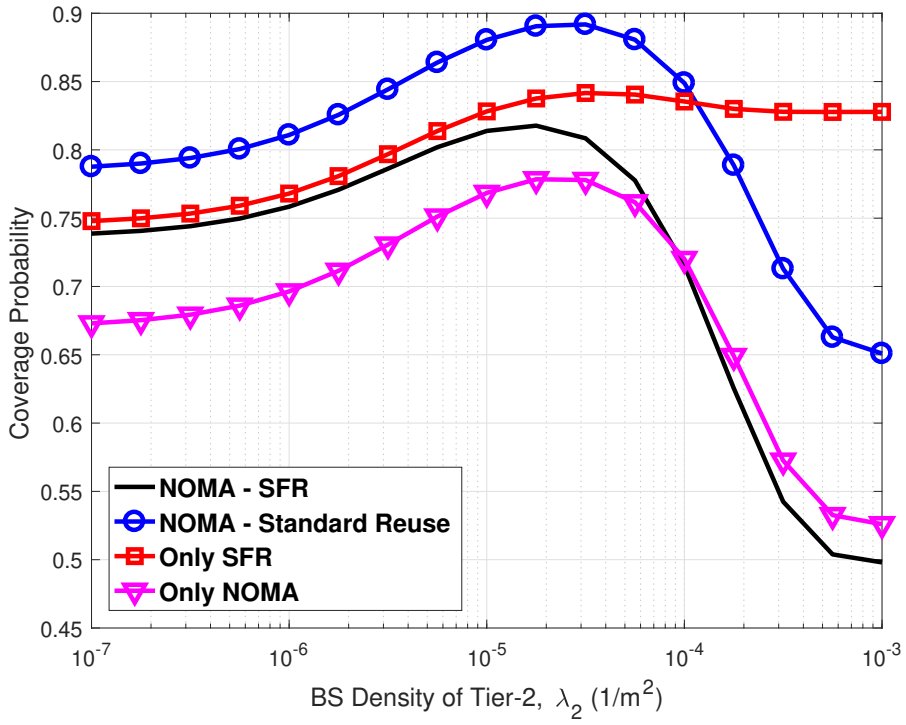

(a) Open access.

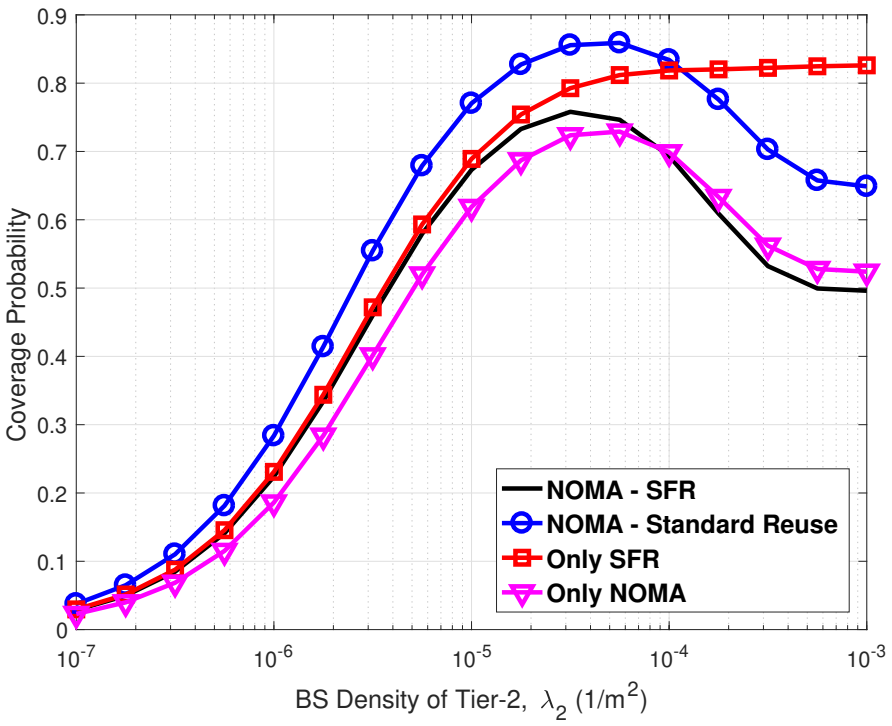

(b) Closed access ($t = 2$).

Figure 5.4. Coverage probability for SFR in NOMA network.

to follow the same poor performance for denser networks, while their spectral efficiency is expected to provide satisfactory performance due to full spectrum usage.

5.4. Conclusion

This chapter presents an extensive analysis of coexistence of NOMA with strict FFR and SFR techniques. Strict FFR and SFR techniques are modelled regarding avoidance of interference from K-tier heterogeneous network. The derivations of coverage probability are presented by including every frequency part of the spectrum. The numerical results reveal potential performance gain in denser heterogeneous networks.

6. COEXISTENCE OF NOMA AND OMA FOR INTERFERENCE MITIGATION

NOMA promises network capacity gain, while complicating experienced interference with the addition of intra-cell interference. The performance gain by conventional ICIC techniques in NOMA network is presented in Chapter 5. However, the performance of NOMA depends on a variety of different design parameters comparing to OMA. In NOMA, the optimization of power levels and pairing promise sum-rate or fairness gains, so can be used to improve edge user performance. On the other hand, serving only the edge users with OMA also provides potential edge user performance improvement as the intra-cell interference gets suppressed. In this chapter, we present a capacity analysis for NOMA-based heterogeneous networks. The capacity analysis in this chapter includes power level optimization and user pairing to provide more realistic results. A hybrid multiple access method, where interior users are served with NOMA and edge users are served with OMA, is proposed and compared with only OMA and only NOMA cases with power level optimization and pairing for a fair and extensive comparison.

In the rest of the chapter, SINR definitions are presented in Section 6.1. Capacity analysis of OMA, NOMA, and hybrid model is presented in Section 6.2, along with the pairing and power optimization methods. The numerical results are presented in Section 6.3 and the conclusion is presented in Section 6.4.

6.1. System Model

The analysis environment is considered as a 2-tier heterogeneous network with macro and pico (or femto) tiers (see Figure 6.1). The BS's of macro and pico tiers are randomly located as a PPP on an infinite 2D plane with respective deployment densities of λ_M and λ_P. In this work, the analysis will be limited to the pico-tier BS's, but it is straight-forward to obtain analysis for macro-tier by following the same

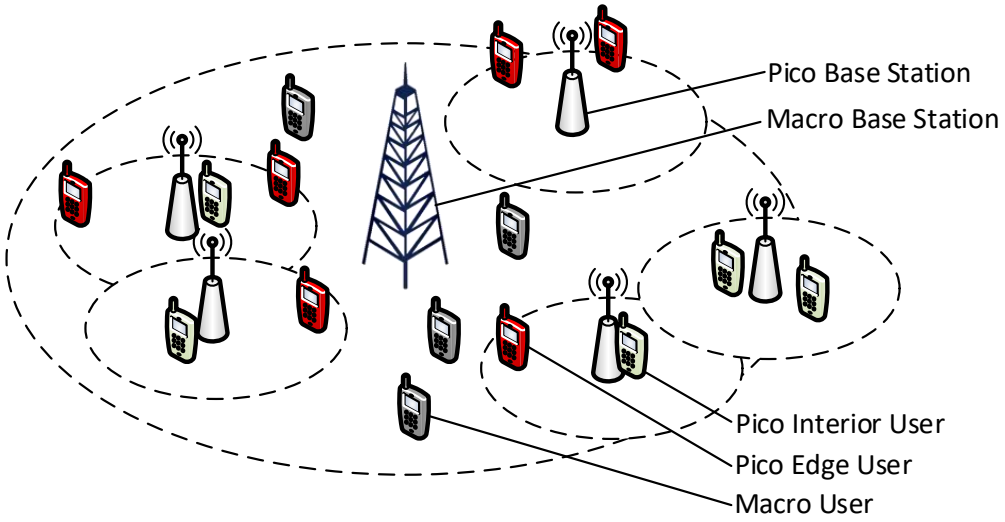

Figure 6.1. Topology of the heterogeneous network.

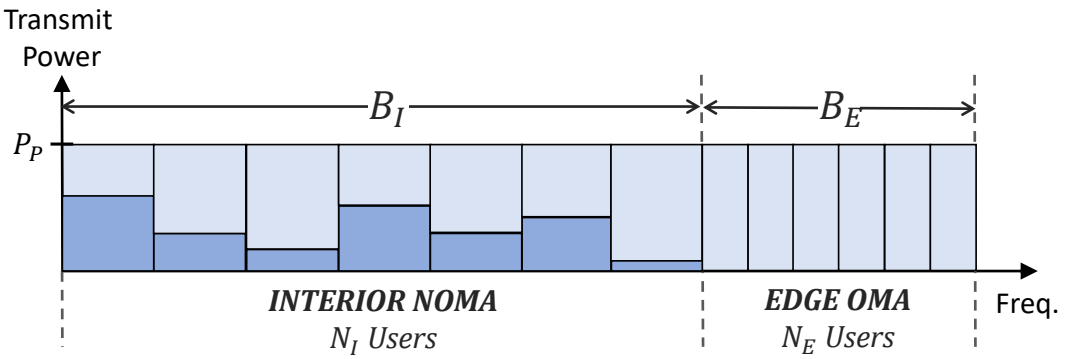

Figure 6.2. Hybrid model, NOMA and OMA serves in the same frequency spectrum.

methodology. Pico users are further grouped as interior and edge users, whose services differ depending on the spectrum usage strategy.

Three different spectrum usage strategies are considered; OMA, NOMA, and hybrid model. When conventional OMA or NOMA is deployed, all of the spectrum is utilized with the same spectrum access strategy to serve all kinds of users. In the hybrid model, the spectrum is divided into two parts for interior and edge users as shown in Figure 6.2. The interior users are served with NOMA to provide better rates to them. In contrast, the edge users are served with OMA to eliminate intra-cell interference and to obtain better signal quality. The users are assumed to have full buffer downlink traffic and the same amount of bandwidth. Power-domain NOMA is employed where the paired users are scheduled to the same RB with different power levels as in [43]. For

a fair comparison, OMA users are served with half the bandwidth of a single NOMA user.

The received SINR of a conventional OMA user is defined as

$$\Psi_{\mathrm{P}} = \frac{P_{\mathrm{P}} h r^{-\alpha}}{\sigma^2 + I_{P|P} + I_{M|P}}, \tag{6.1}$$

where P_{P} is the pico BS transmit power, h is the power gain of the small-scale channel coefficient of the user, r is the distance between serving BS and the user, α is the pathloss exponent, σ^2 is noise power, and $I_{P|P}$ and $I_{M|P}$ are the respective pico and macro interference experienced by a pico user as defined in Sections 2.1.1 and 2.1.2.

The SINR values of NOMA users are different from OMA users, since the signal of two users are superposed. Two NOMA users with superposed signals are referred to as near and far users depending on their distance to the serving BS. SIC technique is implemented in the receivers of the user devices to separate the signals [12]. To decode the signal of the far user, the near user's signal is treated as intra-cell interference. Considering that the i-th and j-th users are paired ($i < j$), the SINR of the j-th (far) user is defined similar to [58] as

$$\Psi_{i,j}^{\mathrm{F}} = \frac{a_{i,j}^{\mathrm{far}} P_{\mathrm{P}} h r^{-\alpha}}{\sigma^2 + a_{i,j}^{\mathrm{near}} P_{\mathrm{P}} h r^{-\alpha} + I_{P|P} + I_{M|P}}, \tag{6.2}$$

where $a_{i,j}^{\mathrm{near}}$ and $a_{i,j}^{\mathrm{far}}$ are user power coefficients of the i-th (near) user and the j-th (far) user, respectively. In equation (6.2), $a_{i,j}^{\mathrm{far}} P_{\mathrm{P}} h r^{-\alpha}$ term from numerator is the received power of far users signal and $a_{i,j}^{\mathrm{near}} P_{\mathrm{P}} h r^{-\alpha}$ term from denominator is the near user's signal, which is received by far user as intra-cell interference as defined in Section 2.1.3. To decode the signal of the near user, the near user should first decode the far user's signal, then decode its own signal. Considering that the i-th and j-th users are paired ($i < j$), the SINR of the j-th (far) user received by the i-th (near) user is given as

$$\Psi_{i,j}^{\mathrm{N(F)}} = \frac{a_{i,j}^{\mathrm{far}} P_{\mathrm{P}} h r^{-\alpha}}{\sigma^2 + a_{i,j}^{\mathrm{near}} P_{\mathrm{P}} h r^{-\alpha} + I_{P|P} + I_{M|P}} \tag{6.3}$$

and the SINR of the i-th (near) user are given as

$$\Psi_{i,j}^{\mathrm{N}} = \frac{a_{i,j}^{\mathrm{near}} P_{\mathrm{P}} h r^{-\alpha}}{\sigma^2 + I_{P|P} + I_{M|P}}. \tag{6.4}$$

The NOMA power coefficients are assumed to satisfy $a_{i,j}^{\mathrm{near}} + a_{i,j}^{\mathrm{far}} = 1$ rule to ensure fair comparison between OMA and NOMA.

6.2. Capacity Analysis

The users are assumed to be selecting the BS tier by measured RSRP values. Therefore, tier selection probabilities and the PDF of the distance to the serving BS is presented in Section 2.3.2. After the user connects the closest BS from the selected tier, the service of the users are differentiated by their SINR measurements. The users are first grouped as interior and edge users depending on their SINR measurements. The probability of the user to be selected as edge user is complementary to coverage probability, $\mathcal{P}_{\mathrm{P}}^{\mathrm{E}} = 1 - \kappa_{\mathrm{P}}(\gamma_{\mathrm{P}})$, as presented in Section 2.4.2. The coverage probability of pico users, $\kappa_{\mathrm{P}}(\cdot)$, can be obtained by following similar steps in Appendix A without including bandwidth and the transformation step from coverage probability to the capacity [90]. Hence, the probability of the user being selected as edge user is given as

$$\begin{aligned} \mathcal{P}_{\mathrm{P}}^{\mathrm{E}} &= 1 - \kappa_{\mathrm{P}}(\gamma_{\mathrm{P}}) \\ &= 1 - \int_0^{\infty} f_{r_P}(r) e^{-\frac{\gamma_{\mathrm{P}} r^{\alpha} \sigma^2}{P_{\mathrm{P}}} - \pi r^2 \left(\lambda_P \rho_1(\gamma_{\mathrm{P}}) + \lambda_M \rho_{z_{\mathrm{MP}}}\left(\gamma_{\mathrm{P}} \frac{P_{\mathrm{M}}}{P_{\mathrm{P}}}\right)\right)} dr. \end{aligned} \tag{6.5}$$

For a pico BS with N_{P} connected users, the average numbers of interior and edge users are calculated by multiplying probabilities in equation (6.5) with the number of users as

$$\begin{aligned} \bar{N}_{\mathrm{P}}^{\mathrm{I}} &= \lfloor \kappa_{\mathrm{P}}(\gamma_{\mathrm{P}}) N \rfloor_2, \\ \bar{N}_{\mathrm{P}}^{\mathrm{E}} &= \lfloor (1 - \kappa_{\mathrm{P}}(\gamma_{\mathrm{P}})) N \rfloor_1, \end{aligned} \tag{6.6}$$

where $\lfloor x \rfloor_y$ is round-down operator that gives the biggest integer value equal or lower than x divisible to y. The interior users are averaged to an even number since NOMA serves to even number of users.

After the user grouping, their coverage probability definitions are changed with the condition of being interior or edge. By the evaluation of Bayes' Theorem, the coverage probability of an interior and edge users are given as

$$\kappa_{\mathrm{P}}^{\mathrm{I}}(\tau) = \Pr\left(\Psi_{\mathrm{P}} > \tau \mid \Psi_{\mathrm{P}} > \gamma_{\mathrm{P}}\right) = \frac{\Pr\left(\Psi_{\mathrm{P}} > \tau, \Psi_{\mathrm{P}} > \gamma_{\mathrm{P}}\right)}{\Pr\left(\Psi_{\mathrm{P}} > \gamma_{\mathrm{P}}\right)} = \begin{cases} \frac{\kappa_{\mathrm{P}}(\tau)}{\kappa_{\mathrm{P}}(\gamma_{\mathrm{P}})} & \tau > \gamma_{\mathrm{P}}, \\ 1 & \tau \leq \gamma_{\mathrm{P}} \end{cases} \tag{6.7}$$

and

$$\begin{aligned} \kappa_{\mathrm{P}}^{\mathrm{E}}(\tau) &= \Pr\left(\Psi_{\mathrm{P}} > \tau \mid \Psi_{\mathrm{P}} < \gamma_{\mathrm{P}}\right) = \frac{\Pr\left(\Psi_{\mathrm{P}} > \tau\right) - \Pr\left(\Psi_{\mathrm{P}} > \tau, \Psi_{\mathrm{P}} > \gamma_{\mathrm{P}}\right)}{1 - \Pr\left(\Psi_{\mathrm{P}} > \gamma_{\mathrm{P}}\right)} \\ &= \begin{cases} \frac{\kappa_{\mathrm{P}}(\tau) - \kappa_{\mathrm{P}}(\gamma_{\mathrm{P}})}{1 - \kappa_{\mathrm{P}}(\gamma_{\mathrm{P}})} & \tau < \gamma_{\mathrm{P}}, \\ 1 & \tau \geq \gamma_{\mathrm{P}}. \end{cases} \end{aligned} \tag{6.8}$$

The order of the received SINR measurements of the users has significant importance for further analysis of NOMA users. In this work, the users are ordered from the highest to the lowest SINR values ($\Psi_1 > \Psi_2 > \cdots > \Psi_N$ for N users). In hybrid mode, only interior users are ordered by their SINR values. When $\tau > \gamma_{\mathrm{P}}$ condition holds, the coverage probability of the i-th SINR-ordered interior user is given as

$$\kappa_i(\tau) = \sum_{j=i}^{\bar{N}_{\mathrm{P}}^{\mathrm{I}}} \binom{\bar{N}_{\mathrm{P}}^{\mathrm{I}}}{j} \left(1 - \frac{\kappa_{\mathrm{P}}(\tau)}{\kappa_{\mathrm{P}}(\gamma_{\mathrm{P}})}\right)^{\bar{N}_{\mathrm{P}}^{\mathrm{I}} - j} \left(\frac{\kappa_{\mathrm{P}}(\tau)}{\kappa_{\mathrm{P}}(\gamma)}\right)^{j}, \tag{6.9}$$

which is obtained by CDF of ordered random variables in [97].

The capacity derivations include two different performance metrics; capacity of a BS and an average edge user for the three different spectrum usage strategies. Starting with the hybrid model, the capacity of a BS is given as

$$\begin{aligned} \mathbb{C}_{\mathrm{P.BS}}^{\mathrm{Hybrid}} &= 2\mathcal{B}_{\mathrm{I}}\mathrm{E}\left[\log(1+\Psi_{\mathrm{P}}) \mid \mathrm{NOMA}, \mathrm{Interior}\right] \\ &\quad + \mathcal{B}_{\mathrm{E}}\mathrm{E}\left[\log\left(1+\Psi_{\mathrm{P}}\right) \mid \mathrm{OMA}, \mathrm{Edge}\right] \\ &\cong \frac{2\mathcal{B}_{\mathrm{I}}}{\bar{N}_{\mathrm{P}}^{\mathrm{I}}} \sum_{(i,j)\in\mathbb{P}\left(\bar{N}_{\mathrm{P}}^{\mathrm{I}}\right)} \left[\mathcal{C}_{i,j}^{\mathrm{near}} + \mathcal{C}_{i,j}^{\mathrm{far}}\right] + \mathcal{B}_{\mathrm{E}}\mathcal{C}^{\mathrm{OMA}}, \end{aligned} \tag{6.10}$$

which is the sum of the total interior and edge capacities. In equation (6.10), $\mathcal{B}_{\mathrm{I}}$ and $\mathcal{B}_{\mathrm{E}}$ are bandwidth parts for interior and edge service (see Figure 6.2), $\mathbb{P}(\cdot)$ is the set of

user pairs, $\mathcal{C}_{i,j}^{\text{near}}$ is NOMA near user capacity of the i-th interior user paired with the j-th interior user, $\mathcal{C}_{i,j}^{\text{far}}$ is NOMA far user capacity of the j-th interior user paired with the i-th interior user, and $\mathcal{C}^{\text{OMA}}$ is the capacity of an edge OMA user. The expected value of the total interior user capacity is multiplied by 2 since the NOMA users reuse the same bandwidth twice (see Figure 6.2) by their superposed signals. Each BS serves to N_{P} users, and $\bar{N}_{\text{P}}^{\text{I}}$ and $\bar{N}_{\text{P}}^{\text{E}}$ values are calculated by equation (6.6). As the number of users is constant, the total interior capacity is approximated by the summation of capacities of interior users.

The near user first decodes far user's signal as a first step then decodes its own signal. $\log(1+\Psi_{i,j}^{\text{N(F)}}) \geq \log(1+\Psi_{i,j}^{\text{F}})$ condition should hold to guarantee that the near user correctly decodes far user's signal and achieves the same bit-rate in the first step of decoding. As the NOMA users are ordered by their respective SINRs, the near user is always able to decode far user's signal [52]. By the definitions in equations (6.2) and (6.3), $\log(1+\Psi_{i,j}^{\text{N(F)}})$ is always equal to or greater than $\log(1+\Psi_{i,j}^{\text{F}})$. For the capacity analysis, we employ the integral transformation from the coverage probability such that

$$\text{E}[\log(1+\Psi)] = \int_0^\infty \frac{\Pr(\Psi > \tau)}{\tau+1} d\tau, \tag{6.11}$$

which is widely employed in the stochastic geometry literature as in [90]. Therefore, the capacity of the i-th NOMA near user paired with the j-th far user is given as

$$\begin{aligned} \mathcal{C}_{i,j}^{\text{near}} &= \text{E}\left[\log(1+\Psi_{i,j}^{\text{N}}) \mid \Psi_{\text{P}} > \gamma_{\text{P}}\right] \\ &= \int_0^\infty \kappa_i\left(\frac{\tau}{a_{i,j}^{\text{near}}}\right)\frac{1}{\tau+1} d\tau, \end{aligned} \tag{6.12}$$

where $\Psi_{\text{P}} > \gamma_{\text{P}}$ condition stands for the interior user and the argument of $\kappa_i(\cdot)$ function is obtained by moving τ and $a_{i,j}^{\text{near}}$ terms to the right-hand side of $a_{i,j}^{\text{near}} > \tau$ condition. Moreover, the capacity of the j-th NOMA far user paired with the i-th near user is given as

$$\mathcal{C}_{i,j}^{\text{far}} = \text{E}\left[\log(1+\Psi_{i,j}^{\text{F}}) \mid \Psi_{\text{P}} > \gamma_{\text{P}}\right] \tag{6.13}$$

$$= \int_0^{\frac{a_{i,j}^{\text{far}}}{a_{i,j}^{\text{near}}}} \kappa_j \left(\frac{\tau}{a_{i,j}^{\text{far}} - a_{i,j}^{\text{near}} \tau} \right) \frac{1}{\tau + 1} d\tau,$$

where the argument of $\kappa_i(\cdot)$ function is obtained by leaving τ, $a_{i,j}^{\text{near}}$, and $a_{i,j}^{\text{far}}$ terms on the right-hand side of $a_{i,j}^{\text{far}} > \tau$ condition. The integral in equation (6.13) has a constant upper limit, since $\kappa_i(\cdot)$ is not applicable for a negative argument. The capacity of an OMA user is given as

$$\begin{aligned} \mathcal{C}^{\text{OMA}} &= \text{E}\left[\log(1 + \Psi_{\text{P}}) \mid \Psi_{\text{P}} < \gamma_{\text{P}}\right] \\ &= \int_0^{\infty} \frac{\kappa_{\text{P}}^{\text{E}}(\tau)}{\tau + 1} d\tau, \end{aligned} \tag{6.14}$$

where $\Psi_{\text{P}} < \gamma_{\text{P}}$ condition stands for the edge user.

The average edge user capacity in hybrid mode, is given as

$$\begin{aligned} \mathbb{C}_{\text{Edge P.User}}^{\text{Hybrid}} &= \text{E}\left[\frac{\mathcal{B}_{\text{E}}}{N_{\text{P}}^{\text{E}}} \log\left(1 + \Psi_{\text{P}}\right) \mid \Psi_{\text{P}} < \gamma_{\text{P}} \right] \\ &\cong \frac{\mathcal{B}_{\text{E}}}{\bar{N}_{\text{P}}^{\text{E}}} \mathcal{C}^{\text{OMA}}, \end{aligned} \tag{6.15}$$

which is implemented as an approximation by $\bar{N}_{\text{P}}^{\text{E}}$ users.

When the BS works in NOMA mode, its capacity is given as

$$\begin{aligned} \mathbb{C}_{\text{P.BS}}^{\text{NOMA}} &= 2\mathcal{B}\, \text{E}\left[\log\left(1 + \Psi_{\text{P}}\right) \mid \text{NOMA}\right] \\ &\cong \frac{2\mathcal{B}}{N_{\text{P}}} \sum_{(i,j) \in \mathbb{P}(N_{\text{P}})} \left[\mathcal{C}_{i,j}^{\text{near}}(\gamma_{\text{P}} \to 0) + \mathcal{C}_{i,j}^{\text{far}}(\gamma_{\text{P}} \to 0) \right], \end{aligned} \tag{6.16}$$

where equations (6.12) and (6.13) are employed with $\gamma_{\text{P}} \to 0$ condition, because all users are NOMA users. Similarly, the average capacity of the edge users in the NOMA mode is given as

$$\begin{aligned} \mathbb{C}_{\text{Edge P.User}}^{\text{NOMA}} &= \text{E}\left[\frac{2\mathcal{B}}{N_{\text{P}}} \log\left(1 + \Psi_{\text{P}}\right) \mid \text{NOMA}, \text{Edge} \right] \\ &\cong \frac{2\mathcal{B}}{N_{\text{P}}\, \bar{N}_{\text{P}}^{\text{E}}} \sum_{j=\bar{N}_{\text{P}}^{\text{I}}+1}^{\bar{N}_{\text{P}}^{\text{I}}+\bar{N}_{\text{P}}^{\text{E}}} \mathcal{C}_{i,j}^{\text{far}}(\gamma_{\text{P}} \to 0), \end{aligned} \tag{6.17}$$

which is an approximation obtained by averaging the capacities of the furthest $\bar{N_E}$ users.

In OMA mode, the capacity of the BS is expressed as

$$\mathbb{C}_{\text{P.BS}}^{\text{OMA}} = \text{E}\left[\mathcal{B}\log\left(1+\Psi_{\text{P}}\right) \mid \text{OMA}\right] = \mathcal{B}\mathcal{C}^{\text{OMA}}(\gamma_{\text{P}} \to \infty), \tag{6.18}$$

where equation (6.14) is employed with $\gamma_{\text{P}} \to \infty$ condition, because all users are OMA users. Lastly, the average capacity of the edge users in OMA mode is given as

$$\mathbb{C}_{\text{Edge P.User}}^{\text{OMA}} = \text{E}\left[\frac{\mathcal{B}_{\text{E}}}{N_{\text{P}}^{\text{E}}}\log\left(1+\Psi_{\text{P}}\right)\middle|\text{OMA, Edge}\right] \cong \frac{\mathcal{B}_{\text{E}}}{\bar{N}_{\text{P}}}\mathcal{C}^{\text{OMA}}, \tag{6.19}$$

which is an approximation obtained by division by the $\bar{N}_{\text{P}}^{\text{E}}$ value.

6.2.1. Pairing

The type of pairing is defined by the pairing set $\mathbb{P}(\cdot)$. Two types of pairing methods are employed to illustrate a competent comparison on fairness and sum-rate trade-off.

6.2.1.1. Near-to-Far Pairing. NF pairing is considered to be an optimal for the maximization of BS sum-rate [49]. In this method, the lowest and highest SINR users are paired, then the second lowest and the second highest SINR users are paired, and pairing is continued until the last pair of users in this order. The pairing set is given as

$$\mathbb{P}(n) = \left\{(i,j) \mid j = n+1-i; i = 1,2,\ldots,\frac{n}{2}\right\} \tag{6.20}$$

for n users.

6.2.1.2. Near-to-Near Pairing. NN pairing is an another known method given in [58]. According to this method, the first half of the users are grouped as near users, and the others are grouped as far users. The nearest user of the near user group and the

nearest user of the far-user group are paired. The pairing set is given as

$$\mathbb{P}(n) = \left\{(i,j) \mid j = i + \frac{n}{2}; i = 1, 2, \ldots, \frac{n}{2}\right\} \tag{6.21}$$

for n users.

6.2.2. Power Level Optimization

The power levels of the paired users have significant importance on the performance of NOMA. In this work, we employ two power optimization solutions to reveal performance trade-offs of NOMA; one aiming to maximize the fairness and the other the sum-rate. The optimization problems are modelled within two paired users to optimize $a_{i,j}^{\text{near}}$ and $a_{i,j}^{\text{far}}$ power coefficients. As their summation equals to 1 (Section 2.1.3), they are represented as

$$\begin{aligned} a_{i,j}^{\text{near}} &= a, \\ a_{i,j}^{\text{far}} &= 1 - a \end{aligned} \tag{6.22}$$

in this section for ease of presentation. As the power allocated to far user's signal is higher, the optimization problems are solved to find optimal a (a^*) in the feasible region given as

$$0 \leq a \leq \frac{1}{2}. \tag{6.23}$$

6.2.2.1. Maximum Fairness. To provide the maximum fairness, the problem is modeled as

$$\max_{a} \left[\min\left\{\mathcal{C}_{i,j}^{\text{near}}(a), \mathcal{C}_{i,j}^{\text{far}}(a)\right\}\right] \tag{6.24}$$

to find the optimal a value that maximizes the minimum capacity among the paired users. The derivations for the optimal solution is presented in Appendix F, where the optimal solution is achieved by

$$\mathcal{C}_{i,j}^{\text{near}}(a^*) = \mathcal{C}_{i,j}^{\text{far}}(a^*) \tag{6.25}$$

condition. a^* that achieves the maximum fairness is found by solving equation (6.25) by the root finding algorithms.

6.2.2.2. Maximum Sum-Rate. The maximum sum-rate problem is given as

$$\begin{aligned} \max_{a} \quad & \mathcal{C}_{i,j}^{\text{near}}(a) + \mathcal{C}_{i,j}^{\text{far}}(a), \\ \text{subject to} \quad & \mathcal{C}_{i,j}^{\text{near}}(a) \geq \epsilon_{6.1}, \\ & \mathcal{C}_{i,j}^{\text{far}}(a) \geq \epsilon_{6.1}, \end{aligned} \tag{6.26}$$

where $\epsilon_{6.1}$ is a constant lower bound for the minimum capacity for a user. The derivations for the optimal solution is introduced in Appendix G, where the optimal solution is achieved by

$$\mathcal{C}_{i,j}^{\text{far}}(a^*) = \epsilon_{6.1}, \tag{6.27}$$

where a^* can be obtained by the root finding algorithms, similar to maximum fairness problem.

Table 6.1. General parameters for numerical results.

Parameters	Values
Density of Macro BS, λ_M	5×10^{-6} [BS/m^2]
Density of Pico BS, λ_P	5×10^{-5} [BS/m^2]
BS transmit power, P_{M} / P_{P}	40 / 1 [Watts]
Edge probability, $\mathcal{P}_{\text{P}}^{\text{E}}$	0.2
Bias, $\mathfrak{b}$	2
Pathloss exponent, α	3
Noise power, σ^2	10^{-10} [Watts]
Bandwidth, $\mathcal{B}$	20 MHz ($\times \log_2(e)$)
Interior and edge bandwidths, $\mathcal{B}_{\text{I}}$ / $\mathcal{B}_{\text{E}}$	16 / 4 MHz ($\times \log_2(e)$)
Number of users per BS, F	50
Average int. and edge users per BS, $\bar{N}_{\text{P}}^{\text{I}}$ / $\bar{N}_{\text{P}}^{\text{E}}$	40 / 10
Minimum user-rate for sum-rate opt., $\epsilon_{6.1}$	0.005 / 0.0005

6.3. Numerical Results

The parameters of the analysis environment are given in Table 6.1. Even though the analysis is limited to the performance of pico users, macro and pico tier parameters are provided for the interference model. γ_{P} threshold is numerically calculated for every instance by the inverse of $\mathcal{P}_{\mathrm{P}}^{\mathrm{E}}$ definition in equation (6.5) for given edge probability from the table. Then, $\bar{N}_{\mathrm{P}}^{\mathrm{I}}$ and $\bar{N}_{\mathrm{P}}^{\mathrm{E}}$ are as calculated by equation (6.6). $\mathcal{B}_{\mathrm{I}}$ and $\mathcal{B}_{\mathrm{E}}$ values are selected to keep a fair bandwidth usage between the interior and edge users with the consideration of the edge probability ($\mathcal{B}_{\mathrm{E}} = \mathcal{B}\mathcal{P}_{\mathrm{P}}^{\mathrm{E}}$).

Prior to the system level analysis, the CDFs, $\mathcal{F}_{\Psi_{\mathrm{P}}}(\tau)$, of user SINRs are shown in Figure 6.3. In a BS with $N_{\mathrm{P}} = 50$ users, 4 prominent users are selected to illustrate the general effect of power optimization and pairing methods. The SINRs of OMA users are shown in Figure 6.3(a) where the user's signal is not manipulated by power coefficients. As the power coefficients degrade the signal quality, the OMA user CDFs provide an upper bound to the NOMA user CDFs. Figures 6.3(b) and 6.3(c) show the SINR CDFs with the sum-rate optimization. In these plots, far users (26 and 50) have the same level of SINR due to the minimum capacity limit $\epsilon_{6.1}$. In the sum-rate optimization, the SINR of user 1 in the NF pairing is worse than its counterpart in the NN pairing, since it compensates the capacity of user 50 to $\epsilon_{6.1}$ by reducing its performance. When user 1 is paired with user 26 in the NN pairing, user 1 gets better SINR, since the compensation of capacity of user 26 is easier. Figures 6.3(d) and 6.3(e) show the SINRs under the fairness optimization, where paired users provide the same capacity by optimized power levels. In Figure 6.3(d), the SINRs of the paired users are around the same level, where near user SINRs are significantly degraded to compensate for the far user performance. In Figure 6.3(e), SINR or user 1 is significantly reduced to compensate for the performance of the worst performing user (user 50). From these results, one important design aspect of the system emerges as the selection of the users who are paired with the worst performing users (user 50 in Figure 6.3) to compensate for their performance.

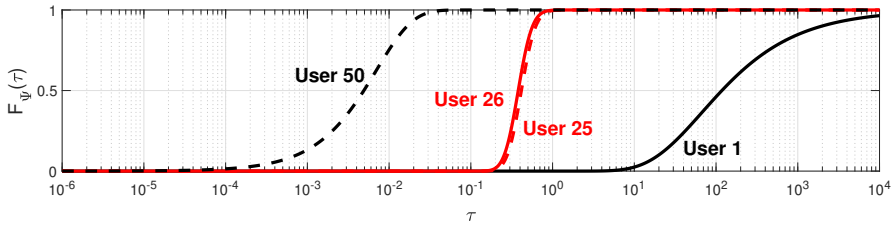

(a) OMA.

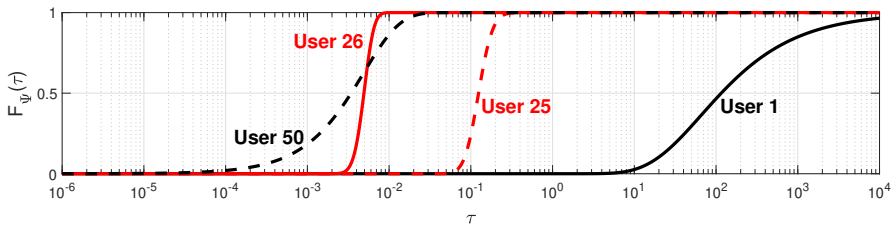

(b) NOMA, maximum sum-rate, NN pairing: (1,26), (25,50).

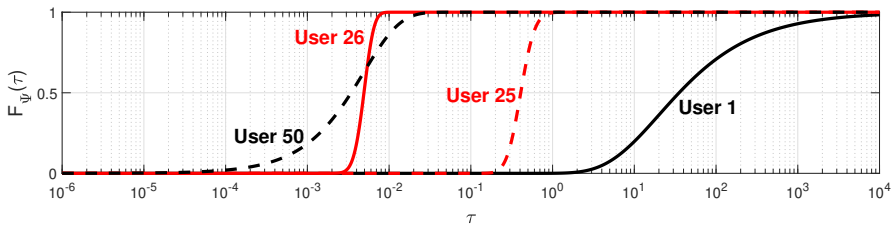

(c) NOMA, maximum sum-rate, NF pairing: (1,50), (25,26).

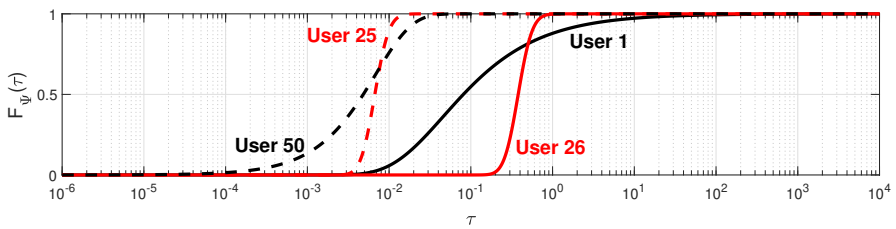

(d) NOMA, maximum fairness, NN pairing: (1,26), (25,50).

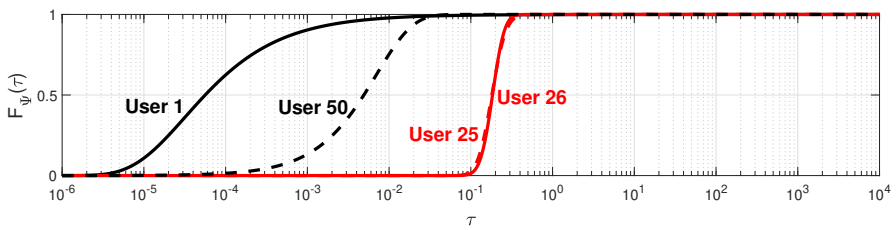

(e) NOMA, maximum fairness, NF pairing: (1,50), (25,26).

Figure 6.3. CDFs of effective SINR for user 1, 25, 26, and 50 for different power optimization and pairing alternatives (open access, $N = 50$, and $\epsilon_{6.1} = 0.005$).

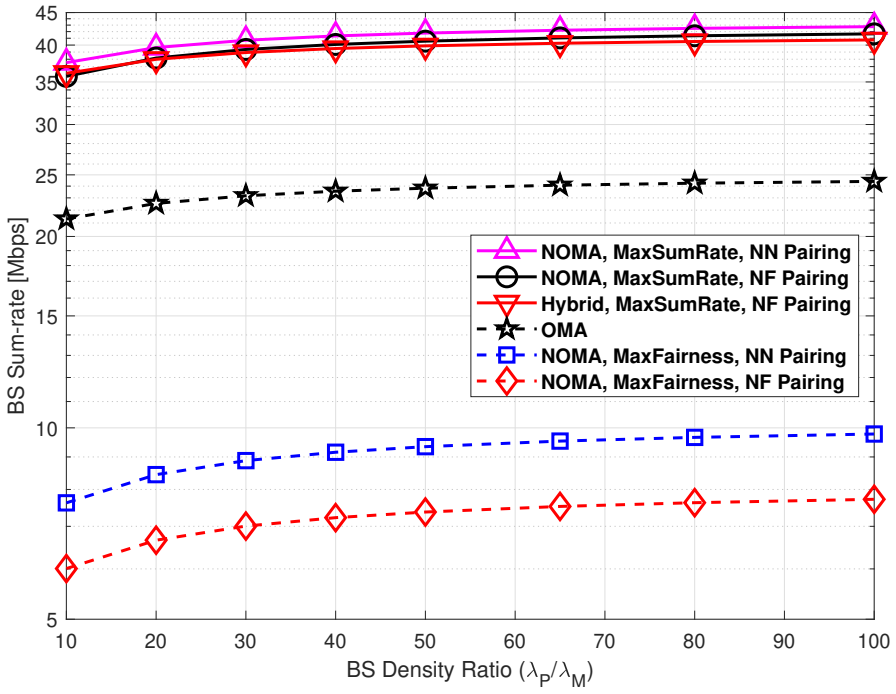

(a) BS sum-rate.

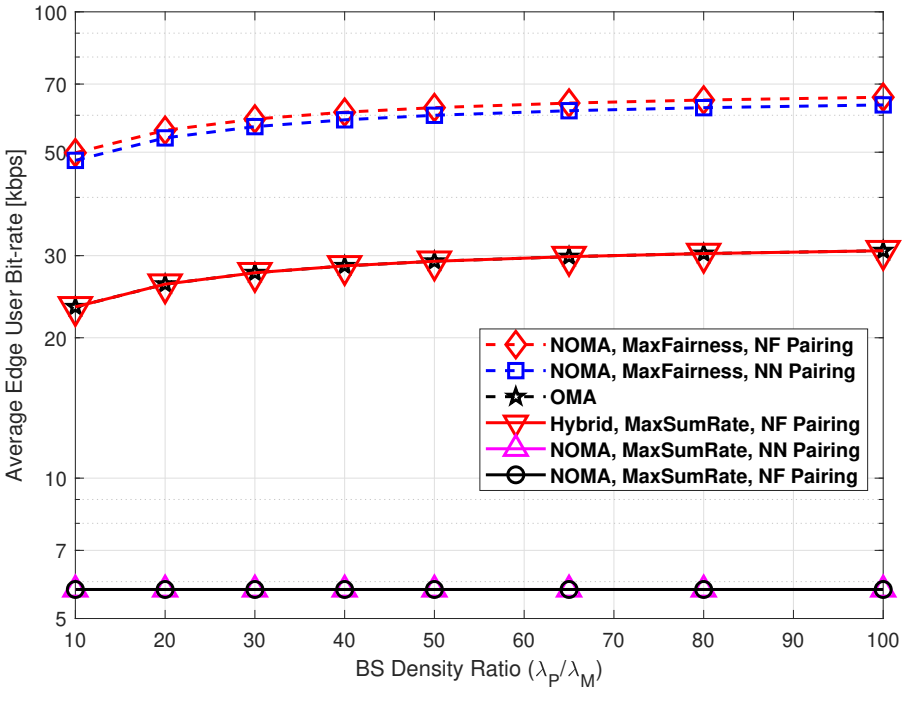

(b) Average edge user bit-rate.

Figure 6.4. Capacity comparison of hybrid model for different BS density ratios in open access network ($\epsilon_{6.1} = 0.005$).

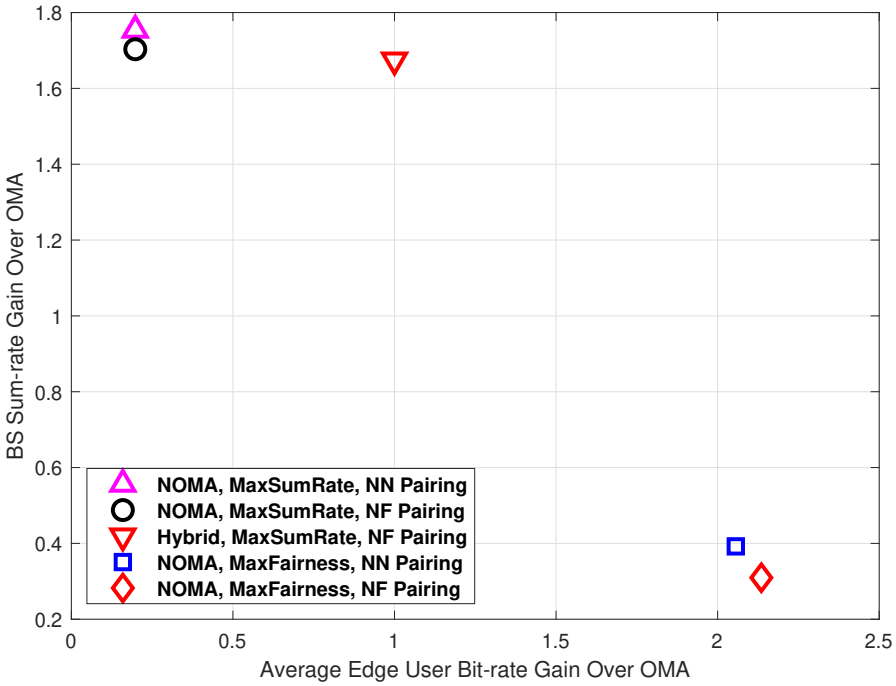

Figure 6.5. Capacity gain over OMA for constant BS density ratio ($\lambda_P/\lambda_M = 50$) in open access network.

Capacity comparison of hybrid model in an the open access network for changing BS density ratio are shown in Figures 6.4 and 6.5. The different values of BS density ratio on the x-axis are provided by keeping macro BS density constant (see Table 6.1) and changing pico BS density. In Figure 6.4(a), maximum sum-rate curves provide a lot better performance compared to the others. Among maximum sum-rate curves, hybrid model follows other NOMA curves with a similar performance. Maximum fairness curves provide a lot worse sum-rate compared to the other curves. NF pairing for maximum fairness results in the worst sum-rate, since its best users compensate for the worst user's signal (also illustrated in Figure 6.3(e)). In Figure 6.4(b), maximum fairness curves provide better edge performance, where NF pairing improves the performance a little over the NN pairing. Hybrid model and OMA curves overlap, since they serve edge users with OMA. Edge user performance of maximum sum-rate curves remain constant, since both provide constant rate of $\epsilon_{6.1}$ to the far users. In Figure 6.5, comparison of the capacity gains provides insight on the flexibility of NOMA to outperform OMA in different performance metrics. In the open access system, NOMA can provide around 1.8 times sum-rate gain and over 2 times average edge capacity gain

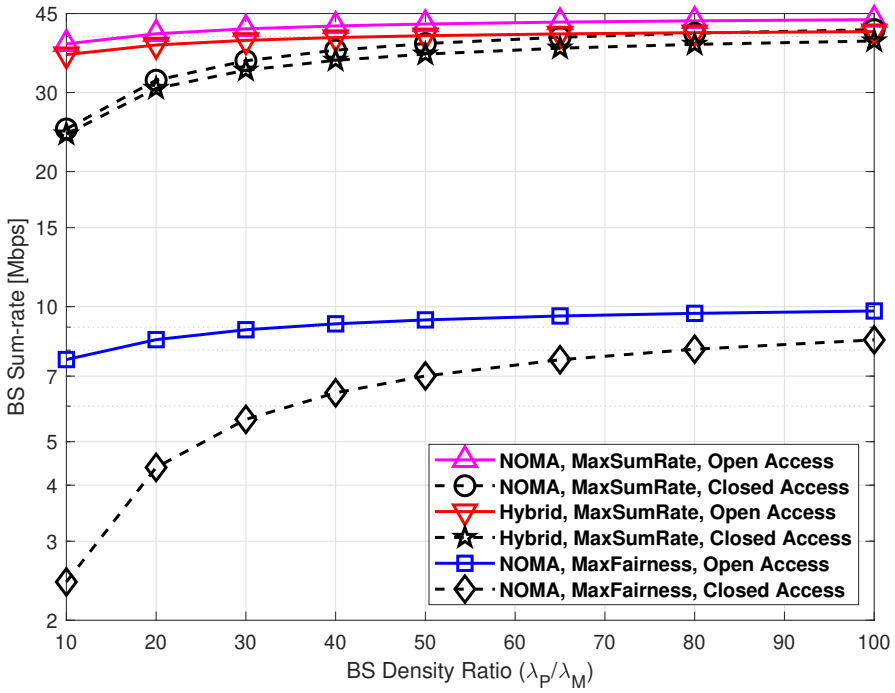

(a) BS sum-rate.

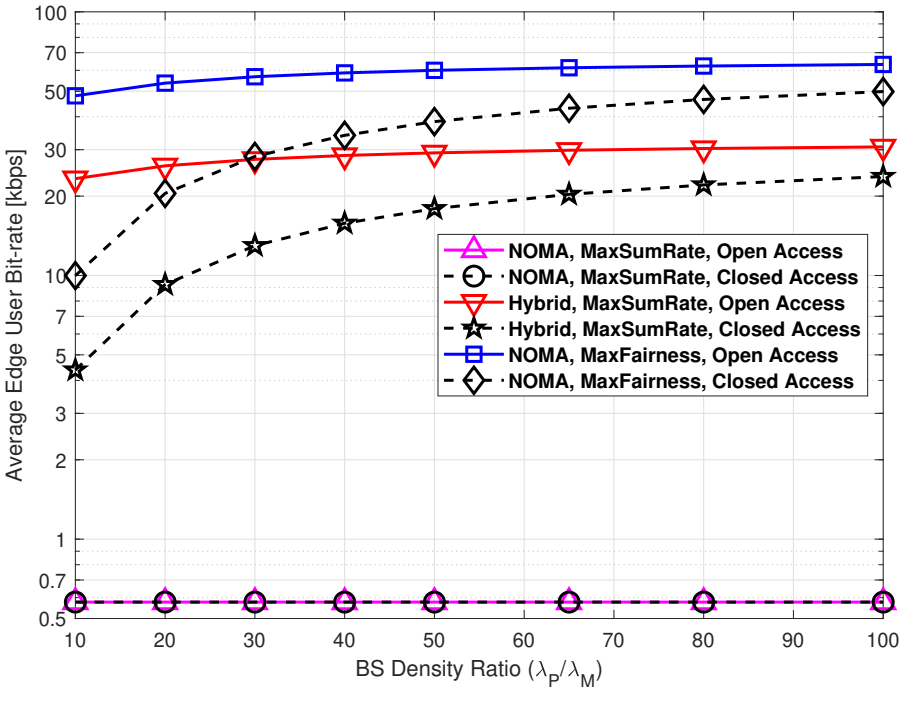

(b) Average edge user bit-rate.

Figure 6.6. Capacity comparison of open and closed access networks for different BS density ratios (NN pairing, $\epsilon_{6.1} = 0.0005$).

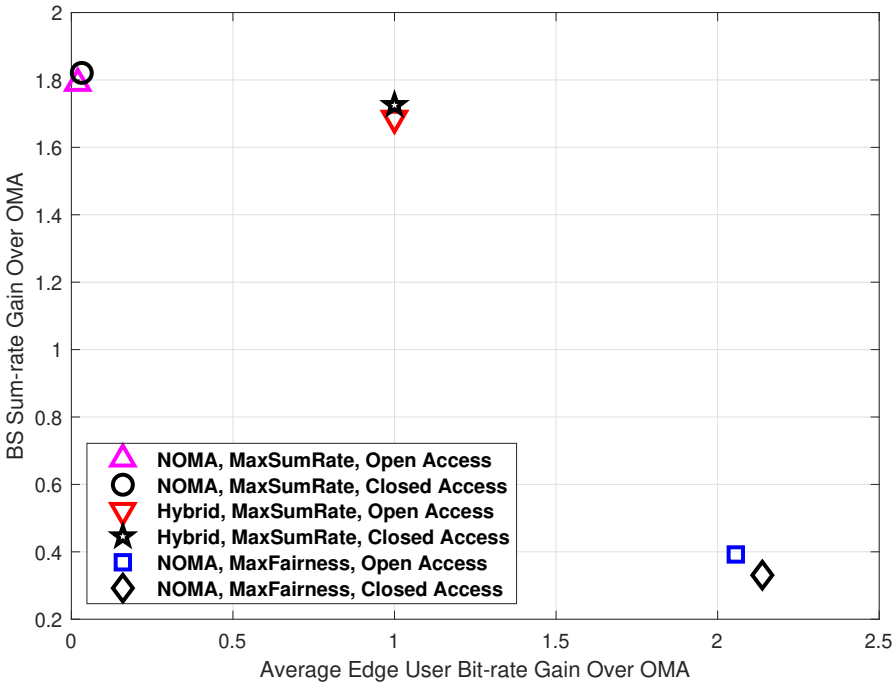

Figure 6.7. Comparison of open and closed access networks by capacity gain over OMA for constant BS density ($\lambda_P/\lambda_M = 50$).

in different operating instances. However, Hybrid model achieves a similar sum-rate performance to the NOMA model in in terms of maximum sum-rate without reducing the edge user performance.

The comparison of capacity results between the open and closed access networks is presented in Figure 6.6. In contrast to the previous results, $\epsilon_{6.1}$ is selected to be a lower value (0.0005) as closed access network cannot satisfy higher capacity requirements for distant users. In Figures 6.6(a) and 6.6(b), the capacity results are given for different BS densities. Pico users are observed to have lower BS and edge capacity for low BS density ratios due to high interference of macro BS's. For higher BS density ratios, the capacity results in closed access converge to the capacity results of open access, because users are served by the nearer pico BS's. Hybrid model is observed to achieve close performance to max. sum-rate curves of NOMA in Figure 6.6(a), and to max. fairness curves of NOMA in Figure 6.6(b). In Figure 6.7, the capacity gains of open and closed access networks employing NOMA are compared. OMA provides poor capacity for closed access user due to high interference. Closed access network is observed to

provide one-step better capacity gain for NOMA over OMA, since OMA suffers more from high interference in closed access. Hybrid model, similar to Figure 6.5, provides close performance to max. sum-rate NOMA, while achieving the same performance with OMA for edge users in Figure 6.7.

6.4. Conclusion

In this chapter, a stochastic geometry analysis of a heterogeneous network where users are served with a hybrid spectrum access model (NOMA and OMA can be employed in the same spectrum band) is presented in this work. The analysis include two alternative power optimization and pairing methods. The numerical results indicate that NOMA can decently improve the edge user performance by power optimization with the cost of reduced sum-rate. The results also indicate that the hybrid model provides adequate edge user performance while providing a sum-rate similar to that achieved by the only NOMA case.

7. UPLINK DECODER DESIGN FOR NOMA WITH POWER CONSTRAINTS

The performance of uplink NOMA is affected by intra-cell interference. For SIC-based receiver in BS, the performance of the firstly decoded user is degraded by intra-cell interference caused by the signal of the other user in the same pair. Therefore, the selection of decoding order potentially avoids the interference for the selected user among the paired users. Joint optimization of decoding order and transmit powers of users is essential for achieving satisfactory sum-rate. If the user with low channel power will be decoded first, its received power should guarantee a certain level of power to ensure its bit-rate demand. This contradicts with low EC KPI for uplink NOMA in [16]. In this chapter, an optimization problem of user transmit power and decoding order is presented with closed-form solution. By the solution to this problem, thresholds on bit-rate and power constraints of the user is derived for the feasibility of switching decoding order.

For the rest of the chapter, the signal model is presented in Section 7.1, the power level optimization is presented in Section 7.2, the decoding order optimization and power limit are presented in Section 7.3, numerical results are presented in Section 7.4, and conclusions are presented in Section 7.5.

7.1. System Model

A wireless environment consists of a single BS and randomly distributed users is considered. The users are assumed to be homogeneously distributed in a disc coverage area, where the BS is located in the center. Each user is served through a channel with power $g_i = hr^{-\alpha}$ where h is small-scale channel power by Rayleigh fading, r is distance between user and BS, and α is pathloss exponent. Two users are scheduled to each RB. The users are referred as user 1 and user 2 for the rest of the chapter, where user 1 is the with stronger channel power. Under configurable decode order, their optimal

sum-rate is given as

$$\max_{p_1,p_2} \left\{ \mathcal{C}_{1\to2}^{\text{Up.RB}}, \mathcal{C}_{2\to1}^{\text{Up.RB}} \right\}, \tag{7.1}$$

where p_1 and p_2 are respective transmit powers of user 1 and 2, $\mathcal{C}_{1\to2}^{\text{Up.RB}}$ is sum-rate when user 1 is decoded before user 2, and $\mathcal{C}_{2\to1}^{\text{Up.RB}}$ is vice versa. Sum-rate definitions by determined are defined as

$$\mathcal{C}_{1\to2}^{\text{Up.RB}} = \log_2\left(1+\Phi_1^{1\to2}\right) + \log_2\left(1+\Phi_2^{1\to2}\right), \tag{7.2}$$

$$\mathcal{C}_{2\to1}^{\text{Up.RB}} = \log_2\left(1+\Phi_1^{2\to1}\right) + \log_2\left(1+\Phi_2^{2\to1}\right), \tag{7.3}$$

where $\Phi_1^{1\to2}$ and $\Phi_2^{1\to2}$ are respective SINRs of user 1 and 2 for decode order $(1\to2)$, $\Phi_1^{2\to1}$ and $\Phi_2^{2\to1}$ are respective SINRs of user 1 and 2 for decode order $(2\to1)$, and σ^2 is the noise power. The uplink SINR definitions are presented in Section 2.2. Before achieving global optimal solution for Problem (7.1), $\mathcal{C}_{1\to2}^{\text{Up.RB}}$ by transmit powers is presented in the next section.

7.2. Transmit Power Optimization $(1\to2)$

Optimal transmit powers for maximum sum-rate are presented for the pre-defined decoding order $(1\to2)$ in this section. Each user is assumed to have its own bit-rate demand and transmit power constraint. The definition for the optimization problem is given as

$$\max_{p_1,p_2} \quad \log_2\left(1+\frac{p_1g_1}{\sigma^2+p_2g_2}\right) + \log_2\left(1+\frac{p_2g_2}{\sigma^2}\right) \tag{7.4a}$$

$$\text{subject to} \quad \log_2\left(1+\frac{p_1g_1}{\sigma^2+p_2g_2}\right) \geq D_1 \tag{7.4b}$$

$$\log_2\left(1+\frac{p_2g_2}{\sigma^2}\right) \geq D_2 \tag{7.4c}$$

$$p_1 \leq p_1^{\max} \tag{7.4d}$$

$$p_2 \leq p_2^{\max}, \tag{7.4e}$$

where D_1 and D_2 are respective bit-rate demands and $p_1^{\max}$ and $p_2^{\max}$ are respective transmit power constraints for users 1 and 2.

The solution for Problem (7.4) is obtained by KKT conditions [96]. The Lagrangian function for the problem is given as

$$\begin{aligned} L = & -\log_2\left(1+\tfrac{p_1 g_1}{\sigma^2+p_2 g_2}\right) - \log_2\left(1+\tfrac{p_2 g_2}{\sigma^2}\right) + v_{7.1}\left(2^{D_1}-1-\tfrac{p_1 g_1}{\sigma^2+p_2 g_2}\right) \\ & + v_{7.2}\left(2^{D_2}-1-\tfrac{p_2 g_2}{\sigma^2}\right) + v_{7.3}(p_1 - p_1^{\max}) + v_{7.4}(p_2 - p_2^{\max}) \ , \end{aligned} \tag{7.5}$$

where $v_{7.1}$, $v_{7.2}$, $v_{7.3}$, and $v_{7.4}$ are non-negative Lagrangian multipliers. To achieve optimal closed-form solution, the KKT conditions are given as

$$\frac{\partial L}{\partial p_1} = -\frac{g_1}{\sigma^2+p_2^* g_2}\frac{\sigma^2+p_2^* g_2}{\sigma^2+p_1^* g_1+p_2^* g_2} - \frac{v_{7.1}^* g_1}{\sigma^2+p_2^* g_2} + v_{7.3}^* = 0, \tag{7.6a}$$

$$\frac{\partial L}{\partial p_2} = -\frac{\sigma^2+p_2^* g_2}{\sigma^2+p_1^* g_1+p_2^* g_2}\frac{g_2}{\sigma^2+p_2^* g_2} + \frac{v_{7.1}^* g_2 p_1^* g_1}{(\sigma^2+p_2^* g_2)^2} - \frac{v_{7.2}^* g_2}{\sigma^2} + v_{7.4}^* = 0, \tag{7.6b}$$

$$v_{7.1}^*\left(2^{D_1}-1-\tfrac{p_1^* g_1}{\sigma^2+p_2^* g_2}\right) = 0, \tag{7.6c}$$

$$v_{7.2}^*\left(2^{D_2}-1-\tfrac{p_2^* g_2}{\sigma^2}\right) = 0, \tag{7.6d}$$

$$v_{7.3}^*\left(p_1^* - p_1^{\max}\right) = 0, \tag{7.6e}$$

$$v_{7.4}^*\left(p_2^* - p_2^{\max}\right) = 0. \tag{7.6f}$$

By the signs of summation components in Constraint (7.6a), we see $v_{7.3}^*$ has non-zero value. Hence, p_1^* value equals to its maximum $p_1^{\max}$ by Constraint (7.6e). By the summation components in Constraint (7.6b), we see at least one of $v_{7.1}^*$ or $v_{7.4}^*$ should have non-zero value. Using this fact, the value of p_2^* can be obtained by Constraints (7.6c) or (7.6f). As a result, the optimal transmit powers are given as

$$p_1^* = p_1^{\max}, \tag{7.7}$$

$$p_2^* = \min\left\{p_2^{\max}, \frac{1}{g_2}\left(\frac{p_1^{\max} g_1}{2^{D_1}-1} - \sigma^2\right)\right\}. \tag{7.8}$$

By placing p_1^* and p_2^* into $\mathrm{C}_{1\to 2}^{\mathrm{SR}}$, its optimal value becomes a piece-wise function as

$$\mathcal{C}_{1\to 2}^{\mathrm{Up.RB}*} = -\log_2(\sigma^2) + \log_2\left(\sigma^2 + p_1^{\max} g_1 + g_2 \min\left\{p_2^{\max}, \tfrac{1}{g_2}\left(\tfrac{p_1^{\max} g_1}{2^{D_1}-1} - \sigma^2\right)\right\}\right) \ . \tag{7.9}$$

7.3. Decode Order Optimization

The solution for the global optimization in Problem (7.1) is obtained by the comparison of the sum-rate values with the optimal transmit powers. Therefore, the best decoding order can be decided by

$$\mathcal{C}_{1\to2}^{\text{Up.RB}*} \underset{2\to1}{\overset{1\to2}{\gtrless}} \mathcal{C}_{2\to1}^{\text{Up.RB}*}, \tag{7.10}$$

where the solution for $\mathcal{C}_{2\to1}^{\text{Up.RB}*}$ is exactly the same by switching the indexes in equation (7.9). The comparison can be reduced to

$$g_1 \max\left\{0, p_1^{\max} - \tfrac{1}{g_1}\left(\tfrac{p_2^{\max} g_2}{2^{D_2}-1} - \sigma^2\right)\right\} \underset{2\to1}{\overset{1\to2}{\gtrless}} g_2 \max\left\{0, p_2^{\max} - \tfrac{1}{g_2}\left(\tfrac{p_1^{\max} g_1}{2^{D_1}-1} - \sigma^2\right)\right\} . \tag{7.11}$$

By conditional structure in two sides of Decision Rule (7.11), the optimal decoding order decision should be made by multiple comparisons. These comparisons are given in inequality form as

$$p_1^{\max} > \tfrac{1}{g_1}\left(\tfrac{p_2^{\max} g_2}{2^{D_2}-1} - \sigma^2\right), \tag{7.12a}$$

$$p_2^{\max} > \tfrac{1}{g_2}\left(\tfrac{p_1^{\max} g_1}{2^{D_1}-1} - \sigma^2\right), \tag{7.12b}$$

$$p_1^{\max} g_1 \left(1 + \tfrac{1}{2^{D_1}-1}\right) > p_2^{\max} g_2 \left(1 + \tfrac{1}{2^{D_2}-1}\right) . \tag{7.12c}$$

The resulting inequalities for the optimal decoding order reveal two important remarks.

- When the transmit power constraints, $p_1^{\max}$ and $p_2^{\max}$, are sufficiently high, the optimal decoding order can be obtained by only Inequality (7.12c). If $p_1^{\max}$ and $p_2^{\max}$ are equal values, this case is equivalent to the solution presented in [77].
- When the transmit power constraints, $p_1^{\max}$ and $p_2^{\max}$, are sufficiently low, Inequalities (7.12a) and (7.12b) do not hold and the sum-rate is the same for both decoding orders. This case is called *No-Optimal-Order (NOO)* region. This region is achieved when both sides of Decision Rule (7.11) equals to zero.

The decision logic for the optimal decoding order is summarized by Inequalities (7.12) as

$$\begin{aligned} &! \text{ (7.12a)} \wedge ! \text{ (7.12b)} && \Longrightarrow \text{ NOO,} \\ &\left.\begin{array}{l} \text{(7.12a)} \wedge ! \text{ (7.12b)} \\ \text{(7.12a)} \wedge \text{(7.12b)} \wedge \text{(7.12c)} \end{array}\right\} && \Longrightarrow (1 \rightarrow 2), \\ &\left.\begin{array}{l} ! \text{ (7.12a)} \wedge \text{(7.12b)} \\ \text{(7.12a)} \wedge \text{(7.12b)} \wedge ! \text{ (7.12c)} \end{array}\right\} && \Longrightarrow (2 \rightarrow 1), \end{aligned} \tag{7.13}$$

where ! $(\cdot)$ identifies the inequality $(\cdot)$ does not hold and $\wedge$ is *and* logical operator.

The transmit power and bit-rate constraints of the user 2 are critical for decoding decisions. By Decision Rule (7.13), a lower bound for $p_2^{\max}$, which indicates $(2 \rightarrow 1)$ decoding order provides better sum-rate than $(1 \rightarrow 2)$, is given as

$$p_2^{\max} > \tfrac{1}{g_2} \max\left\{ \tfrac{p_1^{\max} g_1}{2^{D_1}-1} - \sigma^2, p_1^{\max} g_1 \left(\tfrac{2^{D_1}}{2^{D_1}-1}\right)\left(\tfrac{2^{D_2}-1}{2^{D_2}}\right) \right\} . \tag{7.14}$$

This lower bound can be described as the minimum transmit power for the user 2 that makes switching the decoding order advantageous. Similarly, an upper bound on the bit-rate demand of user 2 where decoding order $(2 \rightarrow 1)$ provides better service is given as

$$D_2 < \frac{1}{1 - \frac{p_2^{\max} g_2}{p_1^{\max} g_1} \frac{2^{D_1}-1}{2^{D_1}}} \tag{7.15}$$

with the assumption of $\frac{p_2^{\max} g_2}{p_1^{\max} g_1} \frac{2^{D_1}-1}{2^{D_1}} < 1$. Since the channel powers of users are ordered as $g_1 > g_2$, this assumption is valid for most of the use-cases.

7.4. Numerical Results

This section presents numerical results for varying user bit-rate demands and transmit power constraints. In the wireless environment for the numerical results, the users are uniformly distributed inside a 2D plane disc where the BS is located in the center. The outer radius of the disc is considered as 866 meters and its inner radius is 10 meters similar to MMTC use-case of [8]. By the same use-case, the noise figure of

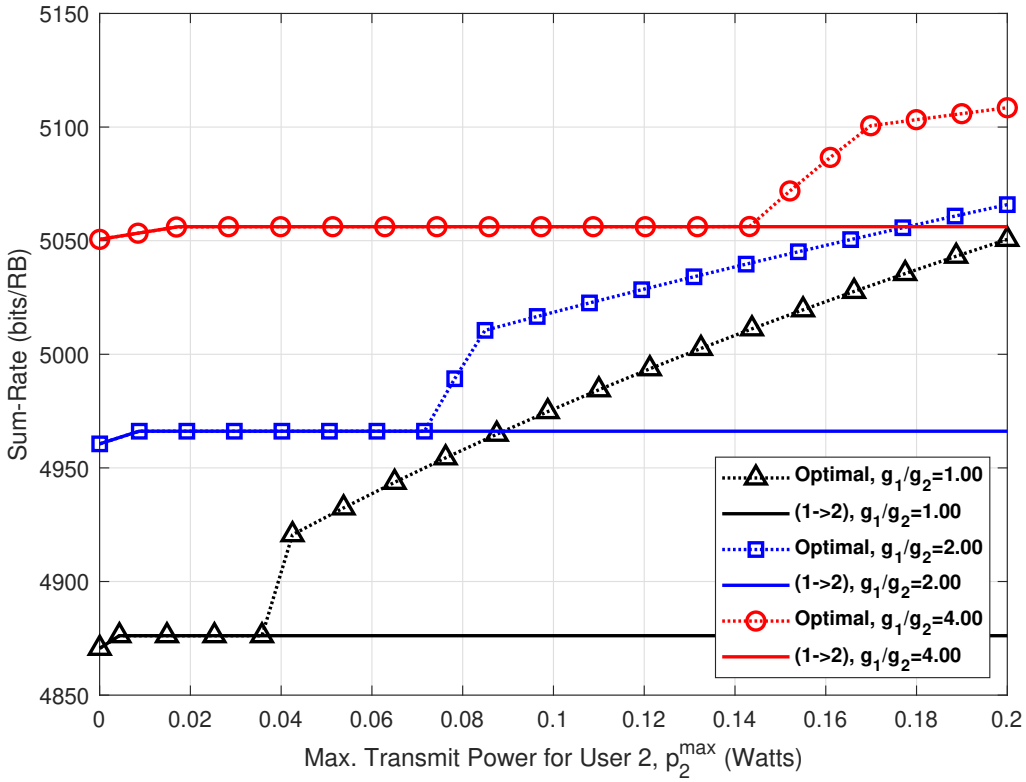

Figure 7.1. Sum-rate comparison of the optimal and the constant $(1 \rightarrow 2)$ decoding order for varying channel power ratios.

the BS is assumed as 5 dB and pathloss exponent, α, is assumed as 2.2 as a line-of-sight model. The maximum transmit power of the user 1, $p_1^{\max}$, is 0.2 Watts. All sum-rate results are obtained for single RB. An RB is considered as 1 ms and 180kHz [98]. Therefore, effective bandwidth for an RB is $B_{\mathrm{RB}} = 0.001 \times 180000 = 180$ 1/RB. In this section, D_1, D_2, and sum-rate values are presented as bits/RB by multiplication with B_{RB}. All of the curves are assumed to have optimized transmit powers as defined in equation (7.8).

Figure 7.1 presents sum-rate results for different channel instances of users. For these curves, the bit-rate demands of the users 1 and 2 are respectively 1000 and 50 bits. The curves are observed to include multiple break points. Equation (7.9) and Decision Rule (7.11) show that the sum-rate for the constant decoding order $(1 \rightarrow 2)$ contains 1 break point, while the sum-rate for the optimal decoding order contains up to 3 break points. The break points where the optimal decoding order starts to provide

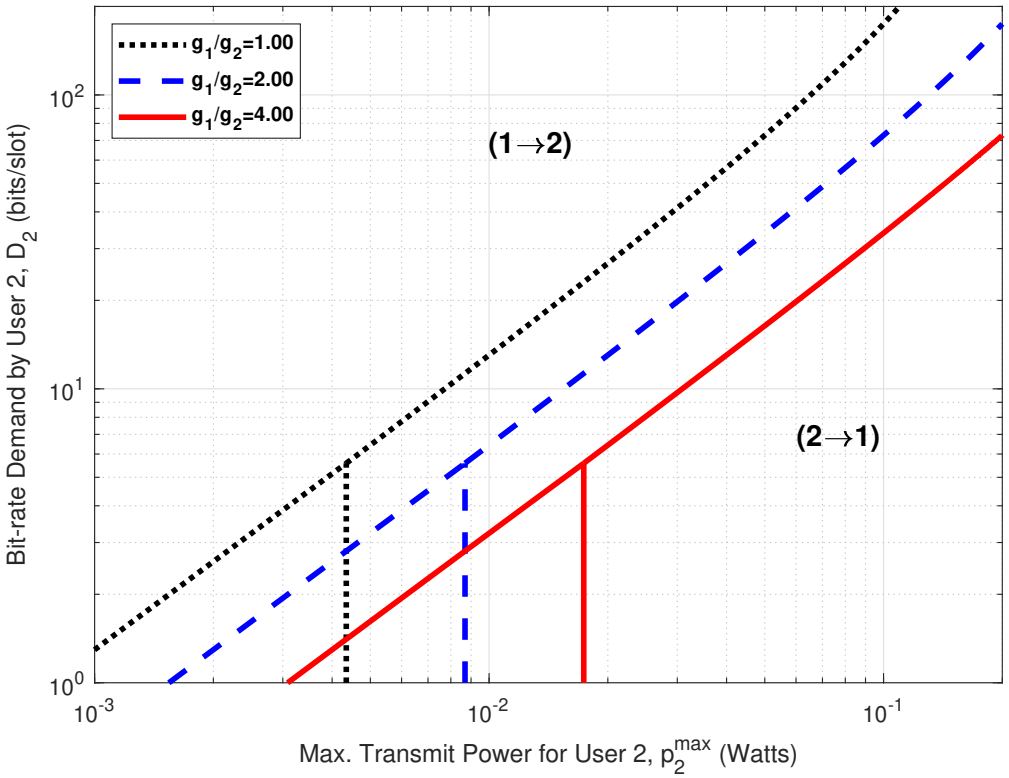

Figure 7.2. The optimal decoding order decision regions from Decision Rule (7.13) for varying channel power ratios.

advantage over constant decoding order $(1 \to 2)$ is determined by Inequality (7.14). As the channel power ratio gets closer to 1, less transmit power by user 2 ($p_2^{\max}$) is required for the decoding order $(2 \to 1)$ to have advantage over $(1 \to 2)$. Moreover, for the lower values of the channel power ratio, the optimization of decoding order provides higher gain over constant decoding order. As discussed also in [71], the received power based decoding order has disadvantage when the channel powers are close to each other. By the difference in bit-rate demands and transmit power constraints, the optimal decoding order provides significant sum-rate gain in the disadvantageous instances of close channel powers.

Figure 7.2 presents the boundaries of the optimal decision logic regions by Decision Rule (7.13) for power and bit-rate constraints of user 2 under different channel ratios. The optimal decoding order decision is $(1 \to 2)$ for the upper-left region above boundaries and $(2 \to 1)$ for the lower-right region below boundaries. The lower-left

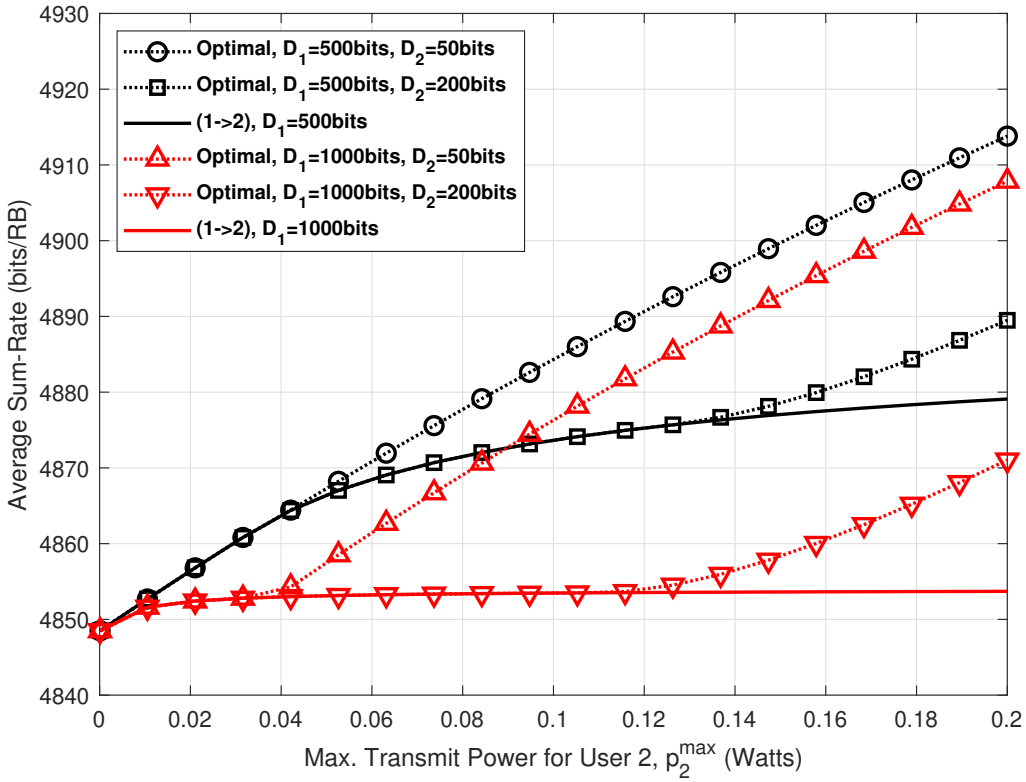

Figure 7.3. Average sum-rate comparison by Monte-Carlo simulations for varying user bit-rate demands.

triangle regions for each boundary curve illustrate NOO region. Among the boundary curves, NOO region is observed to be present only for low bit-rate demands of user 2. For the instances of higher channel power ratio, the required transmit power of user 2 becomes higher to achieve the advantage of decoding order $(2 \rightarrow 1)$. The boundaries between $(1 \rightarrow 2)$ and $(2 \rightarrow 1)$ regions are close to linear. The boundaries between the optimal decision regions shows that the user 2 requires higher transmit to sustain the advantage of switching decoding order for increased bit-rate demand. When the channel ratio get higher, decoding order $(2 \rightarrow 1)$ region gets smaller and it becomes a less desirable solution.

Figure 7.3 presents Monte-Carlo simulation results of average RB sum-rate for varying user bit-rate demands. Average sum-rate values are calculated by 10^6 instances of random channel powers where the infeasible instances of channel pairs are ensured to be below 100 for each point. Comparing curves for $D_1 = 500$ and $D_1 = 1000$ bits,

lower bit-rate demand by user 1 achieves better sum-rate as it limits the transmit power of user 2. The sum-rate of the constant decoding order, $(1 \rightarrow 2)$, is not affected by the bit-rate demand of user 2, D_2. Comparing curves with different D_2 values, the optimization of decoding order by low D_2 value is capable of achieving performance gain for lower transmit powers. When D_2 is increased, the transmit power required for the performance gain becomes higher. Coming to an overall result, the performance gain of optimal decoding order is achievable under high transmit power by Inequality (7.14) and low bit-rate demand by Inequality (7.15), and their thresholds are monotonically affecting each other.

7.5. Conclusion

In this chapter, joint optimization of user transmit powers and decoding order are presented under transmit power and bit-rate demand constraints. The results include theoretical limits for transmit power and bit-rate demand of the user to ensures sum-rate gain by switching decoding order. The numerical results indicate that switching decoding order provides significant performance gain when the channel powers of the users are close to each other. Moreover, a detailed analysis of optimal decision regions by power and bit-rate constraints is presented.

8. CONCLUSION AND FUTURE WORK

In this thesis, most of the numerical results are obtained by stochastic geometry analysis. The mathematical derivations on heterogeneous networks are obtained by regarding the tier selection model [92]. For future studies, the definitions in Section 2.3.2 presents a simplified model to include open and closed access easily to any probabilistic analysis. Besides, in most cases the parameter optimization problems are modelled by utilizing the derivations from capacity analysis. Comparing to the other parameter optimization work in the literature, optimization by capacity analysis with the help of stochastic geometry provides insight for the selection of the parameters for irregular deployments.

In Chapters 3 and 4, stochastic geometry analysis and parameter optimization problems are presented for strict FFR and ABS techniques for OMA networks. The numerical results indicate that idling RB's as in strict FFR is more energy efficient technique than adjusting transmit power for improvement of the edge user performance. For ABS in heterogeneous networks, including macro ABS is observed to be saving more energy that pico ABS, as the macro BS's consumes more energy. However, pico ABS is required when macro edge users are subject to severe interference from pico BS's. Especially in closed access networks, macro ABS is more important as macro BS's cause higher inter-tier interference. Regarding the numerical results and state of the other works from the literature, following future works are considered for the parameter optimization of ICIC techniques.

- The next step for ICIC parameter optimization is to include CRE bias to the optimization problem and to solve it jointly. The numerical results reveal that the choice of the bias parameter has significant impact on the performance.
- One other possible future direction is to include the adaptation to different RB sizes in the interference coordination. Even though this changes the nature of the problem, it has significance as varying RB sizes are practically implemented

in 5G and latter technologies (e.g. F-OFDM [99]).

In Chapters 5 and 6, stochastic geometry analysis of NOMA-deployed heterogeneous network is presented for a variety of spectrum usage options for interference mitigation and network performance improvement. The coverage analysis in Chapter 5 reveals superiority of strict FFR over SFR in terms of signal quality. Chapter 6 deploys more detailed stochastic geometry analysis with power level optimization and pairing for NOMA. By the power level optimization, optimization of BS sum-rate degrades edge user performance vitally. In contrast, the optimal fairness achieves significant edge user performance with the cost of poor BS sum-rate. The proposed hybrid model achieves very good BS sum-rate, close to only NOMA case, with satisfactory edge user performance. Moreover, NN and NF pairing methods achieve very close BS sum-rate, where they differentiate in user-specific performance. As a consequence to NOMA-based sequence, following items are considered future work.

- For an ubiquitous analysis, stochastic geometry analysis should be extended with capacity analysis with inclusion of BS or user bandwidth.
- Hybrid model can be further enhanced with inclusion of ICIC techniques. In this case, the performance of users, who experience most sever interference, can be improved by the help of frequency reuse.
- Beside static ICIC techniques like strict FFR or SFR, dynamic ICIC or CoMP are good alternatives to improve edge user performance, so the analysis can be extended with them.

In Chapter 7, joint optimization of user transmit powers and decoding order is presented under transmit power and bit-rate demand constraints. The results include theoretical limits for transmit power and bit-rate demand of the user to ensures sum-rate gain by switching decoding order. The results indicates the performance gain by switching decoding order under varying transmit power constraints. The performance gain of switching decoding order is indicated to be achievable when the channel powers of the users are close, maximum transmit power of distant user is sufficiently high, and

bit-rate requirement of the distant user is sufficiently low.

- As a future work, optimization of the uplink decoding order can be extended by generalizing the optimal solution to more than 2 users transmitting in the same RB.

REFERENCES

1. "Ericsson Mobility Report November 2021", Ericsson, Sweeden, 2021.

2. Zhang, Z., Y. Xiao, Z. Ma, M. Xiao, Z. Ding, X. Lei, G. K. Karagiannidis and P. Fan, "6G Wireless Networks: Vision, Requirements, Architecture, and Key Technologies", *IEEE Vehicular Technology Magazine*, Vol. 14, No. 3, pp. 28–41, 2019.

3. An, J., K. Yang, J. Wu, N. Ye, S. Guo and Z. Liao, "Achieving Sustainable Ultra-Dense Heterogeneous Networks for 5G", *IEEE Communications Magazine*, Vol. 55, No. 12, pp. 84–90, 2017.

4. Anpalagan, A., M. Bennis and R. Vannithamby (Editors), *Design and Deployment of Small Cell Networks*, Cambridge University Press, Cambridge, 2016.

5. Deb, P., A. Mukherjee and D. De, "A Study of Densification Management Using Energy Efficient Femto-Cloud Based 5G Mobile Network", *Wireless Personal Communications*, Vol. 101, No. 4, pp. 2173–2191, 2018.

6. Benjebbour, A., Y. Saito, Y. Kishiyama, A. Li, A. Harada and T. Nakamura, "Concept and Practical Considerations of Non-Orthogonal Multiple Access (NOMA) for Future Radio Access", *2013 International Symposium on Intelligent Signal Processing and Communication Systems*, pp. 770–774, Okinawa, Japan, 2013.

7. "TR 36.859 Study on Downlink Multiuser Superposition Transmission (MUST) for LTE, 13.0.0", 3GPP, 2015.

8. "TR 38.812 Study on Non-Orthogonal Multiple Access (NOMA) for NR, 16.0.0", 3GPP, 2018.

9. Liu, Y., S. Zhang, X. Mu, Z. Ding, R. Schober, N. Al-Dhahir, E. Hossain and X. Shen, "Evolution of NOMA Toward Next Generation Multiple Access (NGMA) for 6G", *IEEE Journal on Selected Areas in Communications*, Vol. 40, No. 4, pp. 1037–1071, 2022.

10. Zhu, Q., H. Li, Y. Fu, C.-X. Wang, Y. Tan, X. Chen and Q. Wu, "A Novel 3D Non-Stationary Wireless MIMO Channel Simulator and Hardware Emulator", *IEEE Transactions on Communications*, Vol. 66, No. 9, pp. 3865–3878, 2018.

11. Wang, C.-X., Z. Lv, X. Gao, X. You, Y. Hao and H. Haas, "Pervasive Wireless Channel Modeling Theory and Applications to 6G GBSMs for All Frequency Bands and All Scenarios", *IEEE Transactions on Vehicular Technology*, Vol. 71, No. 9, pp. 9159–9173, 2022.

12. Saito, Y., A. Benjebbour, Y. Kishiyama and T. Nakamura, "System-Level Performance Evaluation of Downlink Non-Orthogonal Multiple Access (NOMA)", *2013 IEEE 24th Annual International Symposium on Personal, Indoor, and Mobile Radio Communications (PIMRC)*, pp. 611–615, London, UK, 2013.

13. Manap, S., K. Dimyati, M. N. Hindia, M. S. Abu Talip and R. Tafazolli, "Survey of Radio Resource Management in 5G Heterogeneous Networks", *IEEE Access*, Vol. 8, pp. 131202–131223, 2020.

14. Hasan, Z., H. Boostanimehr and V. K. Bhargava, "Green Cellular Networks: A Survey, Some Research Issues and Challenges", *IEEE Communications Surveys Tutorials*, Vol. 13, No. 4, pp. 524–540, 2011.

15. Yuan, Y., S. Wang, Y. Wu, H. V. Poor, Z. Ding, X. You and L. Hanzo, "NOMA for Next-Generation Massive IoT: Performance Potential and Technology Directions", *IEEE Communications Magazine*, Vol. 59, No. 7, pp. 115–121, 2021.

16. Cirik, A. C., N. M. Balasubramanya, L. Lampe, G. Vos and S. Bennett, "Toward

the Standardization of Grant-Free Operation and the Associated NOMA Strategies in 3GPP", *IEEE Communications Standards Magazine*, Vol. 3, No. 4, pp. 60–66, 2019.

17. Mendrzik, R., R. A. J. Castillo, G. Bauch and E. Seidel, "Interference Coordination-Based Downlink Scheduling for Heterogeneous LTE-A Networks", *IEEE Wireless Communications and Networking Conference (WCNC)*, pp. 1–6, Doha, Qatar, 2016.

18. Kosta, C., B. Hunt, A. Quddus and R. Tafazolli, "A Distributed Method of Inter-Cell Interference Coordination (ICIC) Based on Dual Decomposition for Interference-Limited Cellular Networks", *IEEE Communications Letters*, Vol. 17, No. 6, pp. 1144–1147, 2013.

19. Rahman, M. and H. Yanikomeroglu, "Enhancing Cell-Edge Performance: A Downlink Dynamic Interference Avoidance Scheme with Inter-Cell Coordination", *IEEE Transactions on Wireless Communications*, Vol. 9, No. 4, pp. 1414–1425, 2010.

20. Novlan, T. D., R. K. Ganti, A. Ghosh and J. G. Andrews, "Analytical Evaluation of Fractional Frequency Reuse for OFDMA Cellular Networks", *IEEE Transactions on Wireless Communications*, Vol. 10, No. 12, pp. 4294–4305, 2011.

21. Zhang, X. and M. Haenggi, "A Stochastic Geometry Analysis of Inter-Cell Interference Coordination and Intra-Cell Diversity", *IEEE Transactions on Wireless Communications*, Vol. 13, No. 12, pp. 6655–6669, 2014.

22. Tsilimantos, D., J. M. Gorce, K. Jaffrès-Runser and H. V. Poor, "Spectral and Energy Efficiency Trade-offs in Cellular Networks", *IEEE Transactions on Wireless Communications*, Vol. 15, No. 1, pp. 54–66, 2016.

23. Gonzalez, D., M. Garcia-Lozano, S. R. Boque and D. S. Lee, "Optimization of Soft

Frequency Reuse for Irregular LTE Macrocellular Networks", *IEEE Transactions on Wireless Communications*, Vol. 12, No. 5, pp. 2410–2423, 2013.

24. Novlan, T. D., R. K. Ganti, A. Ghosh and J. G. Andrews, "Analytical Evaluation of Fractional Frequency Reuse for Heterogeneous Cellular Networks", *IEEE Transactions on Communications*, Vol. 60, No. 7, pp. 2029–2039, 2012.

25. Zhuang, H. and T. Ohtsuki, "A Model Based on Poisson Point Process for Downlink Tiers Fractional Frequency Reuse Heterogeneous Networks", *Physical Communication*, Vol. 13, Part B, pp. 3–12, 2014.

26. "TS 36.300 Overall description; Stage 2, 15.7.0", 3GPP, 2019.

27. Yunas, S. F., M. Valkama and J. Niemelä, "Spectral and Energy Efficiency of Ultra-Dense Networks under Different Deployment Strategies", *IEEE Communications Magazine*, Vol. 53, No. 1, pp. 90–100, 2015.

28. Virdis, A., G. Stea, D. Sabella and M. Caretti, "A Distributed Power-Saving Framework for LTE HetNets Exploiting Almost Blank Subframes", *IEEE Transactions on Green Communications and Networking*, Vol. 1, No. 3, pp. 235–252, 2017.

29. "R1-113806, Performance Study on ABS With Reduced Macro Power", 3GPP TSG-RAN WG1 Meeting #67, Panasonic, 2011.

30. Merwaday, A., S. Mukherjee and I. Güvenç, "HetNet Capacity with Reduced Power Subframes", *IEEE Wireless Communications and Networking Conference (WCNC)*, pp. 1380–1385, Istanbul, Turkey, 2014.

31. Hu, H., J. Weng and J. Zhang, "Coverage Performance Analysis of FeICIC Low-Power Subframes", *IEEE Transactions on Wireless Communications*, Vol. 15, No. 8, pp. 5603–5614, 2016.

32. Sun, Y., H. Xu, S. Zhang, Y. Wu, T. Wang, Y. Fang and S. Xu, "Energy Efficiency Analysis of FeICIC in Dense Heterogeneous Networks", *15th International Wireless Communications Mobile Computing Conference (IWCMC)*, pp. 711–716, Tangier, Morocco, 2019.

33. Holtkamp, H., G. Auer, V. Giannini and H. Haas, "A Parameterized Base Station Power Model", *IEEE Communications Letters*, Vol. 17, No. 11, pp. 2033–2035, 2013.

34. Sung, D. and J. S. Baras, "Utility-Based Almost Blank Subframe Optimization in Heterogeneous Cellular Networks", *IEEE Global Communications Conference (Globecom)*, pp. 3622–3627, Austin, Texas, USA, 2014.

35. Zheng, J., L. Gao, H. Zhang, H. Wang, J. Niu, X. Li and J. Ren, "Max-Min Energy-Efficient eICIC Configuration in Heterogeneous Network", *IEEE International Conference on Communications (ICC)*, pp. 1–6, Kansas City, MO, USA, 2018.

36. Zheng, J., L. Gao, H. Wang, J. Niu, X. Li and J. Ren, "EE-eICIC: Energy-Efficient Optimization of Joint User Association and ABS for eICIC in Heterogeneous Cellular Networks", *Wireless Communications and Mobile Computing*, Vol. 2017, p. 6768415, 2017.

37. Li, J., X. Wang, Z. Li, H. Wang and L. Li, "Energy Efficiency Optimization Based on eICIC for Wireless Heterogeneous Networks", *IEEE Internet of Things Journal*, Vol. 6, No. 6, pp. 10166–10176, 2019.

38. Merwaday, A. and I. Güvenç, "Optimisation of FeICIC for Energy Efficiency and Spectrum Efficiency in LTE-Advanced HetNets", *Electronics Letters*, Vol. 52, No. 11, pp. 982–984, 2016.

39. Chen, Z., L. Qiu and X. Liang, "Area Spectral Efficiency Analysis and En-

ergy Consumption Minimization in Multiantenna Poisson Distributed Networks", *IEEE Transactions on Wireless Communications*, Vol. 15, No. 7, pp. 4862–4874, 2016.

40. Cierny, M., H. Wang, R. Wichman, Z. Ding and C. Wijting, "On Number of Almost Blank Subframes in Heterogeneous Cellular Networks", *IEEE Transactions on Wireless Communications*, Vol. 12, No. 10, pp. 5061–5073, 2013.

41. Gonzalez, D. G., M. Garcia-Lozano, S. R. Boque and D. S. Lee, "Optimization of Soft Frequency Reuse for Irregular LTE Macrocellular Networks", *IEEE Transactions on Wireless Communications*, Vol. 12, No. 5, pp. 2410–2423, 2013.

42. Dai, L., B. Wang, Y. Yuan, S. Han, C. l. I and Z. Wang, "Non-Orthogonal Multiple Access for 5G: Solutions, Challenges, Opportunities, and Future Research Trends", *IEEE Communications Magazine*, Vol. 53, No. 9, pp. 74–81, 2015.

43. Dai, L., B. Wang, Z. Ding, Z. Wang, S. Chen and L. Hanzo, "A Survey of Non-Orthogonal Multiple Access for 5G", *IEEE Communications Surveys Tutorials*, pp. 1–1, 2018.

44. Lei, L., D. Yuan and P. Värbrand, "On Power Minimization for Non-Orthogonal Multiple Access (NOMA)", *IEEE Communications Letters*, Vol. 20, No. 12, pp. 2458–2461, 2016.

45. Yang, Z., W. Xu, C. Pan, Y. Pan and M. Chen, "On the Optimality of Power Allocation for NOMA Downlinks With Individual QoS Constraints", *IEEE Communications Letters*, Vol. 21, No. 7, pp. 1649–1652, 2017.

46. Huang, Y., J. Wang and J. Zhu, "Optimal Power Allocation for Downlink NOMA Systems", *Multiple Access Techniques for 5G Wireless Networks and Beyond*, pp. 195–227, Springer International Publishing, Springer, Cham, Switzerland, 2019.

47. Oviedo, J. A. and H. R. Sadjadpour, "On the Power Allocation Limits for Down-

link Multi-User NOMA with QoS", *IEEE International Conference on Communications (ICC)*, pp. 1–5, Kansas City, MO, USA, 2018.

48. Chen, X., F. k. Gong, G. Li, H. Zhang and P. Song, "User Pairing and Pair Scheduling in Massive MIMO-NOMA systems", *IEEE Communications Letters*, Vol. PP, No. 99, pp. 1–1, 2017.

49. Zhu, L., J. Zhang, Z. Xiao, X. Cao and D. O. Wu, "Optimal User Pairing for Downlink Non-Orthogonal Multiple Access (NOMA)", *IEEE Wireless Communications Letters*, Vol. 8, No. 2, pp. 328–331, 2019.

50. Nain, G., S. S. Das and A. Chatterjee, "Low Complexity User Selection with Optimal Power Allocation in Downlink NOMA", *IEEE Wireless Communications Letters*, Vol. 7, No. 2, pp. 158–161, 2018.

51. Li, X., C. Li and Y. Jin, "Dynamic Resource Allocation for Transmit Power Minimization in OFDM-Based NOMA Systems", *IEEE Communications Letters*, Vol. 20, No. 12, pp. 2558–2561, 2016.

52. Ding, Z., Z. Yang, P. Fan and H. V. Poor, "On the Performance of Non-Orthogonal Multiple Access in 5G Systems with Randomly Deployed Users", *IEEE Signal Processing Letters*, Vol. 21, No. 12, pp. 1501–1505, 2014.

53. Ali, K. S., M. Haenggi, H. ElSawy, A. Chaaban and M.-S. Alouini, "Downlink Non-Orthogonal Multiple Access (NOMA) in Poisson Networks", *IEEE Transactions on Communications*, Vol. 67, No. 2, pp. 1613–1628, 2019.

54. Han, T., J. Gong, X. Liu, S. M. R. Islam, Q. Li, Z. Bai and K. S. Kwak, "On Downlink NOMA in Heterogeneous Networks With Non-Uniform Small Cell Deployment", *IEEE Access*, Vol. 6, pp. 31099–31109, 2018.

55. Liu, Y., Z. Qin, M. Elkashlan, A. Nallanathan and J. A. McCann, "Non-Orthogonal Multiple Access in Large-Scale Heterogeneous Networks", *IEEE Jour-*

nal on Selected Areas in Communications, Vol. 35, No. 12, pp. 2667–2680, 2017.

56. Liu, C. and D. Liang, "Heterogeneous Networks With Power-Domain NOMA: Coverage, Throughput, and Power Allocation Analysis", *IEEE Transactions on Wireless Communications*, Vol. 17, No. 5, pp. 3524–3539, 2018.

57. Shin, W., M. Vaezi, B. Lee, D. J. Love, J. Lee and H. V. Poor, "Non-Orthogonal Multiple Access in Multi-Cell Networks: Theory, Performance, and Practical Challenges", *IEEE Communications Magazine*, Vol. 55, No. 10, pp. 176–183, 2017.

58. Liu, Y., Z. Qin and Z. Ding, *Non-Orthogonal Multiple Access for Massive Connectivity*, Springer, Cham, Switzerland, 2020.

59. Zhang, C., W. Yi, Y. Liu and Q. Wang, "Multi-cell NOMA: Coherent Reconfigurable Intelligent Surfaces Model With Stochastic Geometry", *IEEE International Conference on Communications (ICC)*, pp. 1–6, Montreal, Canada, 2021.

60. Ali, K. S., H. Elsawy, A. Chaaban and M.-S. Alouini, "Non-Orthogonal Multiple Access for Large-Scale 5G Networks: Interference Aware Design", *IEEE Access*, Vol. 5, pp. 21204–21216, 2017.

61. C. -H. Lee, M. Kobayashi, H. -Y. Wei, S. Saruwatari and T. Watanabe, "Adaptive Resource Allocation for ICIC in Downlink NOMA Systems", *IEEE 90th Vehicular Technology Conference (VTC Fall)*, pp. 1–6, Honolulu, Hawaii, 2019.

62. Budhiraja, I., S. Tyagi, S. Tanwar, N. Kumar and M. Guizani, "Cross Layer NOMA Interference Mitigation for Femtocell Users in 5G Environment", *IEEE Transactions on Vehicular Technology*, Vol. 68, No. 5, pp. 4721–4733, 2019.

63. Su, S.-L., T.-H. Chih and T.-Y. Wu, "Resource Allocation and Interference Suppression with PCA for Multicell MU-MIMO Systems", *Wireless Networks*, Vol. 25, No. 5, pp. 2889–2899, 2019.

64. Umehara, J., Y. Kishiyama and K. Higuchi, "Enhancing User Fairness in Non-Orthogonal Access with Successive Interference Cancellation for Cellular Downlink", *IEEE International Conference on Communication Systems (ICCS)*, pp. 324–328, Omaha, Nebraska, USA, 2012.

65. W. K. New, C. Y. Leow, K. Navaie, Y. Sun and Z. Ding, "Interference-Aware NOMA for Cellular-Connected UAVs: Stochastic Geometry Analysis", *IEEE Journal on Selected Areas in Communications*, Vol. 39, No. 10, pp. 3067–3080, 2021.

66. Ding, Z., Y. Liu, J. Choi, Q. Sun, M. Elkashlan, I. Chih-Lin and H. V. Poor, "Application of Non-Orthogonal Multiple Access in LTE and 5G Networks", *IEEE Communications Magazine*, Vol. 55, No. 2, pp. 185–191, 2017.

67. Marcano, A. S. and H. L. Christiansen, "A Novel Method for Improving the Capacity in 5G Mobile Networks Combining NOMA and OMA", *IEEE 85th Vehicular Technology Conference (VTC-Spring)*, pp. 1–5, Sydney, Australia, 2017.

68. A. Hussein, C. Rosenberg and P. Mitran, "Hybrid NOMA in Multi-Cell Networks: From a Centralized Analysis to Practical Schemes", *IEEE/ACM Transactions on Networking*, Vol. 30, No. 3, pp. 1268–1282, 2022.

69. Tabassum, H., M. S. Ali, E. Hossain, M. J. Hossain and D. I. Kim, "Uplink Vs. Downlink NOMA in Cellular Networks: Challenges and Research Directions", *IEEE 85th Vehicular Technology Conference (VTC-Spring)*, pp. 1–7, Sydney, Australia, 2017.

70. Gao, Y., B. Xia, K. Xiao, Z. Chen, X. Li and S. Zhang, "Theoretical Analysis of the Dynamic Decode Ordering SIC Receiver for Uplink NOMA Systems", *IEEE Communications Letters*, Vol. 21, No. 10, pp. 2246–2249, 2017.

71. Ding, Z., R. Schober and H. V. Poor, "Unveiling the Importance of SIC in NOMA

Systems—Part 1: State of the Art and Recent Findings", *IEEE Communications Letters*, Vol. 24, No. 11, pp. 2373–2377, 2020.

72. Ding, Z., R. Schober and H. V. Poor, "A New QoS-Guarantee Strategy for NOMA Assisted Semi-Grant-Free Transmission", *IEEE Transactions on Communications*, Vol. 69, No. 11, pp. 7489–7503, 2021.

73. Sun, Y., Z. Ding and X. Dai, "A New Design of Hybrid SIC for Improving Transmission Robustness in Uplink NOMA", *IEEE Transactions on Vehicular Technology*, Vol. 70, No. 5, pp. 5083–5087, 2021.

74. Shi, Z., X. Xie, H. Lu, H. Yang and J. Cai, "Deep Reinforcement Learning Based Dynamic User Access and Decode Order Selection for Uplink NOMA System With Imperfect SIC", *IEEE Wireless Communications Letters*, Vol. 10, No. 4, pp. 710–714, 2021.

75. Qian, L. P., C. Yang, H. Han, Y. Wu and L. Meng, "Learning Driven Resource Allocation and SIC Ordering in EH Relay Aided NB-IoT Networks", *IEEE Communications Letters*, Vol. 25, No. 8, pp. 2619–2623, 2021.

76. Kim, J., J. Kim and S.-H. Park, "Joint Design of Power Control and SIC Decoding Order for Max-Min Fairness optimization in Uplink NOMA Systems", *International Conference on Information Networking (ICOIN)*, pp. 339–342, IEEE, Jeju Island, Korea (South), 2021.

77. Zhang, J., L. Zhu, Z. Xiao, X. Cao, D. O. Wu and X.-G. Xia, "Optimal and Sub-Optimal Uplink NOMA: Joint User Grouping, Decoding Order, and Power Control", *IEEE Wireless Communications Letters*, Vol. 9, No. 2, pp. 254–257, 2020.

78. Rao, J. B. and A. O. Fapojuwo, "A Survey of Energy Efficient Resource Management Techniques for Multicell Cellular Networks", *IEEE Communications Sur-*

veys Tutorials, Vol. 16, No. 1, pp. 154–180, 2014.

79. Li, Y., H. Celebi, M. Daneshmand, C. Wang and W. Zhao, "Energy-efficient femtocell networks: challenges and opportunities", *IEEE Wireless Communications*, Vol. 20, No. 6, pp. 99–105, 2013.

80. Soh, Y. S., T. Q. S. Quek, M. Kountouris and H. Shin, "Energy Efficient Heterogeneous Cellular Networks", *IEEE Journal on Selected Areas in Communications*, Vol. 31, No. 5, pp. 840–850, 2013.

81. Holtkamp, H., G. Auer, S. Bazzi and H. Haas, "Minimizing Base Station Power Consumption", *IEEE Journal on Selected Areas in Communications*, Vol. 32, No. 2, pp. 297–306, 2014.

82. Rao, J. B. and A. O. Fapojuwo, "An Analytical Framework for Evaluating Spectrum/Energy Efficiency of Heterogeneous Cellular Networks", *IEEE Transactions on Vehicular Technology*, Vol. 65, No. 5, pp. 3568–3584, 2016.

83. Peng, J., P. Hong and K. Xue, "Energy-Aware Cellular Deployment Strategy Under Coverage Performance Constraints", *IEEE Transactions on Wireless Communications*, Vol. 14, No. 1, pp. 69–80, 2015.

84. Kosta, C., B. Hunt, A. U. Quddus and R. Tafazolli, "Distributed Energy-Efficient Inter-Cell Interference Coordination (ICIC) in Multi-Cell HetNets", *77th Vehicular Technology Conference (VTC-Spring)*, pp. 1–5, Dresden, Germany, 2013.

85. Mahmud, A. and K. A. Hamdi, "A Unified Framework for the Analysis of Fractional Frequency Reuse Techniques", *IEEE Transactions on Communications*, Vol. 62, No. 10, pp. 3692–3705, 2014.

86. Xu, Y., G. Gui, H. Gacanin and F. Adachi, "A Survey on Resource Allocation for 5G Heterogeneous Networks: Current Research, Future Trends, and Challenges", *IEEE Communications Surveys & Tutorials*, Vol. 23, No. 2, pp. 668–695, 2021.

87. Haenggi, M., *Stochastic geometry for wireless networks*, Cambridge University Press, Cambridge, UK, 2013.

88. Stoyan, D., W. S. Kendall and J. Mecke, *Stochastic Geometry and Its Applications*, John Wiley & Sons Inc, Chichester W. Sussex ; New York, USA, 1987.

89. Altay, C. and M. Koca, "Capacity Analysis and Optimization for Energy Efficient Heterogeneous Networks", *IEEE Wireless Communications and Networking Conference (WCNC)*, pp. 1–6, Marrakech, Morocco, 2019.

90. Andrews, J. G., F. Baccelli and R. K. Ganti, "A Tractable Approach to Coverage and Rate in Cellular Networks", *IEEE Transactions on Communications*, Vol. 59, No. 11, pp. 3122–3134, 2011.

91. "TS 36.304 Evolved Universal Terrestrial Radio Access; User Equipment (UE) Procedures in Idle Mode, 12.3.0", 3GPP, 2014.

92. Jo, H. S., Y. J. Sang, P. Xia and J. G. Andrews, "Heterogeneous Cellular Networks with Flexible Cell Association: A Comprehensive Downlink SINR Analysis", *IEEE Transactions on Wireless Communications*, Vol. 11, No. 10, pp. 3484–3495, 2012.

93. "TS 36.331 Evolved Universal Terrestrial Radio Access; Radio Resource Control (RRC); Protocol specification, 15.0.1", 3GPP, 2018.

94. Ibe, O., *Fundamentals of Applied Probability and Random Processes*, Academic Press, Cambridge, Massachusetts, USA, 2005.

95. Byrd, R. H., J. C. Gilbert and J. Nocedal, "A Trust Region Method Based on Interior Point Techniques for Nonlinear Programming", *Mathematical Programming*, Vol. 89, No. 1, pp. 149–185, 2000.

96. Boyd, S. and L. Vandenberghe, *Convex Optimization*, Cambridge University

Press, New York, USA, 2004.

97. David, H. A. and H. N. Nagaraja, *Order statistics*, John Wiley, Hoboken, N.J, USA, 2003.

98. "TS 38.101-1 NR; User Equipment (UE) radio transmission and reception; Part 1: Range 1 Standalone, 16.13.0", 3GPP, 2022.

99. Zhang, X., L. Chen, J. Qiu and J. Abdoli, "On the Waveform for 5G", *IEEE Communications Magazine*, Vol. 54, No. 11, pp. 74–80, 2016.

100. Amazigo, J. C., *Advanced Calculus and Its Applications to the Engineering and Physical Sciences*, John Wiley & Sons Inc, New York, USA, 1981.

APPENDIX A: Base Station Capacity for Almost Blank Sub-Frame

In this section, we present the derivations for a single BS average interior and edge capacities, when ABS is employed in 2-tier network. Firstly, the average sum capacity for interior of a macro BS

$$\begin{aligned}
\mathbb{C}^{\mathrm{I}}_{\mathrm{M.BS}} &= \mathrm{E}\left[\mathcal{B}\tfrac{K-k_M-k_P}{K}\ln\left(1+\Psi^{\mathrm{I}}_{\mathrm{M}}\right)\right] \qquad (A.1)\\
&= \mathcal{B}\tfrac{K-k_M-k_P}{K}\int_0^{\infty}\tfrac{1}{\tau+1}\Pr\left(\tfrac{P_{\mathrm{M}}hr^{-\alpha}}{\sigma^2+I_{\mathrm{M|M}}+I_{\mathrm{P|M}}}>\tau\middle|\mathrm{Macro,Interior}\right)d\tau\\
&= \mathcal{B}\tfrac{K-k_M-k_P}{K}\int_0^{\infty}\tfrac{\Pr\left(h>\frac{\tau r^{\alpha}}{P_{\mathrm{M}}}\left(\sigma^2+I_{\mathrm{M|M}}+I_{\mathrm{P|M}}\right)\middle|\mathrm{Macro,Interior}\right)}{\tau+1}d\tau\\
&= \mathcal{B}\tfrac{K-k_M-k_P}{K}\int_0^{\infty}\mathrm{E}_r\left[\tfrac{e^{-\frac{\tau r^{\alpha}\sigma^2}{P_{\mathrm{M}}}}}{\tau+1}\mathcal{L}_{I_{\mathrm{M|M}}}\left(\tfrac{\tau r^{\alpha}}{P_{\mathrm{M}}}\right)\mathcal{L}_{I_{\mathrm{P|M}}}\left(\tfrac{\tau r^{\alpha}}{P_{\mathrm{M}}}\right)\middle|\mathrm{Macro,Interior}\right]d\tau
\end{aligned}$$

where the second line is obtained by a common transformation from the coverage probability to the capacity as shown in [90] and the forth line is obtained by the tail probability of the exponential distribution by Rayleigh fading. $\mathrm{E}_r[\ldots|\mathrm{Macro,Interior}]$ is the expected value by r where the pdf $f_{\mathrm{M}}(r)$ from equation (2.13) is used with the condition of the interior probability as $(1-\mathcal{P}^{\mathrm{E}}_{\mathrm{M}})$ from equation (2.16). By applying similar steps, the average sum capacity of edge users of a macro BS can be obtained as

$$\begin{aligned}
\mathbb{C}^{\mathrm{E}}_{\mathrm{M.BS}} &= \mathrm{E}\left[\mathcal{B}\tfrac{k_P}{K}\ln\left(1+\Psi^{\mathrm{E}}_{\mathrm{M}}\right)\right] \qquad (A.2)\\
&= \mathcal{B}\tfrac{k_P}{K}\int_0^{\infty}\mathrm{E}_r\left[\tfrac{e^{-\frac{\tau r^{\alpha}\sigma^2}{P_{\mathrm{M}}}}}{\tau+1}\mathcal{L}_{I_{\mathrm{M|M}}}\left(\tfrac{\tau r^{\alpha}}{P_{\mathrm{M}}}\right)\mathcal{L}_{I_{\mathrm{P|M}}}\left(\tfrac{\eta\tau r^{\alpha}}{P_{\mathrm{M}}}\right)\middle|\mathrm{Macro,\ Edge}\right]d\tau
\end{aligned}$$

where $\mathrm{E}_r[\ldots|\mathrm{Macro,\ Edge}]$ is the mean value of r where the pdf $f_{\mathrm{M}}(r)$ from equation (2.13) is conditioned on the edge probability by the equation (2.16). $\mathcal{L}_{I_{\mathrm{P|M}}}(\cdot)$ and $\mathcal{L}_{I_{\mathrm{M|M}}}(\cdot)$ are Laplace transforms of interference by pico and macro interferers to the typical macro user, respectively ($I_{\mathrm{P|M}}$ and $I_{\mathrm{M|M}}$). The Laplace transform of $I_{\mathrm{P|M}}$ is derived as

$$\mathcal{L}_{I_{\mathrm{P|M}}}\left(sr^{\alpha}\right) = \mathrm{E}\left[\exp\left\{-sr^{\alpha}\sum_{r_i\geq\sqrt{z_{\mathrm{PM}}}r}P_{\mathrm{P}}h_i r_i^{-\alpha}\right\}\right] \qquad (A.3)$$

$$
\begin{aligned}
&= \mathrm{E}\left[\prod_{r_i \geq \sqrt{z_{\mathrm{PM}}} r} \frac{1}{1+sr^{\alpha} P_{\mathrm{P}} r_i^{-\alpha}}\right] \\
&= \exp\left\{-2\pi\lambda_P \int_{\sqrt{z_{\mathrm{PM}}} r}^{\infty} \left(1 - \frac{1}{1+s\left(\frac{r}{u}\right)^{\alpha} P_{\mathrm{P}}}\right) u du\right\} \\
&= \exp\left\{-\pi\lambda_P r^2 \rho_{z_{\mathrm{PM}}}\left(sP_{\mathrm{P}}\right)\right\}
\end{aligned}
$$

where lower bound $r_i \geq \sqrt{z_{\mathrm{PM}}} r$ on pico cell interferers is obtained by equation (2.14), the second line is derived by Laplace transform of exponential distribution of h_i, the third line is obtained by inserting the probability generating functional of PPP as in [90], and $\rho_x(y)$ is as defined in equation (3.9). By similar steps, Laplace transform of $I_{\mathrm{M|M}}$ is obtained as

$$
\mathcal{L}_{I_{\mathrm{M|M}}}\left(sr^{\alpha}\right) = \exp\left\{-\pi\lambda_M r^2 \rho_1\left(sP_{\mathrm{M}}\right)\right\} . \tag{A.4}
$$

Beside macro BS capacity, pico BS capacity can be derived with the same course of action. By similar steps, $\mathbb{C}^{\mathrm{I}}_{\mathrm{P.BS}}$ and $\mathbb{C}^{\mathrm{E}}_{\mathrm{P.BS}}$ can be obtained by swapping λ_M and λ_P, P_{M} and P_{P}, z_{MP} and z_{PM}, and utilizing $\mathrm{E}_r[\ldots|\text{Pico, Interior}]$, $\mathrm{E}_r[\ldots|\text{Pico, Edge}]$.

APPENDIX B: The Worst-User Capacity for Almost Blank Sub-Frame

The worst-region capacity definitions for edge and interior macro users are respectively given as

$$\begin{aligned} \mathbb{C}^{\text{E-W}}_{\text{M.User}} &= \mathrm{E}\left[\mathcal{B}\frac{k_P}{K}\frac{\ln\left(1+\Psi^{\text{E}}_{\text{M}}\right)}{N^{\text{E}}_{\text{M}}}\middle| r>\omega_{\text{M}}\right] \\ &\approx \mathcal{B}\frac{k_P}{K}\frac{\mathrm{E}\left[\ln\left(1+\Psi^{\text{E}}_{\text{M}}\right)\middle| r>\omega_{\text{M}}\right]}{\mathrm{E}\left[N^{\text{E}}_{\text{M}}\right]}, \end{aligned} \tag{B.1}$$

$$\begin{aligned} \mathbb{C}^{\text{I-W}}_{\text{M.User}} &= \mathrm{E}\left[\mathcal{B}\frac{K-k_M}{K}\frac{\ln\left(1+\Psi^{\text{I}}_{\text{M}}\right)}{N_{\text{M}}}\middle| r>\omega_{\text{M}}\right] \\ &\approx \mathcal{B}\frac{K-k_M}{K}\frac{\mathrm{E}\left[\ln\left(1+\Psi^{\text{I}}_{\text{M}}\right)\middle| r>\omega_{\text{M}}\right]}{\mathrm{E}[N_{\text{M}}]} \end{aligned} \tag{B.2}$$

where N^{E}_{M} and N_{M} are the number of edge-macro users and all macro users, respectively. We employ $\mathrm{E}\left[\frac{\ln(1+\Psi)}{N}\right] \approx \frac{\mathrm{E}[\ln(1+\Psi)]}{\mathrm{E}[N]}$ approximation for the worst-region capacity derivations. The definition of $\mathbb{C}^{\text{I-W}}_{\text{M.User}}$ includes expected value of all users as there is no edge user in the case of $k_P = 0$ (explained in Section 4.2.2). The expected value of number of users in the denominator is obtained by using equations (2.11) and (2.16) as

$$\begin{aligned} \mathrm{E}\left[N^{\text{E}}_{\text{M}}\right] &= \frac{\lambda_u}{\lambda_M}\mathcal{P}^{\text{E}}_{\text{M}}\mathfrak{p}_{\text{M}} = \frac{\lambda_u e^{-\pi\left(\frac{P_{\text{M}}}{\lambda_M}\right)^{2/\alpha}(\lambda_M+\lambda_P z_{\text{PM}})}}{\lambda_M+\lambda_P z_{\text{PM}}} \\ \mathrm{E}\left[N_{\text{M}}\right] &= \frac{\lambda_u}{\lambda_M}\mathfrak{p}_{\text{M}} = \frac{\lambda_u}{\lambda_M+\lambda_P z_{\text{PM}}} \end{aligned} \tag{B.3}$$

where λ_u is the user density of the area. By the tail probability of equation (2.13), the worst-region distance lower bound, ω_{M}, in equation (4.8) is derived by solving $\int_{\omega_{\text{M}}}^{\infty} f_{\text{M}}(r)\,dr = p_{\text{worst}}$. By the worst region condition and following similar steps to equations (A.2) and (A.1), the expected values for the edge and interior worst-user capacity formulation are respectively derived as

$$\mathrm{E}\left[\ln\left(1+\Psi^{\text{E}}_{\text{M}}\right)\middle| r>\omega_{\text{M}}\right] = \int_0^{\infty} \mathrm{E}_r\left[\frac{e^{-\frac{\tau r^{\alpha}\sigma^2}{P_{\text{M}}}}}{\tau+1}\mathcal{L}_{I_{\text{M}|\text{M}}}\left(\frac{\tau r^{\alpha}}{P_{\text{M}}}\right)\mathcal{L}_{I_{\text{P}|\text{M}}}\left(\frac{\eta\tau r^{\alpha}}{P_{\text{M}}}\right)\middle|\text{Macro}, r>\omega_{\text{M}}\right] d\tau \tag{B.4}$$

$$= \int_0^{\infty} \int_{\omega_{\mathrm{M}}}^{\infty} \frac{f_{\mathrm{M}}(r)}{p_{\mathrm{worst}}} \frac{e^{-\frac{\tau r^{\alpha} \sigma^2}{P_{\mathrm{M}}}}}{\tau+1} \mathcal{L}_{I_{\mathrm{M|M}}}\left(\frac{\tau r^{\alpha}}{P_{\mathrm{M}}}\right) \mathcal{L}_{I_{\mathrm{P|M}}}\left(\frac{\eta \tau r^{\alpha}}{P_{\mathrm{M}}}\right) dr d\tau$$

$$\begin{aligned} \mathrm{E}\left[\ln\left(1+\Psi_{\mathrm{M}}^{\mathrm{I}} \middle| r > \omega_{\mathrm{M}}\right)\right] =& \mathrm{E}\left[\ln\left(1+\Psi_{\mathrm{M}}^{\mathrm{E}} \middle| r > \omega_{\mathrm{M}}, \eta = 1\right)\right] \\ =& \int_0^{\infty} \int_{\omega_{\mathrm{M}}}^{\infty} \frac{f_{\mathrm{M}}(r)}{p_{\mathrm{worst}}} \frac{e^{-\frac{\tau r^{\alpha} \sigma^2}{P_{\mathrm{M}}}}}{\tau+1} \mathcal{L}_{I_{\mathrm{M|M}}}\left(\frac{\tau r^{\alpha}}{P_{\mathrm{M}}}\right) \mathcal{L}_{I_{\mathrm{P|M}}}\left(\frac{\tau r^{\alpha}}{P_{\mathrm{M}}}\right) dr d\tau. \end{aligned} \tag{B.5}$$

By inserting these auxiliary definitions into equations (B.1) and (B.2), equations (4.12) and (4.11) are obtained. The derivation can be re-created for the pico cells by replacing macro and pico parameters for obtaining equations (4.13) and (4.14).

APPENDIX C: Sign of the Derivative of EE with Respect to γ_{P} and γ_{M} for Almost Blank Sub-Frame

EE is defined as ratio of ASE to AEC. AEC is not affected by γ_{M} and γ_{P}. Hence, the derivative of EE is given as

$$\begin{aligned} \frac{d\mathrm{EE}}{d\gamma_{\mathrm{P}}} &= \frac{\lambda_P}{\mathrm{AEC}}\left(\frac{d\mathbb{C}^{\mathrm{E}}_{\mathrm{M.BS}}}{d\gamma_{\mathrm{P}}}+\frac{d\mathbb{C}^{\mathrm{I}}_{\mathrm{M.BS}}}{d\gamma_{\mathrm{P}}}\right) \\ &= \frac{\lambda_P\mathcal{B}}{\mathrm{AEC}}\int_0^{\infty}\frac{1}{\tau+1}\left[\frac{k_M}{K}\frac{d\Pr(\Psi^{\mathrm{E}}_{\mathrm{P}}>\tau)}{d\gamma_{\mathrm{P}}}+\frac{K-k_P-k_M}{K}\frac{d\Pr(\Psi^{\mathrm{I}}_{\mathrm{P}}>\tau)}{d\gamma_{\mathrm{P}}}\right]d\tau \end{aligned} \tag{C.1}$$

whose sign depends on the summation of coverage probabilities for edge and interior users. The derivative of coverage probability for Pico-Edge users is given as

$$\frac{d\Pr(\Psi^{\mathrm{E}}_{\mathrm{P}}>\tau)}{d\gamma_{\mathrm{P}}}=\frac{d}{d\gamma_{\mathrm{P}}}\left\{\frac{\int_{\zeta}^{\infty}f_{\mathrm{P}}(r)g^{\mathrm{E}}_{\mathrm{P}}(r)dr}{\int_{\zeta}^{\infty}f_{\mathrm{P}}(r)dr}\right\}=\frac{\frac{\zeta}{\alpha\gamma_{\mathrm{P}}}f_{\mathrm{P}}(\zeta)\int_{\zeta}^{\infty}\left(g^{\mathrm{E}}_{\mathrm{P}}(\zeta)-g^{\mathrm{E}}_{\mathrm{P}}(r)\right)f_{\mathrm{P}}(r)dr}{\left(\int_{\zeta}^{\infty}f_{\mathrm{P}}(r)dr\right)^2} \tag{C.2}$$

where

$$\begin{aligned} \zeta &= \left(\frac{P_{\mathrm{P}}}{\gamma_{\mathrm{P}}}\right)^{1/\alpha}, \\ g^{\mathrm{E}}_{\mathrm{P}}(r) &= e^{-\frac{r^{\alpha}\sigma^2\tau}{P_{\mathrm{P}}}-\pi r^2\left(\lambda_P\rho_1(\tau)+\lambda_M\rho_{z_{\mathrm{MP}}}\left(\eta\frac{P_{\mathrm{M}}\tau}{P_{\mathrm{P}}}\right)\right)}, \end{aligned} \tag{C.3}$$

and $f_{\mathrm{P}}(r)$ is the PDF defined in equation (2.13). The distance r is considered only between ζ and ∞, so its PDF is conditionally implemented. The term $\int_{\zeta}^{\infty}f_{\mathrm{P}}(r)dr$ in the first line of equation (C.2) is a part of the conditional PDF. $g^{\mathrm{E}}_{\mathrm{P}}(r)$ is a strictly monotonically decreasing function of r. Considering equation (C.2), $g^{\mathrm{E}}_{\mathrm{P}}(\zeta)$ is always bigger than $g^{\mathrm{E}}_{\mathrm{P}}(r)$ as r is between ζ and ∞. Therefore, $\frac{d\Pr(\Psi^{\mathrm{E}}_{\mathrm{P}}>\tau)}{d\gamma_{\mathrm{P}}}$ has always a positive sign. The derivative of coverage probability for Pico-Interior users can be derived as

$$\frac{d\Pr(\Psi^{\mathrm{I}}_{\mathrm{P}}>\tau)}{d\gamma_{\mathrm{P}}}=\frac{d}{d\gamma_{\mathrm{P}}}\left\{\frac{\int_{0}^{\zeta}f_{\mathrm{P}}(r)g^{\mathrm{I}}_{\mathrm{P}}(r)dr}{\int_{0}^{\zeta}f_{\mathrm{P}}(r)dr}\right\}=\frac{\frac{\zeta}{\alpha\gamma_{\mathrm{P}}}f_{\mathrm{P}}(\zeta)\int_{0}^{\zeta}\left(g^{\mathrm{I}}_{\mathrm{P}}(r)-g^{\mathrm{I}}_{\mathrm{P}}(\zeta)\right)f_{\mathrm{P}}(r)dr}{\left(\int_{0}^{\zeta}f_{\mathrm{P}}(r)dr\right)^2} \tag{C.4}$$

where

$$g^{\mathrm{I}}_{\mathrm{P}}(r)=e^{-\frac{r^{\alpha}\sigma^2\tau}{P_{\mathrm{P}}}-\pi r^2\left(\lambda_P\rho_1(\tau)+\lambda_M\rho_{z_{\mathrm{MP}}}\left(\frac{P_{\mathrm{M}}\tau}{P_{\mathrm{P}}}\right)\right)}$$

where $g^{\mathrm{I}}_{\mathrm{P}}(r)$ is strictly monotonically decreasing with r. Hence, $g^{\mathrm{I}}_{\mathrm{P}}(r)$ is always bigger

than $g_{\mathrm{P}}^{\mathrm{I}}(\zeta)$ where r is between 0 and ζ. This property proves that the sign of the $\frac{d\mathrm{EE}}{d\gamma_{\mathrm{P}}}$ is always positive.

APPENDIX D: Derivations on NOMA - Strict Fractional Frequency Reuse

Because of the presence of the SIC receiver, the correct demodulation of low power signal depends on initial demodulation of the overlapping high power signal. Hence, the coverage probability of low power signal and overlapping high power signal are considered jointly. For both FFR techniques, type of overlapping high power signal differs due to frequency RB position as shown in Figure 5.1. Starting with the interior, the coverage probability of near users that uses interior RB's is written as

$$\begin{aligned}
&\Pr\left(\Psi_t^{\text{N-I}} > \tau, \Psi_t^{\text{F-I}} > \mathcal{T}\right) \qquad \text{(D.1)}\\
&= \mathrm{E}_r\left[\Pr\left(\tfrac{a_t^{\text{near}} P_t h r^{-\alpha}}{\sigma^2 + I_t^{\text{sFFR-I}}} > \tau, \tfrac{a_t^{\text{far}} P_t h r^{-\alpha}}{\sigma^2 + a_t^{\text{near}} P_t h r^{-\alpha} + I_t^{\text{sFFR-I}}} > \mathcal{T}\right)\middle| P_t r^{-\alpha} > \varphi_t\right]\\
&= \mathrm{E}_r\left[\Pr\left(h > \max\left\{\tfrac{\tau r^{\alpha}}{a_t^{\text{near}} P_t}, \tfrac{\mathcal{T} r^{\alpha}}{a_t^{\text{far}} P_t - \mathcal{T} a_t^{\text{near}} P_t}\right\}\left(\sigma^2 + I_t^{\text{sFFR-I}}\right)\right)\middle| P_t r^{-\alpha} > \varphi_t\right]\\
&= \mathrm{E}_r\left[\exp\left(-\tfrac{\tau r^{\alpha}\sigma^2}{a_t^{\text{near}} P_t}\right)\mathcal{L}_{I_t^{\text{sFFR-I}}}\left(\tfrac{\tau r^{\alpha}}{a_t^{\text{near}} P_t}\right)\middle| P_t r^{-\alpha} > \varphi_t\right]\\
&= \int_0^{(P_t/\varphi_t)^{1/\alpha}} \exp\left(-\tfrac{\tau r^{\alpha}\sigma^2}{a_t^{\text{near}} P_t}\right)\mathcal{L}_{I_t^{\text{sFFR-I}}}\left(\tfrac{\tau r^{\alpha}}{a_t^{\text{near}} P_t}\right)\tfrac{f_{r_t}(r)}{1-\mathfrak{P}_t} dr
\end{aligned}$$

where the forth line is obtained by CDF of exponential distribution and following rule

$$a_t^{\text{near}} P_t \left(1 + \frac{1}{\tau}\right) \leq \frac{a_t^{\text{far}} P_t}{\mathcal{T}}. \qquad \text{(D.2)}$$

In case of that the relationship above does not hold, the coverage probability of the low power signal becomes equal to coverage probability high power signal, either interior or edge depending on the RB region.

The coverage probability of near users that uses edge RB's is

$$\begin{aligned}
\Pr\left(\Psi_t^{\text{N-E}} > \tau, \Psi_t^{\text{F-E}} > \mathcal{T}\right) &= \sum_{s=1}^{T} \tfrac{1}{T} \Pr\left(\Psi_{t,s}^{\text{N-E}} > \tau, \Psi_t^{\text{F-I}} > \mathcal{T}\middle| \textit{edge-s}, P_t r^{-\alpha} > \varphi_t\right) \qquad \text{(D.3)}\\
&= \sum_{s=1}^{T} \tfrac{1}{T} \int_0^{(P_t/\varphi_t)^{1/\alpha}} \exp\left(-\tfrac{\tau r^{\alpha}\sigma^2}{a_t^{\text{near}} P_t}\right)\mathcal{L}_{I_{t,s}^{\text{sFFR-E}}}\left(\tfrac{\tau r^{\alpha}}{a_t^{\text{near}} P_t}\right)\tfrac{f_{r_t}(r)}{1-\mathfrak{P}_t} dr
\end{aligned}$$

where the coverage probability is divided into coverage probabilities of each RB group *edge*-j. We assume that the probability of usage of each RB is the same. Hence, the

probability of selection of *edge-s* among all edge RB's is $\frac{1}{T}\left(1-\frac{\mathrm{F_I}}{\mathrm{F}}\right)$ and the probability of selection of *interior* is $\mathrm{F_I}/\mathrm{F}$. Equation (5.10) is obtained by combining both edge and interior RB coverage probabilities of low power signal. Moreover, the coverage probabilities of far-interior and far-edge users can be similarly obtained by marginal probability of their SINR values.

Coverage probabilities of near, far-interior, and far-edge users are affected by LT of the interference. For Strict FFR technique, LT varies for edge or interior RBs in use. The LT of interior interference is obtained as

$$\begin{aligned}
\mathcal{L}_{I_t^{\text{sFFR-I}}}(x) &= \mathrm{E}\left[\exp\left(-xI_t^{\text{sFFR-I}}\right)\right] \\
&= \mathrm{E}\left[\exp\left(-x\sum_{j=1}^{T}\sum_{r_i>q_{j|t}} P_j h_i r_i^{-\alpha}\right)\right] \\
&= \prod_{j=1}^{T}\mathrm{E}\left[\prod_{r_i>q_{j|t}} \tfrac{1}{1+xP_j r_i^{-\alpha}}\right] \\
&= \prod_{j=1}^{T}\exp\left(-2\pi\lambda_j\int_{q_{j|t}}^{\infty}\left(1-\tfrac{1}{1+xP_j u^{-\alpha}}\right)udu\right)
\end{aligned} \tag{D.4}$$

where the third lines is obtained by introduction of LT of exponentially distributed h_i, the forth line is obtained by inserting probability generating functional (PGFL) for PPP [90]. Moreover, the LT of edge interference is obtained as

$$\begin{aligned}
\mathcal{L}_{I_{t,s}^{\text{sFFR-E}}}(x) &= \mathrm{E}\left[\exp\left(-xI_{t,s}^{\text{sFFR-E}}\right)\right] \\
&= E\Bigg[\exp\Bigg(-s\sum_{r_i>q_{s|t}}(\delta_{i,s}a_s^{\text{far}}P_s + a_s^{\text{near}}P_s)h_i r_i^{-\alpha} \\
&\quad -x\sum_{\substack{j=1\\ j\neq s}}^{T}\sum_{r_i>z_{j|t}} a_j^{\text{near}}P_j h_i r_i^{-\alpha}\Bigg)\Bigg] \\
&= \mathrm{E}\left[\prod_{r_i>q_{s|t}}\tfrac{1}{1+x(\delta_{i,s}a_s^{\text{far}}P_s+a_s^{\text{near}}P_s)r_i^{-\alpha}}\right]\prod_{\substack{j=1\\ j\neq s}}^{T}\mathrm{E}\left[\prod_{r_i>q_{j|t}}\tfrac{1}{1+xa_j^{\text{near}}P_j r_i^{-\alpha}}\right] \\
&= \exp\left\{-2\pi\lambda_s\int_{q_{s|t}}^{\infty}\left(1-\tfrac{1}{\Delta_s}\tfrac{1}{1+xP_s u^{-\alpha}}-\tfrac{\Delta_s-1}{\Delta_s}\tfrac{1}{1+xa_s^{\text{near}}P_s u^{-\alpha}}\right)udu\right.
\end{aligned} \tag{D.5}$$

$$-2\pi \sum_{\substack{j=1 \\ j \neq s}}^{T} \lambda_j \int_{q_{j|t}}^{\infty} \left(1 - \frac{1}{1+x a_j^{\text{near}} P_j u^{-\alpha}}\right) u du \Bigg\}$$

where the third equality is obtained by introduction of LT of exponentially distributed h_i, and the forth equality is obtained by inserting PGFL for PPP [90] and averaging with respect to $\delta_{i,s}$.

APPENDIX E: Derivations on NOMA - Soft Frequency Reuse

The coverage probability of near users is jointly evaluated with coverage of high power signal similar to Appendix D. For SFR, the signal of near user can be transmitted in the same RB with the signals of far-interior or far-edge users. The coverage probability of near users while sharing the same RB's with far-interior users is given as

$$\begin{aligned}
&\Pr\left(\Psi_t^{\mathrm{N}} > \tau, \Psi_t^{\text{F-I}} > \mathcal{T}\right) \qquad \text{(E.1)}\\
&= \mathrm{E}\left[\Pr\left(h > \max\left\{\tfrac{\tau r^{\alpha}}{a_t^{\text{near}} P_t}, \tfrac{\mathcal{T} r^{\alpha}}{a_t^{\text{far}} P_t - \mathcal{T} a_t^{\text{near}} P_t}\right\}(\sigma^2 + I_t^{\mathrm{SFR}})\right)\middle| P_t r^{-\alpha} > \varphi_t\right]\\
&= \mathrm{E}\left[\Pr\left(h > \tfrac{\tau r^{\alpha}}{a_t^{\text{near}} P_t}(\sigma^2 + I_t^{\mathrm{SFR}})\right)\middle| P_t r^{-\alpha} > \varphi_t\right]\\
&= \int_0^{(P_t/\varphi_t)^{1/\alpha}} \exp\left(-\tfrac{\tau r^{\alpha}\sigma^2}{a_t^{\text{near}} P_t}\right) \mathcal{L}_{I_t^{\mathrm{SFR}}}\left(\tfrac{\tau r^{\alpha}}{a_t^{\text{near}} P_t}\right) \tfrac{f_{r_t}(r)}{1-\mathfrak{P}_t} dr
\end{aligned}$$

where the second equality is obtained by the rule in Inequality (D.2) and the third equality is obtained by similar the steps with all previous proofs. By Inequality (D.2), the coverage probability of near users in edge RB region equals the coverage probability of near user in interior RB region since $a_t^{\text{far}} P_t < \beta_t a_t^{\text{far}} P_t$. Hence, the coverage probability of near users found above is applicable for all available RB's. The coverage probabilities of far-interior and far-edge users can be similarly obtained by marginal probability of their SINR values. LT of interference in SFR-NOMA coexistence is written as

$$\begin{aligned}
&\mathcal{L}_{I_t^{\mathrm{SFR}}}(x) \qquad \text{(E.2)}\\
&= \mathrm{E}\left[e^{-x I_t^{\mathrm{SFR}}}\right]\\
&= E\left[\exp\left\{-x \sum_{j=1}^{T} \sum_{r_i > q_{j|t}} \left(a_j^{\text{near}} P_j + (1-\delta_{i,j}) a_j^{\text{far}} P_j + \delta_{i,j}\beta_j a_j^{\text{far}} P_j\right) h_i r_i^{-\alpha}\right\}\right]\\
&= \prod_{j=1}^{T} \mathrm{E}\left[\prod_{r_i > q_{j|t}} \tfrac{1}{1 + x(a_j^{\text{near}} P_j + (1-\delta_{i,j}) a_j^{\text{far}} P_j + \delta_{i,j}\beta_j a_j^{\text{far}} P_j) r_i^{-\alpha}}\right]
\end{aligned}$$

$$= \prod_{j=1}^{T} \exp\left\{ -2\pi\lambda_j \int_{q_{j|t}}^{\infty} \left(1 - \frac{1}{\Delta_j} \frac{1}{1+x(a_j^{\text{near}} P_j + \beta_j a_j^{\text{far}} P_j) u^{-\alpha}} \right.\right.$$
$$\left.\left. - \frac{\Delta_j - 1}{\Delta_j} \frac{1}{1+x(a_j^{\text{near}} P_j + a_j^{\text{far}} P_j) u^{-\alpha}} \right) u du \right\}$$

where the third equality is obtained by LT of exponential distribution of h_i, the forth equality is obtained by averaging with $\delta_{i,j}$ and inserting PGFL of PPP.

APPENDIX F: Power Levels for Maximum Fairness in Downlink NOMA

Problem (6.24) is firstly converted to

$$\max_{a,\xi} \ \xi \tag{F.1a}$$

$$\text{subject to} \ \ \mathcal{C}_{i,j}^{\text{near}} \geq \xi \tag{F.1b}$$

$$\mathcal{C}_{i,j}^{\text{far}} \geq \xi \tag{F.1c}$$

to be able to model with the KKT conditions [96]. The Lagrangian function for the problem becomes

$$L = -\xi + v_{F.1}(\xi - \mathcal{C}_{i,j}^{\text{near}}) + v_{F.2}(\xi - \mathcal{C}_{i,j}^{\text{far}}) \tag{F.2}$$

where $v_{F.1}$ and $v_{F.2}$ are respective Lagrangian multipliers for near and far user capacity lower bounds. Therefore, KKT conditions for the problem are given as

$$-v_{F.1}\frac{\partial \mathcal{C}_{i,j}^{\text{near}}}{\partial a} - v_{F.2}\frac{\partial \mathcal{C}_{i,j}^{\text{far}}}{\partial a} = 0 \tag{F.3a}$$

$$-1 + v_{F.1} + v_{F.2} = 0 \tag{F.3b}$$

$$v_{F.1}(\xi - \mathcal{C}_{i,j}^{\text{near}}) = 0 \tag{F.3c}$$

$$v_{F.2}(\xi - \mathcal{C}_{i,j}^{\text{far}}) = 0 \tag{F.3d}$$

where equations (F.3a) and (F.3b) are derived from derivative of equation (F.2) with respect to a and ξ. By definition, the sign of $\frac{\partial \mathcal{C}_{i,j}^{\text{near}}}{\partial a}$ and $\frac{\partial \mathcal{C}_{i,j}^{\text{far}}}{\partial a}$ are positive and negative, respectively. Considering the signs of these derivatives, equation (F.3a) and (F.3b) provides that $v_{F.1}$ and $v_{F.2}$ have non-zero values and their sum equals to 1. Using this outcome on equation (F.3c) and (F.3d), the solution is achieved when $\xi = \mathcal{C}_{i,j}^{\text{near}} = \mathcal{C}_{i,j}^{\text{far}}$.

APPENDIX G: Power Levels for Maximum Sum-Rate in Downlink NOMA

The Lagrangian function for Problem (6.26) is given as

$$L = -\mathcal{C}_{i,j}^{\text{near}} - \mathcal{C}_{i,j}^{\text{far}} + v_{G.1}(\epsilon_{6.1} - \mathcal{C}_{i,j}^{\text{near}}) + v_{G.2}(\epsilon_{6.1} - \mathcal{C}_{i,j}^{\text{far}}) \tag{G.1}$$

where $v_{G.1}$ and $v_{G.2}$ are the respective Lagrangian multipliers for the near and far user capacity lower bounds. To solve the problem, the KKT conditions [96] are given as

$$-\frac{\partial \mathcal{C}_{i,j}^{\text{far}}}{\partial a}(1 + v_{G.2}) - \frac{\partial \mathcal{C}_{i,j}^{\text{near}}}{\partial a}(1 + v_{G.1}) = 0 \tag{G.2a}$$

$$v_{G.1}(\epsilon_{6.1} - \mathcal{C}_{i,j}^{\text{near}}) = 0 \tag{G.2b}$$

$$v_{G.2}(\epsilon_{6.1} - \mathcal{C}_{i,j}^{\text{far}}) = 0. \tag{G.2c}$$

The optimal values for $v_{G.1}$, $v_{G.2}$, and a can only be obtained by finding a relationship between $\frac{\partial \mathcal{C}_{i,j}^{\text{far}}}{\partial a}$ and $\frac{\partial \mathcal{C}_{i,j}^{\text{near}}}{\partial a}$. The derivative of the near user capacity can be obtained as

$$\begin{aligned}
\frac{\partial \mathcal{C}_{i,j}^{\text{near}}}{\partial a} &= \int_0^{\infty} \tfrac{1}{\tau} \tfrac{\partial}{\partial a} \Pr\left(\Psi_i > \tfrac{\tau}{a}\right) d\tau \\
&= \int_0^{\infty} \tfrac{\tau}{(\tau+1)a^2} f_{\Psi_i}\left(\tfrac{\tau}{a}\right) d\tau \\
&= \int_0^{\infty} \tfrac{u}{1+au} f_{\Psi_i}(u)\, du \\
&= \int_0^{1/a} \Pr\left(\Psi_i > \tfrac{v}{1-av}\right) dv
\end{aligned} \tag{G.3}$$

where $f_{\Psi_i}(\cdot)$ presents PDF of the i-th user SINR. Through derivations, the first line of equation (G.3) is obtained by moving the derivative inside the integral. The second line of equation (G.3) is obtained by the derivative of the CDF of Ψ_i is its PDF. The third line of equation (G.3) is obtained by $\frac{\tau}{a} = u$ transformation in integral. Lastly, the forth line of equation (G.3) is obtained by $\int_0^{\infty} \Pr(\Psi > g^{-1}(t))dt = \int g(t) f_{\Psi}(t) dt$ transformation between integrals of tail probability and PDF [90] as Ψ is always positive.

Similarly, the derivative of the far user capacity can be obtained as

$$\begin{aligned}
\frac{\partial \mathcal{C}_{i,j}^{\text{far}}}{\partial a} &= \frac{\partial}{\partial a} \int_0^{\frac{1-a}{a}} \frac{1}{\tau+1} \Pr\left(\Psi_j > \frac{\tau}{1-a-a\tau}\right) d\tau \\
&= \int_0^{\frac{1-a}{a}} \frac{1}{\tau+1} \frac{\partial}{\partial a} \left(\Pr\left(\Psi_j > \frac{\tau}{1-a-a\tau}\right)\right) d\tau - \frac{1}{a^2} \Pr\left(\Psi_j > \frac{\frac{1-a}{a}}{1-a-a\frac{1-a}{a}}\right) \\
&= -\int_0^{\frac{1-a}{a}} \frac{\tau}{(1-a-a\tau)^2} f_{\Psi_j}\left(\frac{\tau}{1-a-a\tau}\right) d\tau \\
&= -\int_0^{\infty} \frac{u}{1+au} f_{\Psi_j}(u) du \\
&= -\int_0^{1/a} \Pr\left(\Psi_j > \frac{v}{1-av}\right) dv \ .
\end{aligned} \tag{G.4}$$

In the second line of equation (G.4), the derivative operator moved inside the integral by the Leibniz rule [100]. The second term of the second line in equation (G.4) equals to 0. The third line of equation (G.4) is obtained by the derivative of the CDF of Ψ_i is its PDF. The forth line of equation (G.4) is obtained by integral transformation $u = \frac{\tau}{1-a-a\tau}$. Lastly, the fifth line of equation (G.4) is obtained by the transformation between integrals of tail probability and PDF [90].

As the users are ordered according to their SINRs, $\Psi_i > \Psi_j$ condition is always true for $j > i$. By $\Pr(\Psi_i > x) > \Pr(\Psi_j > x)$ condition and equations (G.3) and (G.4), we can conclude that

$$\frac{\partial \mathcal{C}_{i,j}^{\text{near}}}{\partial a} > -\frac{\partial \mathcal{C}_{i,j}^{\text{far}}}{\partial a} \tag{G.5}$$

condition is always true. Adding equation (G.5) condition to the KKT conditions in equations (G.2a), (G.2b), and (G.2c), the optimal solution is achieved by selecting the Lagrangian multipliers as $v_{G.1} = 0$ and $v_{G.2} > 0$. Therefore, the optimal solution of a can be calculated by finding the root of $\mathcal{C}_{i,j}^{\text{far}} = \epsilon_{6.1}$ equation.